
State-of-the-Art Review and Analysis in Earthquake Forecasting

Master Thesis

Handed in by:
Dipl.-Ing. Andreas Maximilian Schäfer

Ludwig-Maximilians Universität München
Department of Earth and Environmental Science
Institute of Geophysics

Supervised by:
Prof. Dr. Hans-Peter Bunge & Prof. Dr. Heiner Igel

Advised by:
Dr. James Daniell & Dr. Matthias Hackl

February 2014

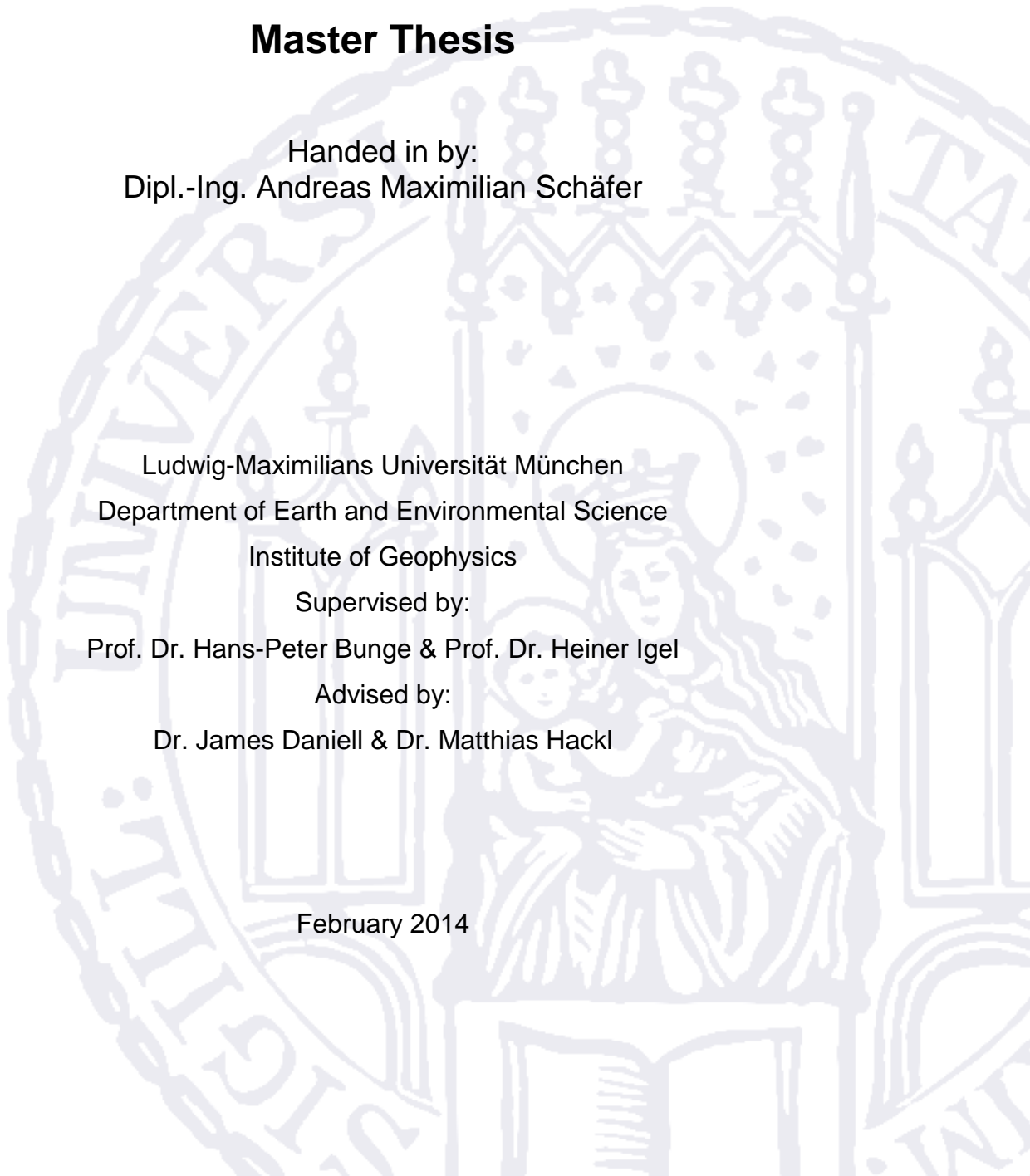


Table of Contents

1	Introduction	1
1.1	Abstract	1
1.2	Introduction and Overview.....	1
1.3	Scientific Objectives	2
2	Theory	4
2.1	Plate Tectonics.....	4
2.1.1	Plate Movement and Interactions.....	4
2.1.2	Subduction Zones	6
2.2	Earthquakes	7
2.2.1	Focal Mechanisms	7
2.2.2	Magnitude Types & Source Parameters	9
2.2.3	Earthquake Statistics	11
2.3	Probabilistic Seismic Hazard Analysis.....	12
2.3.1	Probabilistic Seismic Hazard Methodology	13
2.3.2	Seismic Forecasting.....	13
2.3.3	Seismic Zonation	14
3	Review	16
3.1	Overview of Methods.....	16
3.2	Related Projects.....	17
3.3	Survey Parameters.....	18
3.4	Time-independent Methods.....	19
3.4.1	Relative Intensity (RI).....	19
3.4.2	Earthquake Prediction in California (EPiC)	19
3.4.3	Asperity Likelihood Model (ALM)	20
3.4.4	HAZGRIDX	20
3.4.5	Adaptively Smoothed Seismicity (ASS)	21
3.4.6	PEGASOS EG1b approach	21
3.4.7	Simple Smoothed Seismicity (Triple-S).....	22
3.5	Time-dependent Methods	22
3.5.1	Pattern Information (PI).....	22
3.5.2	Reverse Tracing of Precursors (RTP).....	23
3.5.3	Epidemic-type Aftershock Sequence (ETAS).....	23
3.5.4	Every Earthquake a Precursor According to Scale (EEPAS).....	24
3.5.5	Epidemic Rate-Strain (ERS)	24
3.5.6	Short-term Aftershock Probabilities (StAP)	25

3.5.7	Early Aftershock Statistics (EAST).....	25
3.6	Hybrid Methods	26
3.6.1	Fault Slip and Smoothed Seismicity (FSSS).....	26
3.6.2	Hybrid Seismicity Method (HSM)	26
3.6.3	Long-term Stress Transfer (LtST)	27
3.6.4	Seismic Hazard Inferred from Tectonics (SHIFT)	27
3.6.5	Fault-oriented Earthquake Forecast (FoEF)	28
3.7	Static triggering	29
3.7.1	Overview	29
3.7.2	Theory.....	30
3.8	Catalogue Development.....	32
3.8.1	Catalogue content.....	32
4	Reconstruction.....	33
4.1	Time-independent Method Toolbox.....	33
4.1.1	Declustering.....	34
4.1.2	Smoothing.....	36
4.1.3	Gutenberg-Richter Handling	40
4.2	Time-dependent Method reconstruction.....	42
4.2.1	Pattern Informatics.....	43
4.2.2	Epidemic-Type of Aftershock Sequences	45
4.3	Fault-oriented time-(in-)dependent b-value	49
4.4	Overview and Summary of Coding.....	51
5	Testing.....	53
5.1	Testing Algorithms.....	53
5.1.1	N-Test.....	54
5.1.2	S-Test & M-Test.....	54
5.2	The Testing Range.....	56
5.2.1	Data	56
5.3	Test Results – time-independent.....	59
5.3.1	Methods & Application on Testing Range	59
5.3.2	Results.....	60
5.4	Test Results – time-dependent	66
5.4.1	Test Results – Pattern Informatics.....	66
5.4.2	Test Results – Time-dependent b-value	69
5.4.3	Test Results – Epidemic Type of Aftershock Sequences.....	71
5.5	Test Conclusion.....	75
6	Hybrid Method Development.....	77
6.1	Idea	77
6.2	Theory	78
6.2.1	Data	79
6.2.2	Slip accumulation and release	80

6.3	The Slip Accumulation Method (SAM).....	81
6.3.1	Method description.....	81
6.3.2	Calibration.....	84
6.4	Results	85
7	Case Studies.....	89
7.1	Time-independent Forecast	89
7.2	Time-dependent Forecast	90
7.3	Summarized Forecast	91
8	Conclusion.....	93
8.1	A brief Summary of Earthquake Forecasting.....	93
8.2	Forecasting vs. Prediction	95
8.3	Future Developments	96
8.4	Closing Words.....	97
	Acknowledgements.....	98
	Figures.....	99
	Tables	102
	Literature	103
	Appendix A: Method Catalogue	108
	Appendix B: Time-independent sample Method.....	130
	Appendix C: Time-independent Test Results	136
	Appendix D: Time-independent Method Toolbox	141

1 Introduction

1.1 Abstract

For decades, earthquake prediction and forecasting has remained one of the most challenging tasks in modern geophysics. During this time, a vast number of different algorithms have been developed to calculate earthquake forecasts. To give an overview of the different approaches, a catalogue has been developed that reviews around two dozen methods for earthquake forecasting. This catalogue has been divided into three categories of time-independent, time-dependent and hybrid methods for forecasting, in which each category has been further investigated.

For time-independent methods which are more useful in computing general seismic hazard rather than calculating a real forecast, a toolbox has been assembled and tested from which time-independent smooth seismicity methods can be easily created. Furthermore two different time-dependent methods have been reconstructed and a third one developed and tested to find out their general ability to forecast future seismicity. With rather unsatisfying results due to forecasting accuracy it is shown that a lot of future development is necessary to compute sophisticated and reliable forecasts.

Finally a hybrid method was developed to incorporate slip accumulation and release along tectonic faults to indicate regions of future seismicity. For the beginning, this approach lead to promising results and should be further developed.

Concluding with a small case study of future seismicity in Turkey, the whole area of earthquake forecasting, including the general development of forecasting algorithms and also their related testing procedures, still needs a lot of effort to be able to generate forecasts which are universally applicable and reliable enough within a successful ranges which are good enough to publish via official channels.

1.2 Introduction and Overview

Forecasting earthquakes is still one of the hardest tasks in Geophysics. It is heavily discussed and still controversial. In the last few decades, several methods to forecast and predict damaging earthquake events have been developed. In general, most of the methods lack in accuracy and reliability, which is obviously related to limited knowledge of the earthquake process and the short period of time for which sophisticated observations are available. Anyway there are different approaches

which are able to estimate future behavior up to a certain resolution within the limits of modeling and data. Such theories start from basic Gutenberg-Richter relations and end up with pattern searching algorithms in earthquake occurrence or models to identify static triggering of earthquakes related to stress propagations in the upper crust.

Even with simple assumptions, some methods are able to forecast or predict in the range of years or decades and spatial resolutions related to certain faults or regions. A classic example is the forecast of probably large upcoming events close to San Francisco, Tokyo or Istanbul. For these cities, large events with $M_w \geq 7$ are assumed to occur during the next decades. [e.g. Parsons, 2004]

It is a major task to understand the key aspects of earthquake reoccurrence and triggering. Therefore understanding theories in seismology and structural geology especially for the upper crust are essential. For example relations between the moment magnitude and the rupture length and the average slip of an earthquake or the redistribution of stress after an event which might trigger future earthquakes.

Identifying the different approaches in earthquake forecasting and analyzing the core elements of the forecast algorithms is an important part of this thesis. It is of course not the first attempt to compare different methods. There have been several others like the Collaboratory for the Study of Earthquake Predictability (CSEP) [Werner et al., 2010]. Such projects already applied a useful set of testing procedures, which will be partially applied here to test the general functionality and accuracy of the methods. So additionally a deep background of statistical testing and likelihood estimation must be applied to sophisticatedly test these methods and to compare them to each other. A special focus will be on the overall likelihood, how well a method reflects the events during a testing period, after calibrating the algorithm with a common set of events during a learning period. It can be distinguished between the likelihood due to magnitude and spatial scales and of course the overall number of events which occurred during the testing period.

In general all methods are divided into sub-classes like time-independent, time-dependent and hybrid methods, each with their own characteristics. While the definition is obvious for time-independent and time-dependent methods using in general just historical earthquake data and related statistics, hybrid methods represent approaches which incorporate either physical theories and/or additional datasets. With increasing complexity each category denotes a certain level of accuracy, physical background and application.

1.3 Scientific Objectives

This thesis investigates recently developed methods (approximately during the last two decades) to analyze them. Therefore multiple survey parameters will be used to give a proper review for all of them. The methods are additionally categorized and summarized to develop a general catalogue of earthquake forecasting methods. For time-independent methods, a set of key features will be built and tested, partially

reassembled and applied to a common testing range. This testing range consists of two testing regions, namely datasets for Italy and Turkey. For these areas a common set of tests is used to estimate the accuracy and likelihood of each method. Finally this testing will end up with a retrospective forecast experiment and additionally an outlook of future seismicity.

After testing the methods, the advantages and disadvantages are known for the different approaches. This part of the study will conclude with a general toolbox for time-independent earthquake model creation. Time-dependent models will additionally be rebuilt to test the general efficiency of time-dependent approaches due to short-term forecasting. Two of them are chosen from the catalogue while a third one will be developed by the author.

After reviewing time-independent and time-dependent studies, which in general use only historical earthquake data, a review of so-called hybrid methods is also given. Hybrid methods incorporate additional data sources like focal mechanisms and/or strain-rate patterns and/or incorporate additional physical aspects like Coulomb-stress-changes. To finally round up the overview of state-of-the-art in earthquake forecasting a simple approach in hybrid earthquake forecasting is developed and tested to cover all three kinds of earthquake forecasting methods.

In addition to the classical thesis text work to cover these objectives, a set of appendixes will be made. These appendixes will contain:

1. Earthquake Forecasting Method Catalogue (Appendix A)
2. Development of a sample method, including complete code (Appendix B)
3. Time-independent Test Results (Appendix C)
4. Time-independent method toolbox with readme and code (Appendix D)

The overall scientific objective is to provide a state-of-the-art toolbox in time-independent method development, time-dependent short-term forecast possibilities and an overview of latest method developments.

2 Theory

This chapter covers all basic background topics due to earthquake occurrence. A special focus is made on plate tectonics producing strong earthquake events and the mechanisms behind the process. In addition a short introduction into earthquake hazard analysis is given. The major part of this chapter is based on the publications [Chen and Scawthorn, 2003] and [Stein and Wysession, 2003]

2.1 Plate Tectonics

2.1.1 Plate Movement and Interactions

This chapter will give a slight introduction into plate tectonics, which is the study of the movement of the earth's plates and how these movements lead to the occurrence of earthquakes. The idea of moving plates on the earth surface and the spreading idea of plate tectonics refers back to the 1930s and Alfred Wegener's hypothesis that in the ancient times South America and Africa fit together. Plate tectonics represents the surface expression of the earth's internal convection. The convection is driven by three different mechanisms, also called modes. The first one is the internal heating mode of the earth's mantle, which is driven by radioactive processes. The second one is the plume mode which is driven by heating processes at the core-mantle boundary and leads to relatively small local surface features like Hawaii or the Seychelles and is related to strong surface volcanism. The third and final one is the plate-mode. It is the driving engine of plate tectonics. The plate-mode describes the relative movement of the plates as part of the mantle convection as an upper thermal boundary layer. Its contribution to the convection is the active subduction of cold crust into the mantle. The movement of the plates leads to rifting events where plates get torn apart and hot mantle material can passively rise again to form new oceanic crust by cooling.

So plate tectonics describes the movement of the earth's outer shell, which is differentiated into about 15 larger plates, which are about 100 km thick, depending on if a plate consists continental crust (thicker and less dense) or oceanic crust (thinner and denser), there are also a large number of smaller plates, but their participation to the global plate tectonics is minor due to physical reasons. This outer shell is also known as the earth's lithosphere in contrast to the layer below, the so-called asthenosphere. The plates are moving relative to each other and can be assumed to be rigid. So the deformations, which originate from their movement-related interaction, occur mostly at their boundaries. Typically the movement speed of a plate is in the range of centimeters per year. Some plates are relatively fast like the

Pacific plate, while others seem not to move at all like the African plate. The plate boundaries can be separated into three different kinds. At a ridge, hot mantle material rises to the surface and cools down. Ridges are also defined as divergent plate boundaries where the related plates are moving away from each other. In contrast there are trenches or also called subduction zones, where two plates collide and one of them sinks under the other one downwards to the mantle. The last kind of typical plate boundaries are transversal or transform faults, where the motion of each plate is parallel to the boundary. In this sense figure 2.1 gives a simple overview of the mechanisms and surface features related to plate tectonics.

The different kinds of boundaries create their own earthquake behavior. For example, ridges create quite shallow earthquakes, because the whole process of ocean building happens close to the surface, while subduction zones are able to produce so-called deep seismicity with a depth of several hundred kilometers representing the sinking plate in the upper mantle. Due to different behavior of the faults it is possible to distinguish between two general kinds of movement. The first kind is more common for both divergent and transversal faults, where creep dominates the movement and only weak earthquakes happen. The second type is typical for both convergent and transversal zones where friction locks the movement of the plate boundaries. After exceeding a certain stress, the movement happens quite abrupt with a strong rupture and a large amount of released energy, namely strong earthquakes. After such an event the stress builds up again, due to continuously ongoing movement. This is also called, the seismic cycle [Reid, 1910].

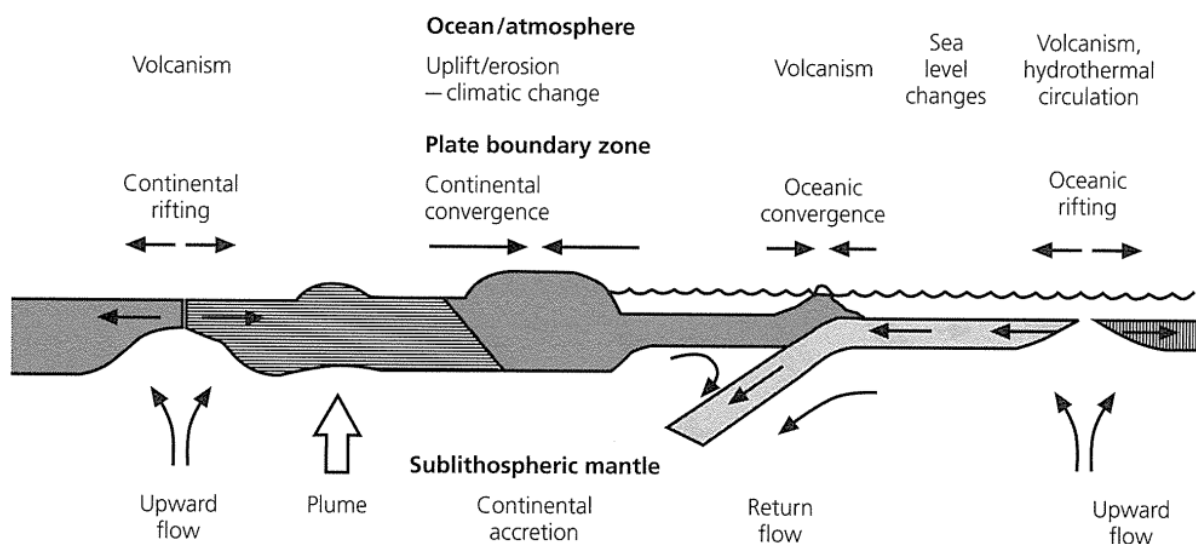


Figure 2.1: A simple cartoonish summary of the main mechanisms and interactions of the earth's surface and its inside and atmosphere. From [Chen and Scawthorn, 2003]

Earthquakes do not only occur at plate boundaries as there are a lot of earthquake hotspots around the world where earthquakes happen far away from any boundary. The reason for this behavior is still heavily debated; some of these events are obviously related to rising hot spots from the deep mantle, which are heated by the

core, while for others the explanation is not so obvious. A popular example is Hawaii, but except for such obvious places where the earthquake activity is related to rising plumes, it is hard to relate events like the Washington earthquake of 2012 in the center of North America to such causes.

In the following we will take a closer look at subduction zones, which are the most common areas of recent disastrous earthquakes. Ridges are not further covered because most of them are below the oceans and do not generate such strong events. Of course there are regions where geophysically speaking rifting occurs like in the East African Ridge or the Rhine Valley, but this won't be explained in detail here, transversal zone are not further explained as well, they are closely related to ridges due to unstable combinations of plate boundaries, earthquakes which occur along transversal zones are relatively shallow and occur mostly in the brittle part of the lithosphere (upper 30 km). The theory behind the stability of plate boundaries and plate movement will not be further explained here.

2.1.2 Subduction Zones

Subduction zones are areas where one plate sinks under another one. Such processes might lead to mountain building like known from the Andes, the Rocky Mountains and so on. These mountain arcs are built by faulting and bending of the overlying plate while in between the plates deep trenches are formed, which might go deep into the crust, popular example is of course the Marianna Trench in the Eastern Pacific. The plate which subducts, sinks with a certain inclination, depending on its movement speed. Fast subducting plates are only slightly inclined, while very slow plates might go down very steep. These inclined plates which are sinking down into the earth's mantle are clearly visible in their seismic activity, which follows the plate downwards. The deep zones of seismic activity due to a subducting slab are known as Wadati-Benioff zones. It should be noted that subduction can only occur if at least one oceanic plate is involved which can be explained with the physical properties like the density difference. If plates of continental material converge, crust thickening happens while one plate goes under the other one. The mountain building might lead to huge mountain belts like the mountain range starting with the Alps in the west to the Himalayans in the East. The seismic activity remains shallow relative to real subduction zones.

Typically a volcanic island arc evolves between the two colliding plates, where partially molten material of the subducting slab rises again. Earthquakes might occur along the trench between the plates and also along the Wadati-Benioff zone downwards into the mantle. This finally leads to a combination of shallow (less than 70 km) and deep (more than 70 km, down to 700 km) earthquakes. While deep earthquakes occur only along the subducting slab, shallow earthquake can happen in both participating plates. In addition to the differentiation of shallow and deep earthquakes it is possible to differ also between intermediate (70 – 300 km) and deep (300 – 700 km) earthquakes. This is related changes in seismicity rates, which

decrease downwards until 300 km and rises again until it finally disappears at around 700 km. Results from seismology show that the events down to a depth of 300 km represent down-dip tension while deeper earthquakes show down-dip compression. The reasons for these differences are still under discussion, but one possibility is to think about that the slab sinks down under its own weight (negative buoyancy) to a depth of 300 km where the surrounding mantle material begins to compress the slab. The first mechanism related to negative buoyancy is also known as “slab pull”. Other possibilities e.g. for the deep mechanism are related to phase transition of the material.

However the really dangerous earthquakes are the shallow ones. Among them are the largest earthquakes that have ever occurred on earth. These events happen in the trench area in the contact zone between both participating plates. Well known examples are the Alaska earthquake of 1964 and the Chilean earthquake of 1960 and of course the Tohoku earthquake of 2011. During these events a fault broke along multiple hundreds of kilometers with a surface slip in the range of tens of meters. Such events release enough energy to affect the earth’s rotation axis and change the elevation of topography features in the rupture area.

2.2 Earthquakes

This Chapter introduces earthquakes and necessary background information to understand how earthquakes are measured to analyze them for forecasting. In general earthquakes are plate ruptures. As described in chapter 2.1 tectonic plates are moving relative to each other. This leads to spatial settings where two sides are moving in the opposite directions, so called faults. Earthquakes almost invariably occur on or along faults. The movement of the plates relative to each other is often locked by friction, while the whole plate continues its absolute movement. Friction occurs on the plate boundaries and prevents the sides from slipping. So the accumulated strain in the rock might overwhelm the strength of the plate and the fault slips. This slipping may happen spontaneously and quickly. This sudden release of energy is called earthquake. The location of this event is often located deep in the crust and called hypocenter, while its projection to the surface is called epicenter. In fact the rupture of a fault happens rather on a plane than a single point, the hypocenter is the centralized location of the fault plane. Earthquakes emit elastic waves which can be measured e.g. by seismographs. These measurements can be used to determine the focal mechanism of the event.

2.2.1 Focal Mechanisms

As described above we can assume that the geometry of a fault is a planar surface along which the sudden movement happens. To give statements about the fault orientation it is described by the direction of the slip along this plane.

2 Theory

The orientation of a plane in three dimensions is defined by three angles. The fault plane is oriented relative to the earth's surface thus the strike angle gives the azimuth or angle relative to the geographic north. The dip angle defines the inclination of the plane relative to the horizontal axis. The slip angle finally gives the movement direction along the inclined fault plane of the upwards moving fault element. Figure 2.2 summarizes the geometry of a fault plane.

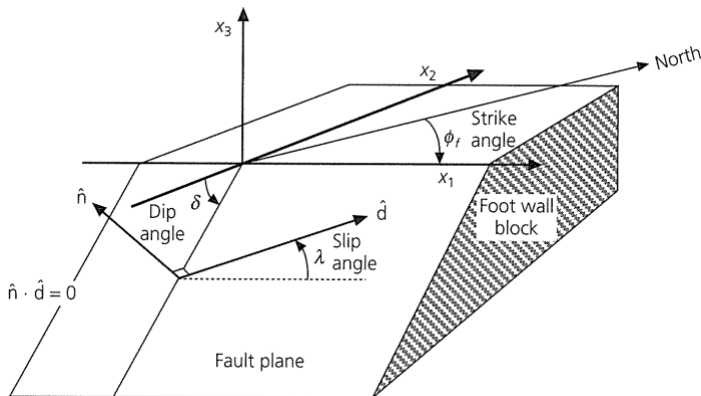


Figure 2.2: Geometry of a fault used to define movement direction of the fault. From [Stein and Wysession, 2003]

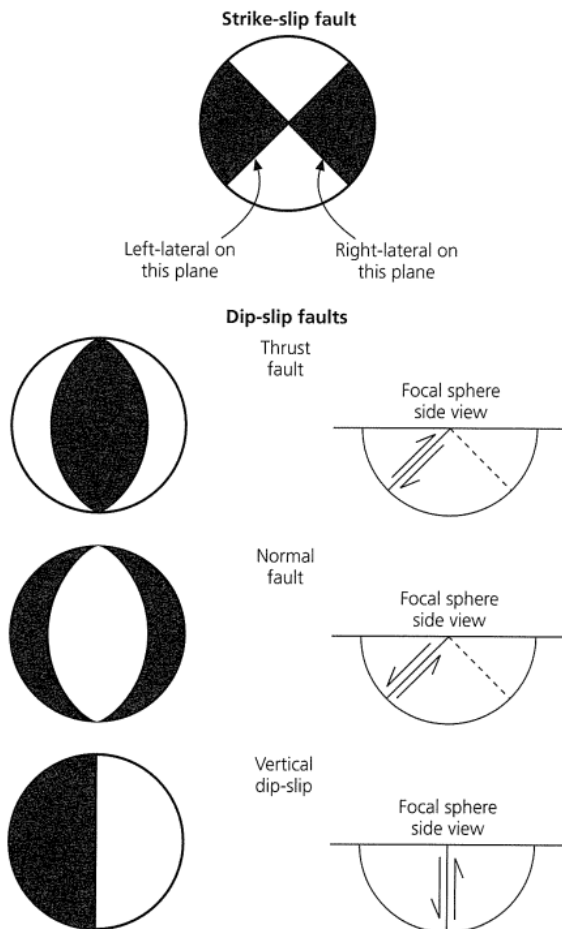


Figure 2.3: Spherical projection of the focal mechanisms. Dark quadrants represent compression, while white ones are for tension. From [Stein and Wysession, 2003]

From the definition the fault orientation we can define four basic types of faulting. The first type is called the strike-slip fault where a 90° dip angle describes a simple horizontal motion of a vertical fault plane. A dip-slip fault represents the movement along a inclined fault plane. If the upper block moves downward, it is called normal, and vice-versa it is called reverse if the upper block moves upwards. The reality is more complex of course, and the fault geometry is often way more complex, but this representation of a fault mechanism is a simple way to understand how an earthquake event was related to the movement of a fault. Almost all possible orientations of these mechanisms are possible.

Measuring fault motion e.g. by an earthquake shows four quadrants of stress around the fault location. If we take the epicenter as a single point in the middle of the fault we have two quadrants for each side. The quadrant in direction of motion is compression while the continuum in the opposite direction is affected by tension or dilatation. This simple explanation for stress propagation in earthquake faults can be used to take a look at final representation of the focal mechanism of an earthquake event.

In conclusion one can represent the focal mechanism as a 2D spherical projection. This projection consists of a sphere of 4 quadrants which represent the 2 times compression and two times tension. Depending on the fault orientation the sphere is rotated and the appearance of its projection changes. The faults describes above can be represented as these projections (also called beach balls). Figure 2.3 shows the basic focal mechanisms, which have been introduced above. For further details, [Stein and Wysession, 2003] describes additional information and theory behind this representation.

2.2.2 Magnitude Types & Source Parameters

Describing earthquakes does not end with explaining how the surface ruptured. Such an event emits, as described, elastic waves through the earth. At the surface this might lead to devastating shaking which might let buildings collapse, trigger tsunamis or landslides. To quantify such events a measurement scale was needed. The first one was the intensity of an earthquake. It is described by its surface effects, e.g. how much damage was caused. However this is rather a subjective observation than a real physical measurement. The first real scale for earthquakes was introduced by Charles Richter in 1935 for earthquake events in California. [Gutenberg and Richter, 1956] It is based on the maximum Amplitude, which was measured with a Wood-Anderson seismometer. This magnitude is called local magnitude M_L and is defined by

$$M_L = \log A + 2.76 \log \Delta - 2.48 \quad (2.1)$$

where A is the amplitude of the signal and Δ the distance between earthquake and seismometer. This special formula was derived for the special case in California with

a certain seismometer. For other locations other functions or scaling laws have to be applied to take the local setting and measurement device into account. Today there exist a couple of other magnitude scales, anyway the local magnitude is still important because its relation the Wood-Anderson seismometer with a resonance about 1 Hz is close to the resonance frequency of building structure and therefore a good indicator for the related structural damage.

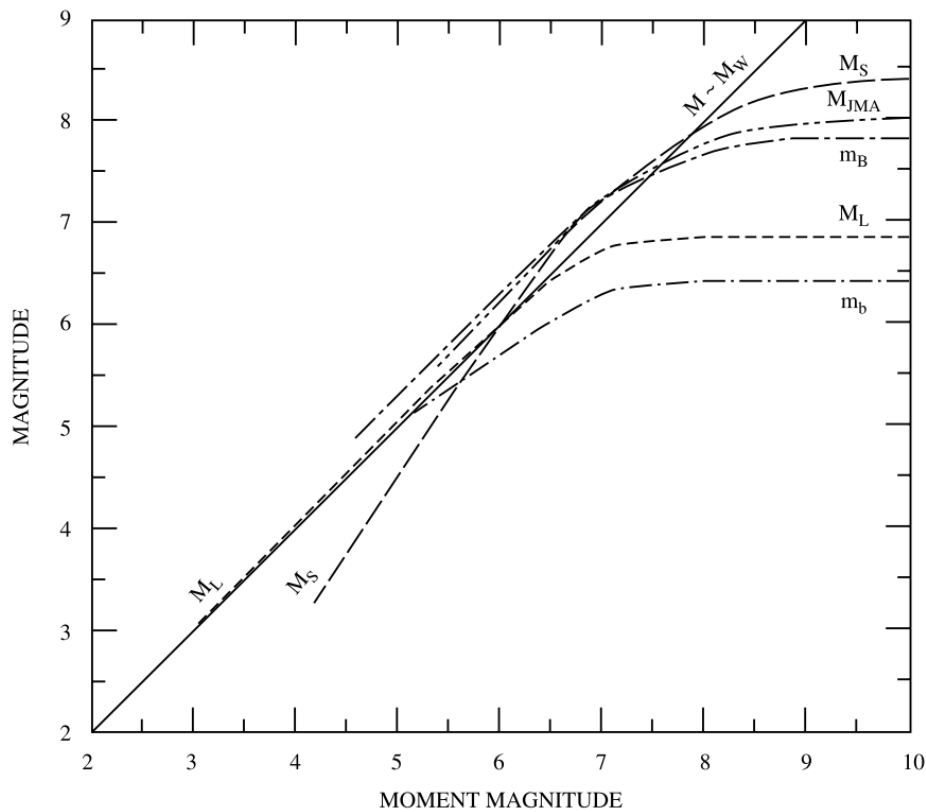


Figure 2.4: Direct comparison of different magnitude scales relative to the moment magnitude. From [Chen and Scawthron, 2003]

Subsequently other magnitude scales were developed for global application, most popular are the surface wave magnitude m_s and the body wave magnitude m_b . The first one measures the obviously the largest amplitude of the measured surface wave while the second one uses the largest amplitude of the body waves. Note that all magnitude have a logarithmic scale that, depending on the additional factor an increase of one magnitude represent an increase by the factor of 10. The largest problem about these magnitudes is related to their saturation, which means that they tend to end in a upper asymptotic boundary, for example it is physically impossible to have $M_L > 8$. Therefore the seismic moment M_0 was introduced as

$$M_0 = \mu A \bar{u} \quad (2.2)$$

Where μ is the material shear modulus, A the area of fault plane rupture and \bar{u} the mean relative displacement between the two fault sides. And in this way a real

physical representation of the earthquake event. Its unit is measured in [dyn-cm] or [Nm]. To transform the seismic moment back to a magnitude scale the moment magnitude M_w was developed, which is in comparison to the local magnitude not bounded. Figure 2.4 shows a comparison of different magnitude scales. These scales have region-specific scaling functions to convert them into each other; this should always be taken into account, because e.g. body wave magnitudes in California might behave not like in Japan.

Quantification of earthquakes is an important step to understand the behavior and scale of such events. Furthermore it was possible to observe statistical relations and pattern related to earthquake occurrence.

Not only is the earthquake occurrence behavior is possible to estimate with statistical methods, a whole branch of research was done to calculate source parameters directly from magnitude scales. [Wells and Coppersmith, 1994] summarized and expanded former results and presents a whole set of transform functions to solve spatial properties of the earthquake rupture like rupture area, rupture width, surface displacement and some more. Most reliable regression functions have been established between rupture length and rupture area and magnitude. The relations are solved depending on the different slip types.

2.2.3 Earthquake Statistics

Earthquake statistics describe general behavior of earthquake occurrence. The most popular and essential element of earthquake statistics was developed and finally published by Gutenberg and Richter in 1956 [Gutenberg and Richter, 1956]. They propose a fundamental relationship between magnitude size and reoccurrence periods. They characterized the term magnitude-frequency with the following generalized Gutenberg-Richter law as

$$\log N(m) = a_N + b_N m \quad (2.3)$$

Where $N(m)$ represents the number of earthquakes equal or larger than magnitude m at a seismic source location per unit time while a_N and b_N are the corresponding parameters. It can be seen as a linear logarithmic regression of a time analysis of all earthquakes in a region. A simple fast-forward evaluation of the parameters can be made with the b -value. It basically describes the ratio of large to small earthquakes. Where large b -values can represent locations with a lot of earthquake swarms and no or rare strong events, while small b -values show the occurrence of more strong earthquakes. The a -value is simply the theoretical intersection between the regression and the zero-magnitude.

This law fits the reality relatively well for a certain intermediate magnitude range. Due to its mathematical nature it does not take physical boundaries into account, which means that the regression of magnitudes continues for large magnitude even if they are physically not possible in that region. Same hold for the lower magnitude scales,

which are limited by the observation. The historical development of magnitude measurements increased its accuracy during the last decades. So there is for example no data of very small earthquake before a certain time when a better measuring device was introduced. Today it is possible to measure even negative magnitude ranges, but for example 50 years ago there was almost no data about magnitudes smaller than 2.5. That's the reason why the completeness magnitude M_C was introduced. It represents the minimum magnitude for which a certain data catalogue of earthquake events contains all events during a certain time window. For example a common value for M_C for the last 30-40 years for Italy is between 3.0 and 4.5.

Another phenomenon, which was statistically observable was firstly mentioned in the late 19th century by [Omori, 1894]. Fusakichi Omori investigated the occurrence of aftershocks after strong earthquakes and proposed a formula, which shows the decrease of aftershock activity over time. This decrease is roughly the reciprocal of the time since the main shock. Omori's formula was later modified by [Utsu, 1961]. This version is today known as the Omori-Utsu formula or the modified Omori law with the following expression. The aftershock rate Λ is represented as

$$\Lambda = \frac{K}{(t+c)^p} \quad (2.4)$$

Where K denotes the aftershock productivity, t is the time since the mainshock, c represents the time delay before the onset of the formula and p is the power-law exponent. The c value can be considered as an artifact which is related to difficulties in detecting earthquakes directly after the mainshock [Shebalin et al., 2011]. The modified Omori law is used widely in the area of time-dependent forecasts and especially short-term models.

2.3 Probabilistic Seismic Hazard Analysis

Probabilistic seismic hazard analysis evaluates the hazard and risk emitted by earthquake events and its following side-effects like tsunamis, landslides, ground shaking and liquefaction. It uses likelihood data for a certain period of interest in a certain region to specify the hazard. Calculation of earthquake likelihood is the major task in generating appropriate hazard maps. A large number of methods was already developed. In the following the basic methodology to calculate seismic hazard is explained with remarks on how some of these methods might differ. One key element to create proper location-specific models is seismic zonation, which shall be explained in more detail. Seismic hazard is often defined as ground motion in terms of the peak ground acceleration or displacement. The displacement and respectively the velocity are often derived from the measured acceleration. Using the peak ground acceleration as a proxy for ground shaking which finally might lead to structural damage.

2.3.1 Probabilistic Seismic Hazard Methodology

Following the description of probabilistic seismic hazard analysis of [Chen and Scawthron, 2003] one can summarize it by the following theorem:

$$\lambda[X \geq x] \approx \sum_{Sources\ i} v_i \int_{M_0}^{M_{max}} \int_{R|M} P[X \geq x|M, R] f_M(m) f_{R|M}(r|m) dr dm \quad (2.5)$$

$\lambda[X \geq x]$ is the annual rate for ground motion which exceeds a certain threshold, while v_i is the annual occurrence rate of the seismic source i , which has a magnitude range between M_0 and M_{max} . $P[X \geq x|M, R]$ gives the probability of to exceed a certain threshold of ground motion with a given magnitude and distance. $f_M(m) f_{R|M}(r|m)$ are two probability density functions which cover the magnitude range and the distance effects between the location and the seismic source. Finally to compute the seismic hazard of a location, the participation in seismic hazard from each seismic source within a certain spatio-temporal computation range is used.

For engineering applications a return period of 10% in a 50 year period is of interest. Therefore a return period of 475 years can be computed [Chen and Scawthorn, 2003]. This is for example also applied in the German industry norm for earthquake engineering DIN4149.

The classic procedure to calculate seismic hazard starts by identifying the seismic source and its geometry, therefore spatial probability density functions are calculated, which are time-independent. The definitions of time-independent and time-dependent methods are given in chapter 2.3.2. It continues further with the calculation of a hazard spectrum, but this shall not be covered here. The main focus is in the calculation of probability density functions and forecasting of earthquakes. This area still lacks in accuracy especially due to forecasting which is still extremely hard and almost impossible. Anyway there are a lot of different approaches to calculate density functions and of course the related forecasting of earthquakes, whose types will be presented in the chapter 3.

Another approach relative to the probability density distribution is to calculate an alarm. Alarm-based methods in general search for certain patterns which precede large earthquakes. If such a pattern was identified, an alarm is spoken, covering a certain period in time and a certain region. If an earthquake occurred within the magnitude-range of the alarm, it is conserved as a successful prediction. If no event happens during the alarm period it is a false alarm. A wrong prediction occurs if an event happens, but outside the forecast region. A good example is the RTP-method [Shebalin et al., 2006], which is introduced in chapter 3.5.3.

2.3.2 Seismic Forecasting

In the last few decades a large number of different forecasting methods have been developed, containing models to calculate probability density maps for seismic hazard assessment or even alarm-based models which should predict earthquakes

on a relatively short timescale. Especially the second approach was not able to give accurate results. This is basically related to the dimension in which earthquake forecasting is possible. Table 2.1 gives an overview of the spatial and temporal dimensions in which earthquake forecasting might get applied to.

After the temporal and spatial setting is determined the basic type of each model has to be identified. There are two substantial kinds of models, the time-independent and the time-dependent approaches. The first one assumes that there is no variation in time due to earthquake occurrence frequencies. Most of them assume an independent Poisson process. This branch of forecasting methods is often directly derived from event catalogues. Depending on the model it finally leads to a general hazard map for each examined location based on the total seismic activities during the modeling period. The second approach takes seismic occurrence patterns into account, which means it assumes that the probability decreases directly after the event and starts to increase with time afterwards. Identifying seismic periods can help to assume of a future event is likely to occur or not based on the recent history. Other approaches might apply the Omori-Utsu formula (see chapter 2.2.3) to detect aftershock activity after large events or investigating earthquake time series for certain patterns to identify precursors of future large events.

Temporal dimension in years		Spatial dimension in km	
Long-term	10	Long-range	Up to 100
Intermediate-term	1	Middle-range	5 – 10
Short-term	0.01 – 0.1	Narrow	2 – 3
Immediate	0.001	Exact	1

Table 2.1: Overview of temporal and spatial dimensions due to earthquake forecasting.

Another important factor in seismic forecasting is related to smoothing. One basic assumption, common in most of the methods, is that future earthquake will happen in regions with former seismic activity. However seismic activity is often biased and variable in its exact location. Thus, this is the reason why spatial smoothing is applied to most of the models to take spatial variation into account.

There are multiple other approaches to identify locations of future earthquakes e.g. by seismic triggering, or incorporating focal mechanisms or geodetic data. The necessary mathematical explanations for certain time-independent and time-dependent approaches are explained in detail in chapter 4. Furthermore a short overview of hybrid methods is added to investigate the range of advanced modeling and data sources which could contribute for better forecasts.

2.3.3 Seismic Zonation

Dividing a region of interest in different zones is often of important interest by modeling a seismic hazard map. Some modeling parameters might be changing due

to spatial variations in seismic activity. A good solution is to determine different regions with common seismic behavior, e.g. by separating certain faults or by identifying the causes for seismic activity and distribute zones for each individual seismic source area, this is also known as identifying asperities.

A typical parameter for which seismic zonation is applied is the b -value and the maximum possible magnitude, which is restricted by physical boundaries like the fault length. Depending on the choice of seismic source zones a model can generate extremely different results especially with respect to a uniform model without zonation. Figure 2.5 shows an example for such a seismic zonation for Italy from [Burkhard and Grünthal, 2009]. With the knowledge of local geography and the tectonic setting it is simple to reconstruct the ideas behind such a specific zonation. Dividing the Apennine into different zones to account for the varying activity along this seismically active fault zone and for example using a zone to area of Vesuvius and the Campi Flegrei to cover the volcano-related seismicity.

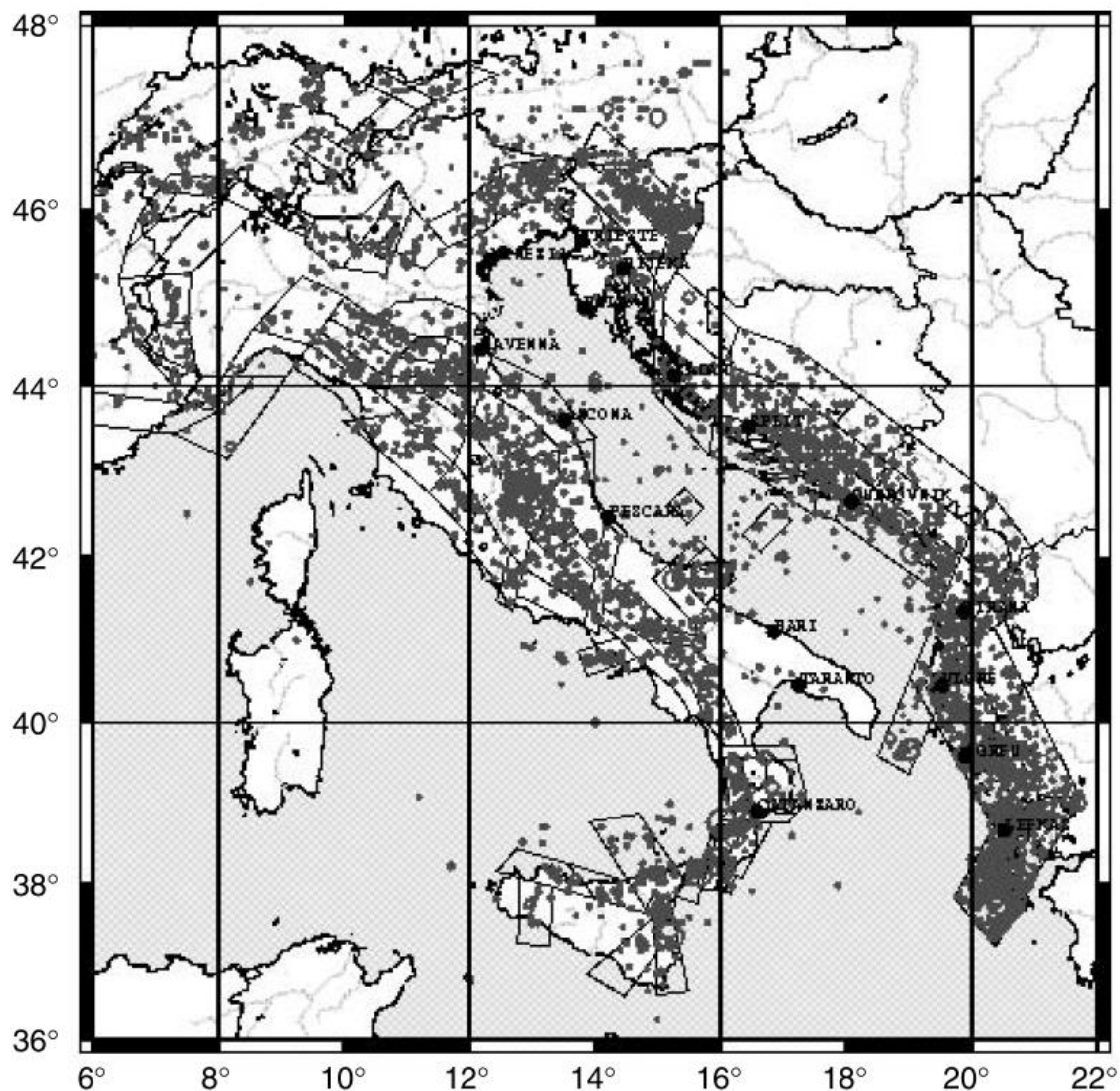


Figure 2.5: Sample map for seismic zonation for Italy with indicated earthquake distribution, after [Burkhard and Grünthal, 2009].

3 Review

This chapter is about collecting and reviewing existing methods for earthquake forecasting and earthquake probability analysis. The research to review these methods is based on presenting latest publications for certain forecasting approaches and evaluating them with a set of survey parameters to distinguish the quality of description. A large number of methods are directly related to recent projects in forecasting like the Collaboratoy of Seismic Earthquake Prediction (CSEP), if that's the case additional information due to the testing procedure and the results of the method are noted. Finally a simple method catalogue is developed to summarize all reviewed and published methods. So this chapter gives an overview of state-of-the-art in earthquake forecasting approaches.

3.1 Overview of Methods

Methods to give a forecast on future earthquake occurrence or for direct earthquake prediction have been developed during the last decades with different basic assumptions. From these assumptions it is possible to derive three different groups of methods:

1. Time-independent methods
2. Time-dependent methods
3. Hybrid methods

The first group is called time-independent, assuming that future earthquake occur in regions with seismic activity during the past. These models apply the statistics of an observed time history of earthquake events to develop a forecast model or map. The second category assumes variations in earthquake occurrence by taking phenomena, e.g. like earthquake frequency patterns or earthquake clustering, into account. The third category, Hybrid methods, applies physical aspects like the rate-and-state friction law or tectonic observations and uses in general additional data sources like focal mechanisms or geodetic data or just combines elements of basic time-independent and time-dependent approaches.

Static triggering is not a real method category than rather a method itself. Static triggering emphasizes a redistribution of static stress after earthquakes which might trigger subsequent events and aftershocks and furthermore might suppress future seismicity depending on the so-called Coulomb stress transfer. Some methods implement static triggering aspects, but instead of presenting one approach, static triggering is generally explained in chapter 3.7.

In the following we will at first introduce a couple of national and international projects during which forecasting methods have been developed and tested. The survey parameters by which the following review is accomplished will be introduced as well as the main foci of evaluation. The method review is based on one of the most recent publications for each method respectively, there are often a lot more papers and research letters covering a certain approach but for the sake of simplification this review will cover the latest developments and applications of the methods.

Afterwards the methods themselves are introduced categorized by in the order described above. The static triggering model is described in more detail. Finally a catalogue is presented, which will summarize the results of this review and give additional information like details to the used algorithm. It should be noted that this chapter evaluates the methods from a theoretical point of view. It does not test the models. It will at least add remarks about results from related projects. Chapter 4 will be focused on the reconstruction of key features of the methods stated in the following while the final testing is shown in the chapter 5.

3.2 Related Projects

Two large projects have been assessed to evaluate methods and models for earthquake predictability and forecasting. The first project is set up by the Regional Earthquake Likelihood Models (RELM) [Zecher et al., 2013] working group for California and adjacent regions. The second project was developed from the first one as a global testing center for earthquake forecasting approaches and is known as the global Collaboratory for the Study of Earthquake Predictability (CSEP) [Werner et al., 2010].

RELM was designed to evaluate and test different forecasting methods under predefined conditions. One of these testing ranges emphasized a 5-year experiment to forecast the number, spatial distribution and magnitude distribution of subsequent target earthquakes.

Both projects defined discretely the spatial location where the methods are applied. In addition the CSEP project predefined the datasets which can be used. Method developers are free to choose which of the proposed datasets they want to implement into their forecast and also the timespan of the dataset. The final forecast which each method shall provide is defined over a certain period, commonly a period of 3-months, 5-years and 10-years. The forecasts are tested within a common testing range, which is based on the likelihood principle. The likelihood is tested versus real occurring earthquakes during the testing period in terms of the total number of events, the magnitude range of the forecasted events, the spatial distribution and other parameters.

Some methods are applied during both projects and/or multiple times for different regions in the CSEP project. If one of the following methods was tested during the stated projects, the project results will be taken into account for the evaluation.

3.3 Survey Parameters

The following review will use a couple of simple parameters for a fast a priori comparison of the different methods. At first the main reference is stated which was used to introduce the method. Furthermore the source of the related project is shown, if it is from the CSEP or the RELM project. An important factor is the region where the method was tested, here not only the region of the stated reference is included, additional regions related to other publications which applied the method are stated and listed in the catalogue in appendix A. Furthermore if the method uses a declustered dataset or not is noted, how declustering might influence results and how it is performed will be explained in chapter 4.1.1. Declustering is more important for time-independent models. In the list of time-dependent methods this point will be replaced with a note whether the method is an alarm-based indicator or an epidemic-type method.

There will be no prior judgment of accuracy and/or quality of the method, except for the results given by CSEP/RELM-tested methods or if there was a general likelihood test already included. The testing range of CSEP and RELM is partially presented in chapter five and will be partially applied again during this study.

A general survey element is to find out how the forecasting itself works in each method, and especially for the first two types, if smoothing is applied, how does it work, what kind of smoothing kernel is used. For the time-dependent methods it is additionally important how the time-dependent aspect of the algorithm works, if it is a pattern algorithm or does it use epidemics, etc. The last types of hybrid methods and every other kind of method will be evaluated the same way accordingly to their core algorithm.

3.4 Time-independent Methods

3.4.1 Relative Intensity (RI)

Reference:

[Nanjo, 2010]

Description:

The RI algorithm uses the fundamental assumption that future events are more likely to occur in areas with higher seismic activity during the past. The algorithm presented here is progressed development of a former alarm-based version of this method, advanced to become a smoothed seismicity model, which uses a simple counting system to calculate the number of future earthquake in a certain region for specified magnitude bins. The smoothing algorithm is based on a simple stencil smoothing by using the Moore neighborhood of each grid cell.

The method was applied during the CSEP project and used for regions in Italy and Japan. Current results for the Italy analysis showed that the RI-algorithm underestimates the number of future events while spatial and likelihood testing of the model lead to relatively well results.

Project	Complexity	Region	Declustering
CSEP	Simple – Medium	Italy Japan	no

3.4.2 Earthquake Prediction in California (EPiC)

Reference:

[Suen et al., 2010]

Description:

This method was developed by Stanford students in the area of computer learning algorithms. This is no “professional” method, but still useful due to its attempts in smoothing and earthquake density maps. It uses a simple Poisson model for spatial smoothing. Furthermore a Fourier analysis was applied to find periodic patterns in time.

Finally one can derive a general form of earthquake densities from these calculations. Due to the method overview there is only the Poisson model presented.

Project	Complexity	Region	Declustering
None	Simple	California	no

3.4.3 Asperity Likelihood Model (ALM)

Reference:

[Gulia et al., 2010]

Description:

The ALM assumes that small variations in the b-value influence the forecasting of future seismicity significantly. This method was applied during the CSEP project for Italy and the RELM project for California. The core of this algorithm calculates local and regional b-values and the corresponding a-values. Applying the Gutenberg-Richter relation with these values leads to a time-independent forecast. Two different approaches were applied, while the first one uses the assumption of a global b-value as a proxy, the second one uses a seismic zonation with a set of b-values depending on the local focal mechanism. This relation between b-value and focal mechanism proved for multiple regions around the world.

Due to the tests of the CSEP method, the ALM results lacked in general likelihood, especially in spatial variations. The second approach additionally underestimated the total number of events during the testing period. Due to the tests of the RELM project ALM lacks only in the spatial likelihood and works well for the general likelihood of forecast.

Project	Complexity	Region	Declustering
CSEP	Medium	Italy	no
RELM		California	

3.4.4 HAZGRIDX

Reference:

[Akinci, 2010]

Description:

HAZGRIDX was developed for the CSEP project in Italy based on a seismic smoothing approach. It uses a two-dimensional Gaussian function to smooth declustered earthquake data. Due to smoothing a 15-km correlation distance was applied based on assumptions on the regional fault geometry. In addition a constant b-value was assumed for the testing area. A large dataset of more than 2000 years was applied using time completeness intervals for different Italian territories. During the testing process of the CSEP project the HAZGRIDX method underestimated the total number of events during the testing period, but behaved well for spatial and temporal likelihood. The bad results of the event number might be related to the conversion of M_w to M_L .

Project	Complexity	Region	Declustering
CSEP	Simple – Medium	Italy	yes

3.4.5 Adaptively Smoothed Seismicity (ASS)

Reference:

[Werner et al., 2010b]

Description:

The ASS method is a complex smoothing method, which applies an isotropic adaptive kernel to the earthquake distribution of a declustered event catalogue. The fact that the event catalogue is declustered is an essential assumption. Its first application was during the RELM project for California and it got further used during the CSEP project in Italy. During the first testing in California further adjustments lead to the continuous application of an adaptive power-law kernel instead of a Gaussian kernel. Additional adjustable parameters are related to the overall smoothing intensity depending on the used dataset and its event density.

The results of the RELM showed that the ASS method has been the most accurate under all tested methods. Due to the CSEP project, the ASS method was again under the most accurate ones, but lacked slightly in the spatial locations of the forecast. The model seems to be not smooth enough and underestimates quiet regions which might become active in the future.

Project	Complexity	Region	Declustering
CSEP	Medium	Italy	yes
RELM		California	

3.4.6 PEGASOS EG1b approach

Reference:

[Burkhard and Grünthal, 2009]

Description:

This approach is not a method in a classical sense. It was part of a larger project called PEGASOS which was addicted to the seismic hazard assessment of four nuclear power plants in Switzerland. The results of PEGASOS EG1b consist of an in-depth analysis of seismic zonation within the study region. It evaluated seismic recurrence for each zone by calculating recurrence parameters of a tapered Gutenberg-Richter relationship based on a declustered earthquake catalogue between 1946 and 2000.

The final results are a set of b-values, which have been computed together with a distribution of possible maximum magnitudes for each seismic source zone.

Project	Complexity	Region	Declustering
none	simple	Europe	yes

3.4.7 Simple Smoothed Seismicity (Triple-S)

Reference:

[Zechar and Jordan, 2010]

Description:

The Triple-S method is a simple approach to generate time-independent forecasts, which assumes that increasing the accuracy of the parameters of simple methods is sufficient to increase the general forecast accuracy instead of increase the method complexity. In this sense, the Triple-S only consists of an appropriate smoothing algorithm, which takes special care of the near field of smoothing when counting the number of events within each spatial bin. In advance, it uses the area skill score testing procedure to find the most accurate smoothing lengthscale. The normalized smoothed seismicity is finally applied to an untapered Gutenberg-Richter relation to generate the final forecast.

Due to the results of the CSEP testing center, the Triple-S method behaved well in general, but tends to underestimate the total number of forecasted events.

Project	Complexity	Region	Declustering
CSEP	Simple – Medium	Italy	no

3.5 Time-dependent Methods

3.5.1 Pattern Information (PI)

Reference:

[Holiday et al., 2007]

Description:

The Pattern Informatics method analyzes changes in seismicity rates. These rates are computed for seismic active areas. If a certain threshold in seismic activity is reached the occurrence of a future event is assumed within the testing period. For identifying the seismic active zones a map based on the relative intensity approach is used. The seismic event catalogue is afterwards divided into multiple periods for which the rates are computed. This leads to so called pixel probabilities for which a Gutenberg-Richter relation is applied to finally end up with a forecasting map.

During the RELM project the PI method generated relatively good results except for the spatial likelihood. Anyway the PI method received the second best score in the testing range.

Project	Complexity	Region	Type
CSEP RELM	Medium	California	Indicator

3.5.2 Reverse Tracing of Precursors (RTP)

Reference:

[Shebalin et al., 2006]

Description:

The RTP method uses short-term spatial and temporal patterns as precursors for short-term earthquake prediction. It searches for these patterns, called precursory chains, to identify future locations of target earthquakes. In this sense, it is a highly time-dependent method using multiple pattern functions and threshold values to identify regions of future seismicity. It was successfully applied during a first testing range in Japan, California, Italy and the Eastern Mediterranean.

After multiple evaluations of different testing ranges with the RTP method, it has been proven that it does not work as well as supposed. The success rate of the forecast is around 25%, containing missed events and failed predictions.

Please note that some failed predictions were only about a couple of kilometers, because the target earthquakes were slightly outside the predicted regions.

Project	Complexity	Region	Type
none	Medium – Complex	Italy Japan California, etc.	Alarm-based

3.5.3 Epidemic-type Aftershock Sequence (ETAS)

Reference:

[Lombardi and Marzocchi, 2010]

Description:

The epidemic-type aftershock sequence (ETAS) model is a time-dependent short-term forecasting model, which uses just observed earthquake data. The 'epidemic' type indicates that each earthquake is a potential triggering event for subsequent events. It combines a calculated background seismicity rate with the magnitude-dependent ability of each aftershock to perturb the rate of earthquake production. The model itself consists of multiple stochastic elements from Omori's law of aftershock occurrence to Gutenberg-Richter relations.

The ETAS formula can be decomposed into the background seismicity rate and the aftershock related activity, which is again decomposed in normal distributions for time and space and the general magnitude-depending ability to produce a certain number of aftershocks. The parameters have to be fitted for each application area by a log-likelihood approach.

The ETAS model can be advanced by adding an ETAS-derived declustering procedure as an additional branching process. The final rate of occurrences is a

superposition of both steps, this approach is called “The Double Branching Model”. There exist several version of ETAS models, like the ERS or the EEPAS methods.

Project	Complexity	Region	Type
CSEP	Complex	Italy Japan	Epidemic

3.5.4 Every Earthquake a Precursor According to Scale (EEPAS)

Reference:

[Rhoades, 2007]

Description:

The EEPAS model is a long-range forecasting method that uses precursory minor earthquakes to forecast the major ones. It uses preliminary information about precursory relations of precursor magnitude to mainshock magnitude, time scale and space occupied by all precursory earthquakes, mainshocks and aftershocks.

The procedure and appearance of it is similar to the ETAS model but uses instead of likelihood estimates the above mentioned preliminary examined relations. The model results depend on the quality of the preliminary investigations and the target magnitude scales for which the precursor events shall be used.

Project	Complexity	Region	Type
RELM CSEP	Complex	California Japan	Epidemic

3.5.5 Epidemic Rate-Strain (ERS)

Reference:

[Console et al., 2007]

Description:

The Epidemic-Rate-Strain (ERS) Model is a close to real-time forecasting model, which is basically related to the ETAS model. Instead of purely stochastic parameters, the ERS incorporates the concept of the rate-and-state friction theory with two free parameters, which additionally increases the computation speed, because standard ETAS models need at least 4-5 free parameters (often more). It simplifies the purely stochastic model by using a empirically generated stress change parameters.

The parameters are estimated based on the log-Likelihood principle. Within a direct comparison to a purely stochastic ETAS model the ERS did not lead to better results. This seems to be related to the more rigid behavior of the algorithm.

Project	Complexity	Region	Type
RELM	Medium – Complex	California	Epidemic

3.5.6 Short-term Aftershock Probabilities (StAP)

Reference:

[Gerstenberger et al., 2004]

Description:

The model of short-term aftershock probabilities was developed to calculate subsequent events after strong mainshocks for the following days. It combines basic occurrence laws like the Gutenberg-Richter relation and the modified Omori-law to define a time-dependent earthquake probability by taking combined aftershock sequences into account. A special focus is set to the spatial distribution which is calculated based on a leveled smoothing algorithm which uses rupture length and aftershock distribution. The method was running for several years to estimate earthquake probabilities after large events in California. Please note that this method does not generate long-term forecasting maps, it is totally focused on aftershock probabilities.

Project	Complexity	Region	Type
None	Complex	California	Epidemic

3.5.7 Early Aftershock Statistics (EAST)

Reference:

[Shebalin et al., 2011]

Description:

The EAST method is a short-term prediction method, designed to detect locations which are more prone to moderate or large earthquakes within an active fault zone. Its main hypothesis assumes that the time delay before the onset of the aftershock decay is anticorrelated with the level of stress in the seismogenic crust. It uses the mean of elapsed time between long-term aftershocks and short-term aftershocks to the mainshock. Calculating their relation, after reaching a certain threshold of the number of aftershocks in each time bin, generates a short term alarm value. The size of the relation between the mean elapsed times denotes which places are more vulnerable to subsequent target events during the next time step. Based on first case studies of Californian earthquakes the method showed promising results.

Project	Complexity	Region	Feature
None	Medium	California	Virtual Fault Map Paleoseismic Data

3.6 Hybrid Methods

3.6.1 Fault Slip and Smoothed Seismicity (FSSS)

Reference:

[Hiemer et al., 2011]

Description:

The FSSS model is a stochastic earthquake source model for intermediate and long-term forecasts. It consists of two types pairs of finally combined density maps. Each pair consists of two types of maps. The first type is a classical smoothed probability density map while the second one is a map of smoothed focal mechanisms. The first pair is made of the data of the historic earthquake catalogue which therefore must also contain information about the focal mechanisms. The second map is constructed by a transformation of the 3D-geometry of a recent fault map to some kind of density map. Via merging both maps with a magnitude-dependent weighting procedure and a tapered Gutenberg-Richter model, future areas of earthquakes are determined

Project	Complexity	Region	Feature
none	Medium – Complex	California	Faultmap Focal Mechanisms

3.6.2 Hybrid Seismicity Method (HSM)

Reference:

[Chan et al., 2010]

Description:

The Hybrid Seismicity Method combines a classic time-independent smoothing algorithm based on a power-law kernel with a time-dependent rate-and-state friction model, which applies Coulomb stress changes. It was used for the CSEP project in Italy. The dataset was both tested for the clustered and declustered case, which resulted in better approximations with declustered datasets. In addition, the application of the rate-and-state friction model lead only to a marginal improvement, just about less than 10%. It was assumed that the improvement should behave better, the authors suggest to use more detailed information for the source fault model, because for this method just estimated scaling laws have been applied to retrieve fault parameters better data and scaling laws might lead to better results. Due to the results of the CSEP project, the HSM overestimated the total number of events during the testing period, but passed most of the applied tests and due to magnitude likelihood adequately forecasted the observed $M_L \geq 7$ events.

Project	Complexity	Region	Feature
CSEP	Medium – Complex	Italy	Coulomb Stress Change

3.6.3 Long-term Stress Transfer (LtST)

Reference:

[Falcone et al., 2010]

Description:

The LTST algorithm is based on the fusion of a statistical renewal model with a physical model. It considers fault interactions, which might increase or decrease future seismicity. The fault interactions are computed based on the co-seismic static permanent Coulomb stress change caused by all earthquakes since the last characteristic event on a certain fault segment.

This model can be used for long-term forecasting intervals by using two parameters, the average interevent time and the aperiodicity. To apply the method additional data, like the focal mechanisms, is necessary to cover the stress changes. Furthermore, the fault parameters of strike, dip, rake, dimensions and average slip are needed to perform computation.

Project	Complexity	Region	Feature
CSEP	Medium – Complex	Italy	Coulomb Stress Change Interevent times

3.6.4 Seismic Hazard Inferred from Tectonics (SHIFT)

Reference:

[Bird and Liu, 2007]

Description:

The SHIFT model for estimating long-term average seismicity of a certain region uses a local kinematic model of surface velocities and an existing global calibration of plate-boundary seismicity. This global calibration is based on former publications of Peter Bird. It uses an approximation of the long-term average seismic moment rate and applies it to a tapered Gutenberg-Richter model.

Due to the testing in the RELM project, the SHIFT model overestimated the number of events, which was related to the overall rates, which were much too high.

Project	Complexity	Region	Feature
RELM	Complex	California	Geodetic Data Geologic Data Stress directions

3.6.5 Fault-oriented Earthquake Forecast (FoEF)

Reference:

[Van Aalsburg et al., 2007]

Description:

FoEF uses topologically realistic numerical simulations for the strike-slip fault system in California to identify future rupture elements of the fault system. The Virtual California fault model was used to apply friction laws and other physical parameters. By tuning the model a stochastic set of earthquake series is calculated and compared to paleoseismic observations. To identify modeled time series which seem to reproduce historic data most accurately a time series score is applied. The models with the highest score are used to generate probability density function spatially distributed for each fault element, stating probabilities for participation in future large earthquake events.

Project	Complexity	Region	Feature
None	Medium – Complex	California	Virtual Fault Map Paleoseismic Data

3.7 Static triggering

3.7.1 Overview

An alternative approach, relative to the rather statistical methods shown above, is the investigation due to *Coulomb stress changes* or so-called static triggering. The simple idea behind static triggering takes the redistribution of stress in the earth's crust after a strong earthquake event as a trigger, which might lead to subsequent events in areas with increased stress, while areas with decreased stress should have less seismicity with respect to the increased areas. The zones with decreased seismicity after a large shock is also called *stress shadow*. A very good overview of the static triggering approach is given by [King et al., 1994]

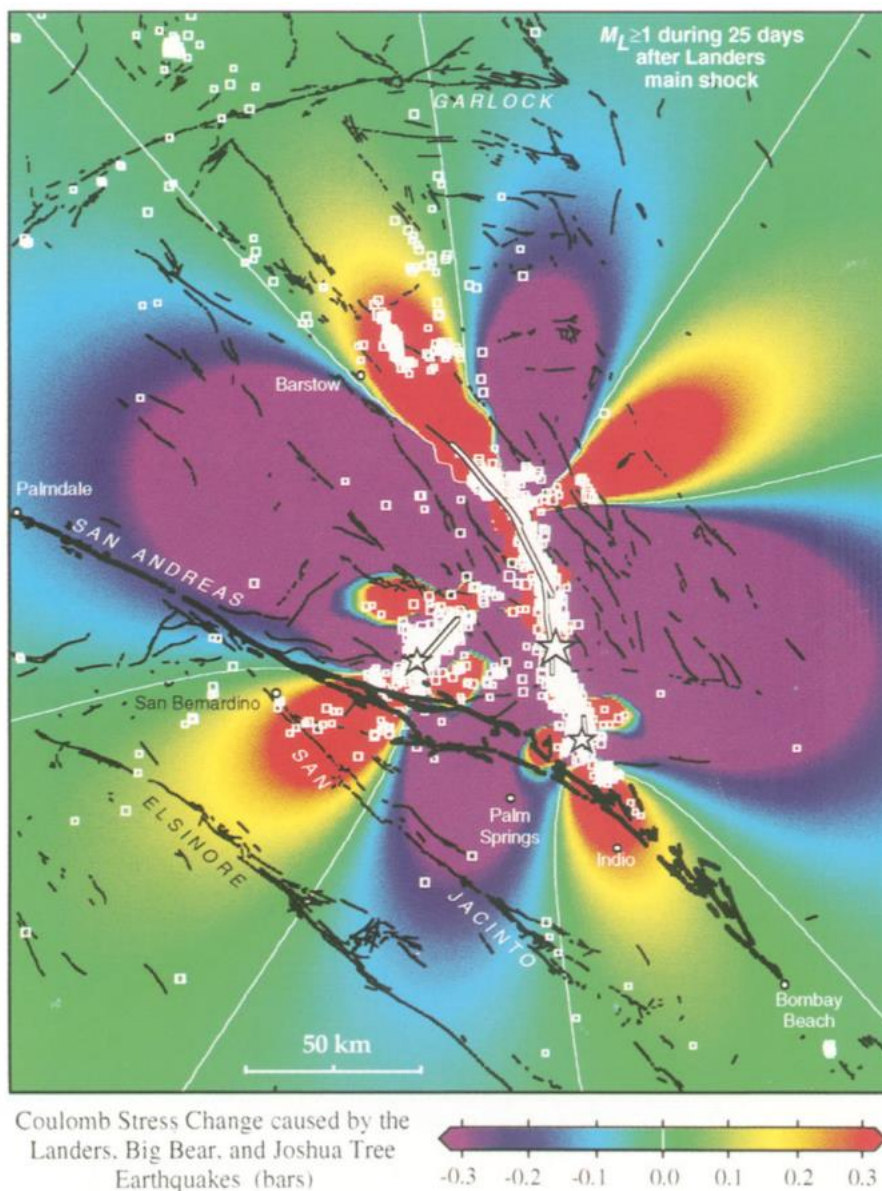


Figure 3.1: Coulomb stress changes after the 1992 earthquake sequence (Joshua Tree, Landers, Big Bear) in California. From [King et al., 1994]

A famous example well examined during the last two decades is the earthquake sequence, starting with the $M_W = 6.1$ Joshua Tree earthquake in April 1992 in California. Two month later the in June 1992 the Landers earthquake happened with a magnitude of $M_W = 7.3$, followed about 3.5 hours later by the Big Bear earthquake with $M_W = 6.3$ (see figure 3.1). The sequence finally seemed to end seven years later with the October 1999 $M_W = 7.1$ Hector Mine earthquake. This sequence shows the time scale of triggered earthquake sequences very well. Stress changes can immediately lead to subsequent events within hours, while it seems to be more common that the time scale is between months and a few years. Another example, from Japan, assumes that the 1995 $M_W = 6.9$ Kobe earthquake was triggered about 50 years earlier by the 1944 $M_W = 8.0$ Tonankai and the 1946 $M_W = 8.2$ Nankaido earthquakes.

Earthquake triggering does not only differ in the time scale, it also differs in the spatial scale. While the described earthquake sequence above is a rather regional phenomenon, it is also assumed that for example the 2002 $M_W = 7.9$ Denali earthquake in Alaska triggered seismicity in the Coso geothermal field in California, more than 3600 km away.

The basic idea behind the regional and the long-distance scales is related to the differences between static and dynamic triggering. While static triggering is related to elastic stress changes in the narrow field, the long distance triggering seems to be induced by the passage of dynamic seismic waves, which might be able to trigger events as well.

3.7.2 Theory

The basic theory about earthquake triggering in this topic is related to Coulomb stress changes. An earthquake occurs when the shear stress exceeds the combination of normal stress and friction. The shear stress works to rupture the fault and is generated by the relative movement of the plates. The balance until the fault ruptures is characterized by the Coulomb failure criterion for which a critical state of stress is defined by σ_c and is given by

$$\sigma_c = \tau - \mu(\sigma_n - p) \quad (3.1)$$

Where τ represents the shear stress parallel to the slip direction and σ_n the normal stress. The pore fluid pressure is introduced as p and μ is the coefficient of friction. Effectively speaking to bring a fault closer to failure the effective normal stress ($\sigma_n - p$) must be decreased and/or the shear stress increased. This theoretical perspective was developed in the laboratory during tests on rock units. Typically it is almost impossible or very hard to directly measure stress in the field, but it is possible to estimate it. Thus, it is finally possible to calculate the normal and shear stresses on

faults from such estimates. Similarly the absolute value of stress is unknown, so it is more common to calculate the change in Coulomb stress. With respect to (3.1) this leads to the following expression

$$\Delta\sigma_c = \Delta\tau - \mu(\Delta\sigma_n - \Delta p) \quad (3.2)$$

The calculation of stress changes leads to the information whether a fault brought closer to rupture or not, (positive or negative stress changes). Changes in pore fluid pressure are often assumed to be proportional to normal stress. Taking the Skempton coefficient B into account, which is the relation between pore pressure and normal stress, it is possible to use the effective friction coefficient μ' . [7]

$$\mu' = \mu(1 - B) \quad (3.3)$$

The Skempton coefficient is typically between 0.5 and 0.9 while the effective friction coefficient is between 0.0 and 0.75. The average assumption is $\mu' = 0.4$. Thus, finally the coseismic stress change takes the form

$$\Delta\sigma_c = \Delta\tau - \mu'\Delta\sigma_n \quad (3.4)$$

This basic formulation can be computed e.g. by using a discrete boundary method algorithm and a given geometry to calculate spatial variations of the stress field. Normal and shear stresses are calculated separately, the superposition then finally leads to the stress change, for which a positive stress change leads to an increase in seismicity and negative stress change leads to a decrease in seismic activity. Such an increase in seismicity implies that the fault with positive stress change is brought closer to rupture and vice versa. This approach is not able to explain the time-dependence of the triggered events, but can indicate areas with larger probability for subsequent events. This increased probability is not restricted to fault areas, it can also increase the probability of earthquakes in areas apart from faults. The best correlation of Coulomb stress change to aftershock distribution was observed a few kilometers away from the fault of the initial mainshock. Far away from the fault the stress distribution is not well known and other events might influence as well, similarly it is for the near-field, where unknown fault geometry makes it impossible to model accurate solutions.

From multiple studies it is assumed that an increase or decrease in stress in the scale of about 0.1 to 0.3 MPa is sufficient to trigger or suppress subsequent events effectively.

3.8 Catalogue Development

3.8.1 Catalogue content

To summarize the findings of this review chapter a catalogue was developed, which covers all aspects of the review above. It contains all method described above with additional details especially about the algorithm itself

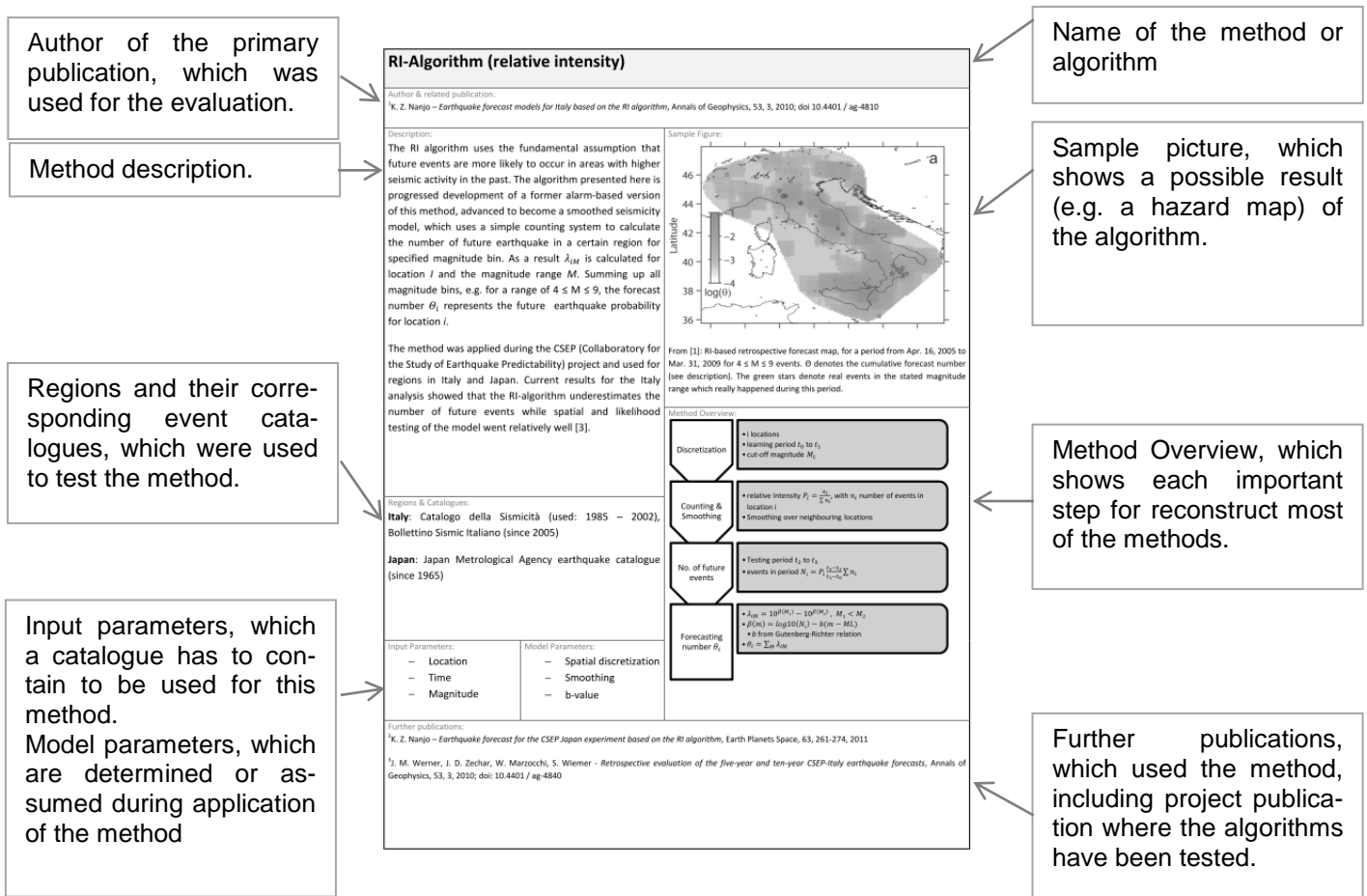


Figure 3.2: Overview of a sample entry of the method catalogue, with descriptions for each catalogue parameter

The catalogue gives a fast overview of current methods for earthquake probability analysis and forecasting. The related publications are cited as well as further information of projects within the model has been tested.

In addition to the above stated survey parameters a general method overview has been created. For most of the methods a direct reconstruction based on this short overview is possible, this overview introduces the major steps of the forecasting algorithm and for certain cases relevant model parameters as well. However some methods are way too complex to summarize their algorithms within a short overview. In such a case the overview just contains the most important calculation steps of the algorithm. The catalogue can be found in Appendix A.

4 Reconstruction

This chapter is focused on the reconstruction of key features which have been used in the methods, introduced in chapter 3. The goal is to build accurate methods to apply them in a testing range for chapter 5. No method is of course exactly rebuilt. In the following the main elements of time-independent methods will be explained and different approaches are introduced. A special focus is here in the area of spatial smoothing and Gutenberg-Richter handling. In addition a short introduction into seismic declustering is given.

Due to time-independent modeling a set of code blocks will be developed with which one can easily assemble a whole model. Furthermore two versions of time-dependent modeling are explained in detail and adopted. One for pattern search, the Pattern Informatics Method and one simplified version of the epidemic type methods. At third one, developed by the author is introduced as well which is based on time variations of the Gutenberg-Richter parameters.

In general, the models which are introduced in the following follow two simple rules:

1. Simplification: The model should only use historical earthquake data (location, time, magnitude). The reason is simple; historical earthquake data is available almost worldwide and for relatively long time periods (up to 2000 years).
2. Speed: The models should be fast, therefore no long and time-intensive iterations or finite element approaches are used. The models developed here are simply enough to be calculated on a standard home computer. All algorithms and programming codes are built in Matlab©.

4.1 Time-independent Method Toolbox

In chapter 3, multiple time-independent methods have been introduced. In general a time-independent model uses a set of basic assumptions. At first it assumes that future earthquakes are likely to occur where earthquakes happened in the past. Secondly, seismic rates do not change over time. Moreover earthquakes do not interact with each other.

A time-independent method in general consists of three steps. The first one is related to the dataset. Data management is the most basic and most essential part in the model development. A model can only work as good as the quality of the dataset allows it to be. In that way, one must consider both seismic clustering and magnitude completeness. Completeness was already explained in chapter 2.2.3, seismic clustering will be explained in chapter 4.1.1 due to what it exactly means, its implications for modeling results and of course how to overcome such effects. The second step is related to spatial smoothing and how the event database is distributed

over the region. The third and final step is focused on the Gutenberg-Richter handling and how the final probability of the forecast is calculated. The Gutenberg-Richter Handling and the spatial smoothing will be explained in detail during the following chapters.

In general the forecast is connected to a Poisson process, because earthquakes are assumed to be homogeneous in time. The Poisson process assumes generally that the process is stationary and follows simplicity and that the earthquakes are independent from each other. Stationary indicates that the probabilistic distribution only depends on the interval length of the forecast. Independence is meant that the number of events occurring in two disjoint time intervals is independent from each other and the simplicity just assumes that two events never occur simultaneously.

$$\Pr\{N(N(t, t + \Delta t) = n\} = \frac{\lambda^n \Delta t^n}{n!} e^{-\lambda \Delta t} \quad (4.1)$$

Formula (4.1) shows the general Poisson probability, that the number of events N during the time step Δt is exactly n , where λ is the average rate per time. For the application in a time-independent model, this relation can be transformed into the probability that time until the next event is smaller than the time step.

$$\Pr\{\tau < t\} = 1 - e^{-\lambda t} \quad (4.2)$$

It should be stated, that the Poisson process is far away from any physical observation. The reality is neither stationary nor independent or simple. However the Poisson process is currently the closest process for modeling time-independent earthquake occurrence. For further details of temporal processes, see [Zhuang et al. 2012].

4.1.1 Declustering

Earthquake occurrence can be differentiated between two kinds of earthquakes. The first group is called independent events or background seismicity, whose offspring is related to tectonic movement, the second group's offspring are previous earthquakes, they are called aftershocks, which are triggered after strong events or vice versa, if an small earthquake is directly followed by a large one it is called a foreshock; these are dependent earthquakes, because they depend on their ancestor, or are themselves smaller predecessors of an upcoming mainshock. It is assumed that the set of independent earthquakes is homogeneous in time, so they can follow the principle of a Poisson process. With this interest it can be assumed that the dataset itself has to lose its aftershock events to represent an independent process. Due to the fact that aftershocks occur in clusters the whole process of removing these events is called declustering.

In the following two straight-forward methods are introduced which are used for declustering. A third one could be taken into account, but it is based on an epidemic process with a stochastic algorithm. This algorithm is introduced in chapter 4.2.2 as the epidemic-type of aftershock sequences, which can also be used to decluster earthquake catalogues.

The first method is in contrast very simple. It is called Window Method and simply assumes that earthquakes within a certain time and space window generate a chain. The largest event in such a chain is denoted as the mainshock. Earthquakes before the mainshock are called foreshocks, earthquakes after the mainshock are called aftershocks. Both of them are removed from the catalogue so that only the mainshock will remain within the catalogue. There have been multiple definitions developed to define such a window, the most often used (during the review) is from [Gardner and Knopoff, 1974].

Space window [km]:

$$d = 10^{0.1238*M+0.983} \quad (4.3)$$

Time window [days]:

$$t = 10^{0.032*M+2.7389} \quad \text{if } M \geq 6.5 \quad (4.4a)$$

$$t = 10^{0.5409*M-0.547} \quad \text{else} \quad (4.4b)$$

With M as the magnitude of the mainshock. Another way to decluster a dataset is to apply the cluster method of [Reasenberg, 1985]. As its name already tells, it denotes clusters to link earthquakes. The temporal and spatial distribution incorporates an decreasing spatial threshold and the Omori formula to account for the decay over time. Here again the linked events are grouped as a cluster from which only the largest one is used for the declustered dataset. The method in general is more dynamic in its application because it can be adjusted with several parameters like the look-ahead time, observation probabilities, magnitude relations and spatial parameters.

Figure 4.1 shows the application of the cluster method on a Turkish dataset. It is obvious that the declustering method especially shrinks the number of events where seismicity peaks occurred (e.g. 1995 – 1999), because large events are in general followed by a certain number of aftershocks, which are removed. While periods with only minor seismicity (e.g. 2000 – 2006) are almost unchanged.

Due to the testing of the time-independent methods, both original and declustered datasets are used. More details are given in chapter 5. Further details about seismic declustering are given in [Van Stiphout et al., 2012]

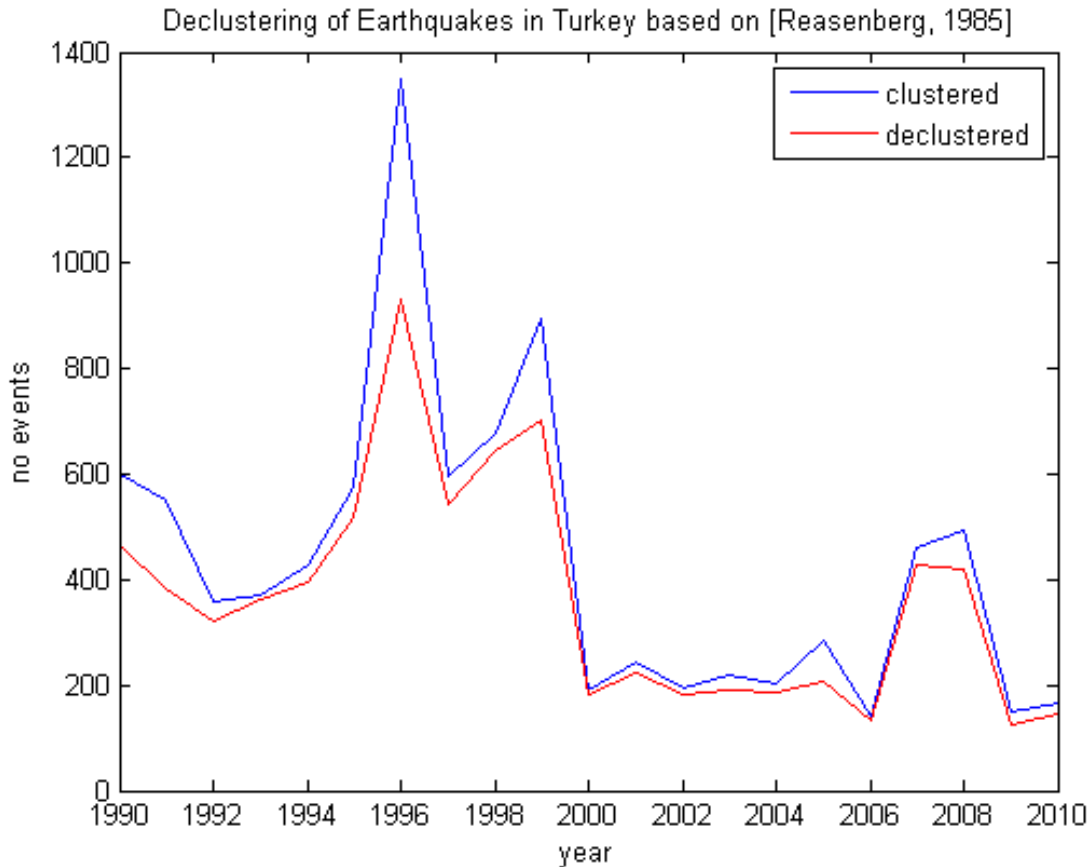


Figure 4.1: A declustered earthquake dataset of turkey from 1990 until 2010. The blue line denotes the original data while the red line indicates the declustered data. Details about the data itself is given in chapter 5

4.1.2 Smoothing

Spatial smoothing is an essential part of almost every model, both time-independent, time-dependent and even Hybrid Methods apply a certain kind of smoothing. The main reason to blur the data is on the one hand in the location uncertainty, which is related to measurement errors and general uncertainty in the development of historical catalogues, where mostly intensity observation have been collected and transformed into a possible magnitude and location. Furthermore due to the assumptions that earthquakes are likely to happen in area with earthquakes during the past, it is on the other hand unlikely that a future earthquake will happen exactly at the same location as the historical one. In that sense, future event will happen “somewhere close” to the former events. This leads to the necessity of redistribution of seismic rates and to spatial discretization of the observation.

In the following tests, the spatial discretization will be based on a $0.1^\circ \times 0.1^\circ$ grid, so approximately a square with an edge length of around 11 km. When distributing the dataset over such a grid, simply the number of events within each grid cell is counted and afterwards redistributed with the application of a stencil or a kernel formula. Such

a formula e.g. uses a Gaussian description to distribute the occurrence over neighboring cells. Most important is that these are normalized functions that the total number of events in the smoothed dataset is the same as the original dataset. Such a formula is mostly controlled by a kernel parameter (or smoothing parameter) to define over which distance the data is smoothed. Stencil smoothing uses static smoothing with an uniform distribution over each participating cell. Therefore so-called stencil over the Moore neighborhood is applied [Nanjo, 2010].

To apply smoothing properly there are two ways to tackle that task. The first one assumes static smoothing, for each grid point the same kernel parameter is applied, which leads to a varying number of events over which it is smoothed. On the other hand, the smoothing parameter can be adaptively changed to smooth over a minimum number k of events around.

For the beginning simple static stencil smoothing is introduced. It was applied within the Relative Intensity Method of [Nanjo, 2010]. Here the events within each grid cell are smoothed over the S -closest neighbors around the cell. That means that e.g. for rectangular smoothing with $S = 1$, the parent cell and the 8 adjacent cells $1/9$ is assigned to each cell, instead of 1 just for the parent cell. It can be easily seen that this approach automatically solves the normalization. In general, smoothing the S -closest neighbors follows the following procedure, that the value $(2S - 1)^{-2}$ is assigned to the parent cell and the $(2S - 1)^2 - 1$ surrounding cells. S represents here the smoothing parameter. With afterwards applied normalization, this approach can also be made for radial smoothing, which is to be preferred. The choice of which smoothing parameter is the most appropriate can be solved by applying the maximum likelihood principle (see chapter 5).

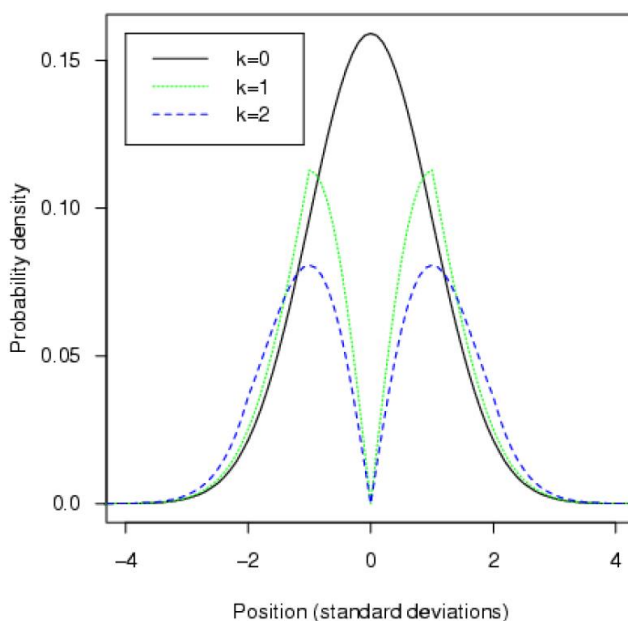


Figure 4.2: From [Rhoades, 2013], a radial cross section through a donut distribution for different κ values (here k). For $\kappa=1$ the donut distribution takes the shape of a standard bivariate Gaussian distribution.

Kernel Smoothing denotes a smoothing algorithm which is based on a distribution function. Two examples are introduced here. The 2D-Gaussian (also called bivariate normal distribution) and the 2D-Power-law has been applied for the Adaptively Smoothed Seismicity algorithm of [Werner et al., 2010b]. Alternatives are for example the donut-distribution, witch's-hat-distribution [Rhoades, 2013] or just a linear distribution. In the following we will concentrate only on the Gaussian and the power-law, because due to [Rhoades, 2013] the other distributions do not increase the information gain of the model, except for the Donut kernel, which are introduced to show a distribution, which sets the density at the center to 0. Figure 4.2 shows different Donut distributions with a normal distribution in comparison.

The Gaussian can be expressed as the following:

$$K_d(r) = C_G(d) * \exp\left[-\frac{|r|^2}{d^2}\right] \quad (4.5)$$

And the power-law as

$$K_d(r) = \frac{C_P(d)}{(|r|^2+d^2)^{1.5}} \quad (4.6)$$

And the donut as

$$K_d(r) = \frac{C_D(\kappa)}{2\pi d^2} \exp\left[-\frac{|r|^2}{2d^2}\right] \quad r \geq d \quad (4.7a)$$

$$K_d(r) = \frac{|r|C_D(\kappa)}{2\pi\kappa d^3} \exp\left[-\frac{|r|^2}{2d^2}\right] \quad r < d \quad (4.7b)$$

With $C(d)$ and $C(\kappa)$ the corresponding normalization factors to bring the integral over an infinite area to 1, r is the distance between data point and location and d is the standard deviation or here denoted as the smoothing distance. For the donut distribution, the additional parameter κ is introduced, which additionally controls the shape of the donut distribution. The normalization parameter for the Gaussian can be calculated as the following:

$$C_G(d) = \frac{1}{\sqrt{\pi}d} \quad (4.8)$$

And for the power-law:

$$C_P(d) = 0.5 * d^2 \quad (4.9)$$

And for the donut:

$$C_D(\kappa) = \frac{2\kappa}{\sqrt{2\pi}\text{erf}(\kappa/\sqrt{2})} \quad (4.10)$$

Another way to generate a smoothing kernel is to normalize the smoothed values with themselves. Instead normalizing by using a normalizing constant, the whole smoothed dataset is neglecting its smoothing multiplication to maintain its original integral sum. The following formula shows how such an approach for a Gaussian kernel can look like. The smoothed number of events $\check{n}(i)$ in cell i is

$$\check{n}(i) = \frac{\sum_{j;r \leq 3d} n(j) * \exp\left[-\frac{|r|^2}{2d^2}\right]}{\sum_{j;r \leq 3d} \exp\left[-\frac{|r|^2}{2d^2}\right]} \quad (4.11)$$

With d as the smoothing parameter and $n(j)$ the observed number of earthquakes in cell j . Thus, the smoothing algorithm is applied over all cells around cell i within three times the smoothing parameter distance.

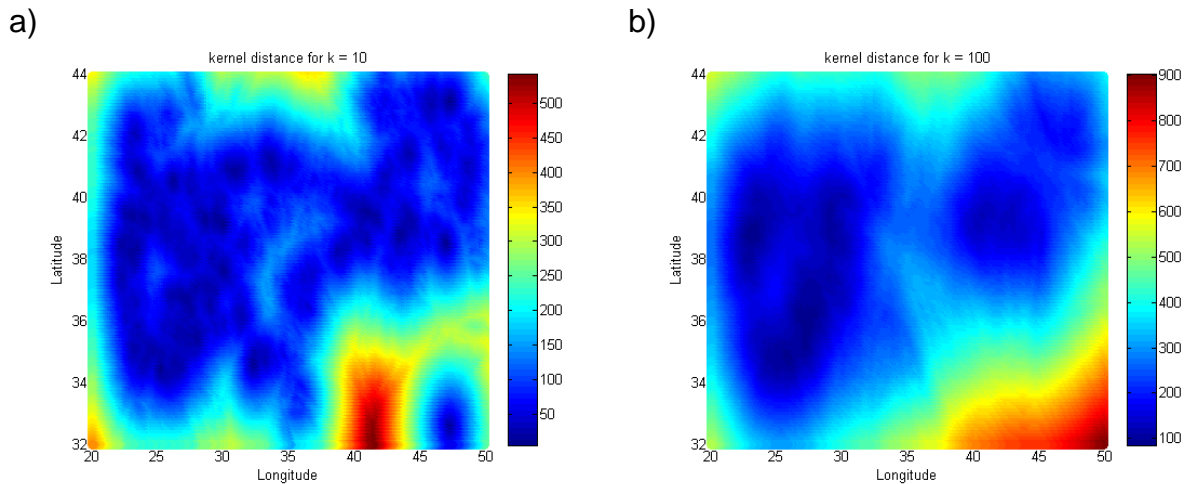


Figure 4.3: Smoothing distance solved for each grid cell. The color indicates the radius of a circle around each grid point with at least k events inside. The minimum value was set to 0.5 km. a) shows the map for $k=10$ and b) for $k=100$.

With this small selection of spatial smoothing algorithm it is already possible to create a wide range of spatial seismic distributions. The first choice to make, is if the algorithm is adaptive or not, so if it is event oriented, or does it use a static smoothing. Secondly there is the choice of smoothing parameter. For static smoothing, here it is important to find out which value of smoothing (S for stencil smoothing, or d for the kernel smoothing) leads to the most likely result. In the adaptive smoothing, instead of defining a global d , a varying kernel distance is calculated. Thus, d represents the radius around each grid point within at least k earthquakes occurred. Figure 4.3 shows two maps of kernel distances, to compare how such a choice might affect the overall smoothing. Large values for k tend to blur the overall seismicity, while too small values generate an accuracy which does not exist and furthermore neglects possible seismicity in between the event locations. Figure 4.4 compares the different smoothing approaches. It can be easily seen, that

the application of an adaptive kernel leads to a better resolution than static smoothing. The donut kernel has been neglected for further studies because its resolution and spatial accuracy tends to lead to worse results than the power-law or Gaussian respectively. However, in general the adaptive kernel leads to an overrepresentation of local seismicity.

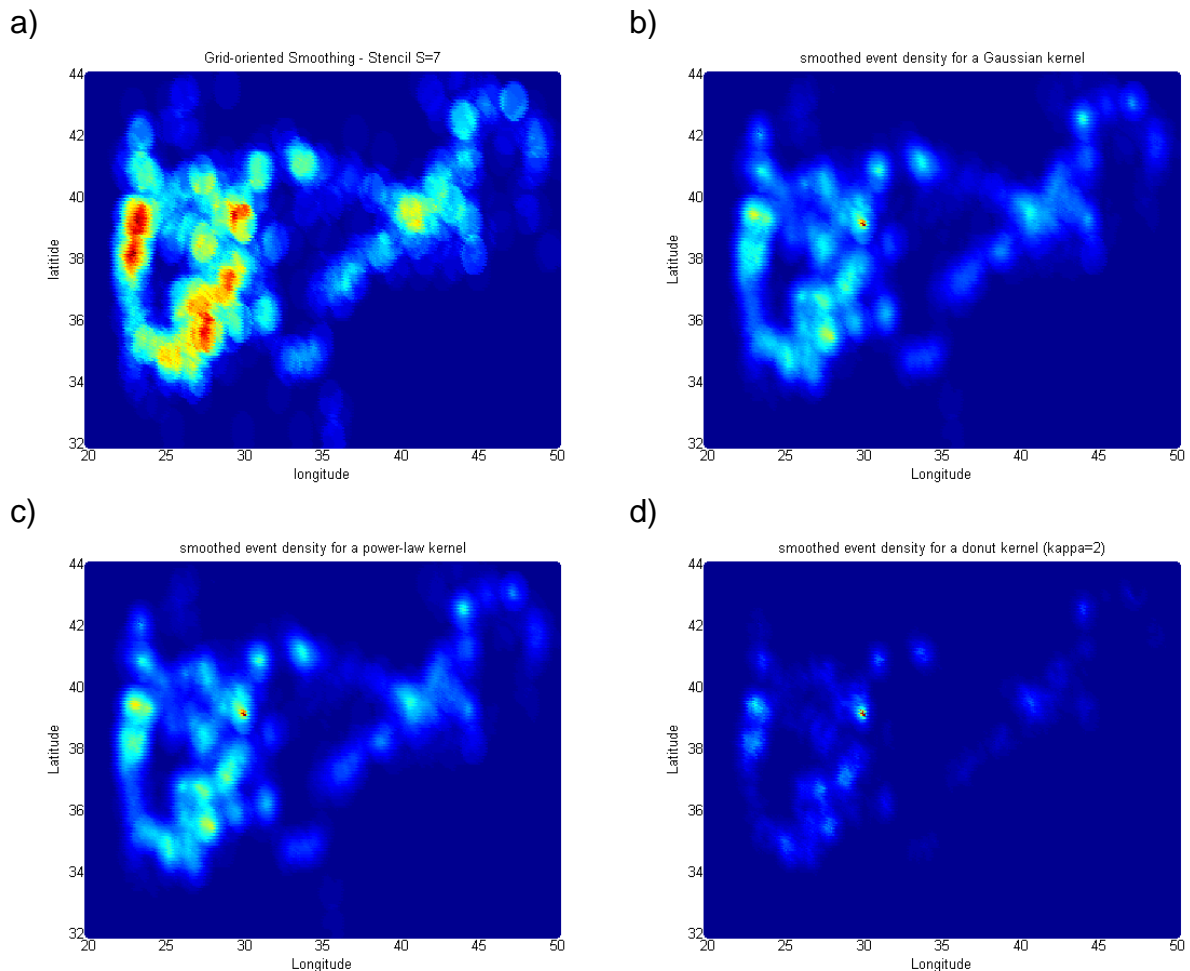


Figure 4.4: Different results for smoothed seismic density for Turkey. a) is a static radial stencil $S=5$, b) an adaptive Gaussian kernel, c) an adaptive power-law kernel, d) an adaptive donut kernel with $\kappa=2$. b)-d) used all the same $k=10$ (minimum events around each location). The color code shows the relative density of events per grid cell, the absolute value should not be taken into account

4.1.3 Gutenberg-Richter Handling

Even more essential than the spatial smoothing of seismicity is the handling of the Gutenberg-Richter relation to finally calculate annual earthquake rates for different magnitudes. In general there are three ways to apply the Gutenberg-Richter relation; a regional b -value without estimating a -values. This approach assumes that the b -value is constant or the whole testing region. With the background that the a -value is nothing else than the theoretical intersection of the linear logarithmic regression with the y -axis (zero magnitude), it is possible just to shift the whole function by

subtracting a minimum magnitude. The number of forecasted earthquakes $N(i, M)$ larger or equal magnitude M at location i is equal

$$N(i, M) = 10^{\log_{10}(\tilde{N}(i)) - b*(M - M_{\min})} \quad (4.12)$$

With $\tilde{N}(i)$ the observed annual rate of earthquakes larger or equal M_{\min} and b as the regional b -value.

Another way is to calculate a -values for each magnitude range and finally calculating the most likely a -value out of this set (e.g. by taking the mean, applying the least squares approach, etc.).

$$N(i, M) = 10^{\bar{a}(i) - b*M} \quad (4.13)$$

With e.g. by applying the mean

$$\bar{a}(i) = \frac{a(i,m)}{n} \quad (4.14)$$

Where n denotes the number of magnitude bins for which an a -value has been calculated.

The most complex approach is to calculate a b -value for each location separately.

$$N(i, M) = 10^{\bar{a}(i) - b(i)*M} \quad (4.15)$$

This idea refers to the Asperity-based Likelihood Method of [Gulia et al., 2010], where local b -values have been calculated to account for different asperities. In the approach of [Gulia et al., 2010] has been adopted. The method generally compares local values vs. a global b -value and chooses the “best” by applying the maximum likelihood principle. This principle uses the probability density equation of the formula for which parameters have to be adjusted. It compares the estimated results of the equation with the observed dataset and finally calculates a likelihood value. This likelihood value is finally applying to the corrected Akkaike Information Criterion (AIC_c) [Kenneth et al., 2002] to estimate how large the information gain of a certain formulation is. Smaller values for the AIC denote better results. In general the likelihood function for the b -value for a certain magnitude in the dataset, where the a -value can be neglected in the shifted approach as described above, can be calculated the following way:

$$L(\beta; H_t) = \sum_{i=1}^n \log_{10} \left(\beta \frac{e^{-\beta(M(i) - M_{\min})}}{1 - e^{-\beta(M_{\max} - M_{\min})}} \right) \quad (4.16)$$

Where H_t represents the dataset with n earthquakes from which M_{min} and M_{max} are the minimum and maximum magnitude respectively. And β is the lognormal transformation of the b -value

$$\beta = b * \ln(10) \quad (4.17)$$

The likelihood is calculated for the regional b -value as well as for different local b -values. The data used to calculate a local b -value is determined by simply using all events within a circle with a certain radius around the location. Depending on the general event density of the dataset and its resolution the local b -values are computed with data circles with radii from 1 to 100 km. Finally the likelihood is compared using the corrected Akkaike Information Criterion as the following:

$$AIC_c = -2 * \ln(L) + 2P + \frac{2P(P+1)}{N-P-1} \quad (4.18)$$

Where P is the number of free parameters and N is the sample size. AIC_c values are compared lowest value is chosen to be the most likely. The final Gutenberg-Richter rate can be computed using one of the methods described above.

Alternatively it is also possible to calculate the b -value based on a seismic zonation or tectonic faults, same holds also for a -values. Finally the average annual rate for a certain magnitude can be computed from the Gutenberg-Richter relation. This rate can then be used for the Poisson process to calculate the final probability of an earthquake with a certain magnitude at a certain location within a certain time period based on the historical data.

4.2 Time-dependent Method reconstruction

While time-independent methods follow a relatively strict way how to build a forecast, the time-dependent methods are a lot more diverse. As it can be seen in chapter 3.5 there are a lot of different approaches. Two major groups exist on the one hand the epidemic-type methods which are in general more focused on the short-term aftershock forecasting. On the other hand there are pattern searching algorithms, which investigate the earthquake occurrence due to certain precursory patterns to indicate regions and period within future earthquakes are most likely. This precursor information can be used either to change time-independent forecasting maps or to generate an alarm which is close to a prediction, because it predicts an earthquake within a certain magnitude, space and time window without declaring its probability.

As the methods within this project should be somehow comparable, the time-dependent approaches introduced in the subsequent chapters should either lead to a map of earthquake rates with time-dependent features to finally build a comparison with time-independent earthquake rates or at least create a map where the locations of future earthquakes are indicated. The first method based on the Pattern

Informatics method of [Holiday et al., 2005] and [Holiday et al., 2007]. It uses time-independent elements of the Relative Intensity approach, which has also been applied by [Nanjo, 2010], from which elements have been described in chapter 4.1.

The second method is a slightly simplified version of the Epidemic-Type of Aftershock Sequence method, which was introduced for the first time by [Ogata, 1988], afterwards applied and modified by [Ogata, 1998] and later multiple times adopted, e.g. by [Zhuang et al., 2002], [Lombardi and Marzocchi, 2010], [Zhuang 2011].

4.2.1 Pattern Informatics

The first elements of the Pattern Informatics approach have been already introduced more than ten years ago by [Rundle et al., 2000] from which followed subsequent developments. These have been applied by [Holiday et al., 2005] and [Holiday et al., 2010]. This approach does not directly predict or forecast. It rather denotes areas where future earthquakes are more likely to happen based on a temporal variation in seismicity patterns.

This method uses precursory information about an increase in seismic activity to denote increased probabilities for future earthquakes. Therefore the dataset is divided into several time intervals within each the seismic activity is calculated. The seismic activity of the final time interval is compared to the activity of the whole interval before that to find locations with anomalous seismic activity. For example if there is a 10-year forecast to make, the last ten years of the dataset are used to compute the anomalous activity relative to the whole rest of the dataset before that period.

The following procedure in general follows the description of [Holiday et al., 2010]. The spatial discretization follows the same way as for the time-independent methods. For the beginning a general smooth seismicity map is calculated with earthquake rates for each location of the spatial grid.

Afterwards, the dataset is divided into two periods. The first period from t_b to t_1 represents the reference period, the second one from t_1 to t_2 is the change interval, which is later compared to the reference period due to seismic activity. A third period from t_2 to t_3 can be defined as the forecasting interval for which the forecast is made. The times are related as $t_0 \leq t_b < t_1 < t_2 < t_3$, where t_0 is the first entry of the dataset and t_2 the most recent. The change interval and the forecasting interval should be of the same length, e.g. ten years. For the dataset a common completeness magnitude M_C as lower threshold is applied for which all earthquake with $M > M_C$ are excluded.

The seismic reference activity is measured by calculating the average seismicity rate, say seismic intensity, in each cell within certain a period from t_b to t the following way:

$$I_i(t_b, t) = \frac{1}{t-t_b} \sum_{t'=t_b}^t N_i(t') \quad (4.19)$$

Where $N_i(t')$ is the number of earthquakes at time t' . The sum is performed over all increments of the time period, e.g. in days or years. Afterwards to compare the seismic intensities of different periods, the seismic intensity in each cell is normalized by subtracting the mean and dividing by the standard deviation. This is performed for all periods and locations by

$$\hat{I}_i(t_b, t) = \frac{I_i(t_b, t) - \langle I(t_b, t) \rangle}{\sigma(t_b, t)} \quad (4.20)$$

Finally the measure of anomalous activity in each cell is calculated by comparing the differences in seismic intensity for the periods from t_b to t_1 with t_b to t_2 by

$$\Delta I_i(t_b, t_1, t_2) = |\hat{I}_i(t_b, t_2) - \hat{I}_i(t_b, t_1)| \quad (4.22)$$

The absolute value used that both seismicity decreases (so-called quiescence) and increases (activation) are taken into account the same way. As a last step, the mean squared change is computed for each cell over each reference period, because it is assumed that the probability of a future earthquake is proportional to the mean squared change.

$$P_i(t_0, t_1, t_2) = \overline{\Delta I_i(t_b, t_1, t_2)^2} = \left[\frac{1}{t_1-t_0} \sum_{t_b=t_0}^{t_1} \Delta I_i(t_b, t_1, t_2) \right]^2 \quad (4.23)$$

This mean squared change is calculated based on multiple reference intervals, t_b is chosen between t_0 and t_1 e.g. in time-steps of five years. Anomalous regions are defined as area where the probability changes drastically with respect to the long-time average in the following way:

$$\Delta P_i(t_0, t_1, t_2) = P_i(t_0, t_1, t_2) - \langle P_i(t_0, t_1, t_2) \rangle \quad (4.24)$$

Where $\langle P_i(t_0, t_1, t_2) \rangle$ is the mean probability over all boxes and defined as the background seismicity. Locations with a high probability of future earthquakes, so-called hotspot pixels, are defined to be regions where $\Delta P_i(t_0, t_1, t_2)$ is larger than a certain threshold (e.g. $\Delta P_i > 0$)

To finally create a hazard map, the smooth seismicity map, calculated in the beginning will be superpositioned with the PI-data. All cells for which the threshold (e.g. top 10% of the pixel probabilities) is reached the probability of the original time-

independent map is replaced with the value 1, which finally just means, that for this certain location an earthquake is most likely to happen.

Afterwards the probability map is normalized and adjusted to the total earthquake rate for the forecast period, which is computed from the regional Gutenberg-Richter relation.

To summarize the Pattern Informatics approach, it can easily be said that it shifts the forecasting probability due to its location. It investigates recent seismic activity, compares it to the historical observations and finally the area with certain change in activity is assumed to have higher probabilities for future earthquakes than the other regions.

The combination with a time-independent method was made by [Holiday et al., 2010] with a Relative Intensity approach [see Nanjo, 2010], but can also be achieved with other smooth seismicity methods. Computational results can be found in chapter 5.

4.2.2 Epidemic-Type of Aftershock Sequences

The ETAS model was in some sense the most popular epidemic model of the last years. It uses age-dependent birth and death processes to calculate aftershock sequences for short-term forecasting. Thus, it describes earthquake clustering of aftershocks, foreshocks and mainshock to give a time-dependent alternative to the time-independent Poisson models.

The procedure described here follows basically the procedure established by [Zhuang et al., 2002], incorporating elements from [Ogata, 1998]. [Zhuang et al., 2002] used the ETAS to stochastically decluster earthquake datasets, so this approach can partially be counted to the declustering methods as well, because the ETAS procedure separates the background seismicity from the aftershock/foreshock seismicity with the help of a stochastic process.

The fundamental formula which describes the ETAS assumes that the distribution of magnitudes m is separable from all the other elements. The algorithm separates furthermore the space and time domain during the calculation of aftershock activity. The number of subsequent events from a parent earthquake depends only on the magnitude of the parent earthquake. Furthermore, the probability distribution function of the time until the next aftershock depends only on the time since the mainshock. The probability distribution of subsequent events in space depends on the distance to the mainshock and the mainshock magnitude. Taking all this together the following formula can be derived:

$$\lambda(t, x, y) = \left[u(x, y) + \sum_{i:t_i < t} \kappa(M_i) g(t - t_i) f(x - x_i, y - y_i | M_i) \right] \quad (4.25)$$

Where $\kappa(M_i)$ represents the magnitude-dependent number of earthquakes from an ancestor event with magnitude M_i and can be calculated the following way

$$\kappa(M_i) = A e^{\alpha(M - M_0)} \quad (4.26)$$

Furthermore $g(t - t_i)f(x - x_i, y - y_i, M_i)$ represent the normalized response functions of time and location, where $f(x - x_i, y - y_i | M_i)$ follows a magnitude-dependent 2D-Gaussian, and $g(t - t_i)$ basically represents a modified version of the Omori-law.

$$g(t - t_i) = \frac{(p-1)c^{p-1}}{(t+c)^p} \quad (4.27)$$

$$f(x - x_i, y - y_i | M_i) = \frac{1}{2\pi d e^{\alpha(M-M_0)}} \exp\left[-\frac{1}{2} \frac{x^2 + y^2}{d e^{\alpha(M-M_0)}}\right] \quad (4.28)$$

Finally $u(x, y)$ is the estimated intensity function for the background seismicity. The parameters (A, α, p, c, d) are estimated by using the maximum likelihood principle, where the following formula has to be maximized

$$\log(L(\theta)) = \sum_{k=1}^N \log(\lambda_{\theta}(t_k, x_k, y_k | \mathcal{H}_t)) - \int_0^T \iint_S \lambda_{\theta}(t_k, x_k, y_k | \mathcal{H}_t) dx dy dt \quad (4.29)$$

Where $\theta = (A, \alpha, p, c, d)$ are the free parameters and \mathcal{H}_t represents the whole historical dataset over the period $[0, T]$ over the study region S .

General problem behind this approach is that the background seismicity is as unknown as the parameter set θ , unfortunately the background seismicity is not computable over the maximum likelihood principle, which would anyway contradict the physical process of the ETAS formula. To calculate the background seismicity based on ETAS calculations using an iteration process, it is necessary to compute the general seismic activity as well as the probabilities for each event to be an offspring or an independent event. Therefore a couple of further formulations have to be introduced. ρ_j is defined as the probability of the j 'th event to be an aftershock. To calculate ρ_j , $\rho_{i,j}$ has to be computed, which is the probability, that the j 'th event is the offspring of the i 'th event. Combining both steps, this leads to

$$\rho_j = \sum_{i=1}^{j-1} \rho_{i,j} = \sum_{i=1}^{j-1} \frac{\kappa(M_i)g(t_j-t_i)f(x_j-x_i, y_j-y_i | M_i)}{\lambda(t_j, x_j, y_j | \mathcal{H}_{t_j})} \quad (4.30)$$

Vice versa, the probability of the j 'th event to be independent is

$$\varphi_j = 1 - \rho_j \quad (4.31)$$

In addition, based on a simple smoothed seismicity approach it is possible to calculate the total seismicity rate (comparable to chapter 4.1). In the following a simple Gaussian distribution function is used to compute the mean seismic rate $m(x, y)$ as

$$m(x, y) = \frac{1}{T} \sum_{j=1}^N k_{d_j}(x - x_j, y - y_j) \quad (4.32)$$

Where k_{d_j} is an adaptive smoothing kernel, similar to the event-oriented smoothing of chapter 4.1.2, where the smoothing parameter d_j depends on the event density k around location j .

$$k_{d_j}(x, y) = \frac{1}{2\pi d_j} \exp\left(-\frac{x^2+y^2}{2d_j}\right) \quad (4.33)$$

In that way the rates of the offspring events γ and the background seismicity u can be calculated separately.

$$\gamma = \frac{1}{T} \sum_j \rho_j k_{d_j}(x - x_j, y - y_j) \quad (4.34)$$

$$u(x, y) = m(x, y) - \gamma(x, y) = \frac{1}{T} \sum_j (1 - \rho_j) k_{d_j}(x - x_j, y - y_j) \quad (4.35)$$

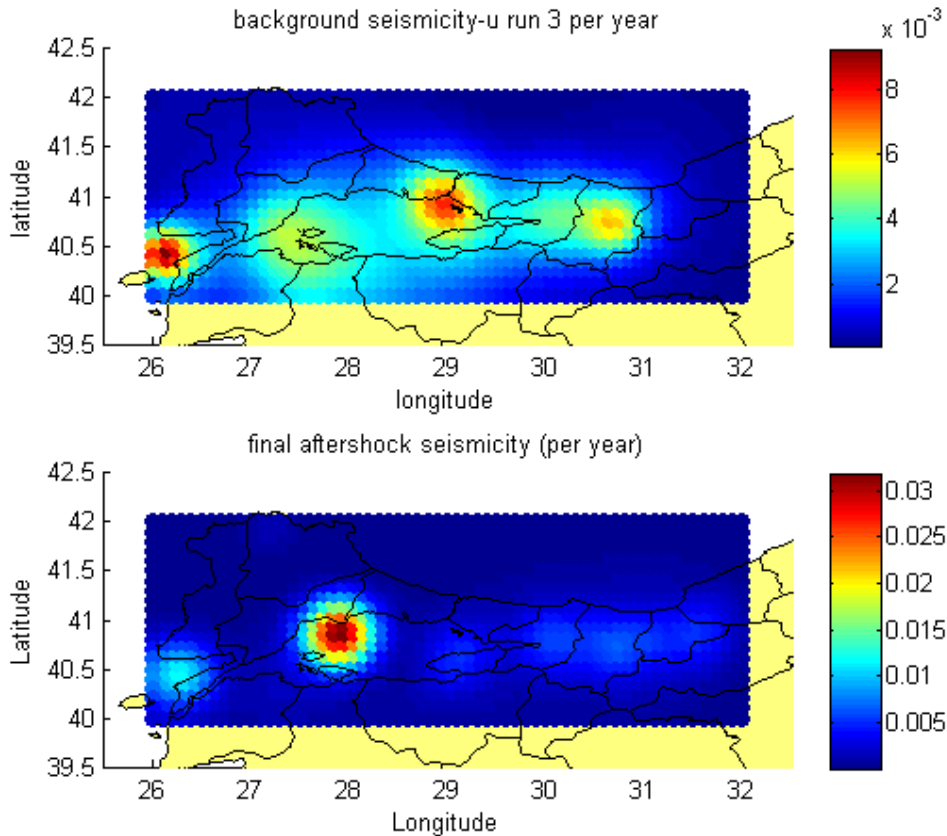


Figure 4.5: Results for an ETAS-analysis of the Marmara Sea region. Top: background seismicity based on a 1000 year dataset for earthquakes with magnitudes $M > 4$. Bottom: aftershock seismicity of the same dataset, the color denotes the earthquake activity in annual rates. For the aftershock seismicity, the annual rate is a theoretical extrapolation of the calculated daily rates.

This iteration process is based on [Zhuang et al., 2002] and can be summarized the following way:

1. Assume a value for k , e.g. $k = 5$ [after Zhuang et al., 2011] and calculate d_j for each event.
2. Set $u^{(0)}(x, y) = 1$ and $l = 1$.
3. Calculate $\lambda(t, x, y)$ using the maximum likelihood principle to estimate all relevant parameters with formula (4.29). One possibility for computation is shown in [Ogata, 1998].
4. Calculate ρ_j for each event based on formula (4.30)
5. Estimate $u^{(l)}(x, y)$ with formula (4.34)
6. If $\max|u^{(l-1)}(x, y) - u^{(l)}(x, y)| > \varepsilon$, set $l = l + 1$, where ε is a small positive number, otherwise, if $\max|u^{(l-1)}(x, y) - u^{(l)}(x, y)| \leq \varepsilon$ assume that $u^{(l)}(x, y)$ is a sufficient estimate of the background seismicity.

After this iteration process $\lambda(t, x, y)$ represents the seismicity rate directly at the end of the observation period $[0, T]$ for earthquakes above M_c .

The forecast of aftershock seismicity is calculated for daily rates. Giving for example a 10-year forecast, the aftershock seismicity of a certain earthquake can be neglected. There are two ways to build a long-term forecast from the ETAS algorithm. The first one is to estimate simply the future seismicity from the time-independent background seismicity, which obviously to a time-independent forecast. Another way is to simulate the earthquake occurrence for the testing period with a stochastic process, but this needs a lot of computation power. Details in simulating ETAS-catalogue forecasts are given in [Zhuang et al., 2011].

Another way to use the ETAS algorithm is to calculate daily short-term forecasts based on the upcoming aftershock seismicity after certain earthquakes. Both the time-independent long-term forecast as well as the short-term aftershock probabilities will be tested in chapter 5.

4.3 Fault-oriented time-(in-)dependent b-value

A third option to bring a time-dependent element into a time-independent calculation is to change Gutenberg-Richter's b -value according to the current seismic state by investigating average inter-event times. This approach is broad up by the author himself and has been developed to be applied both for time-independent and time-dependent forecasting.

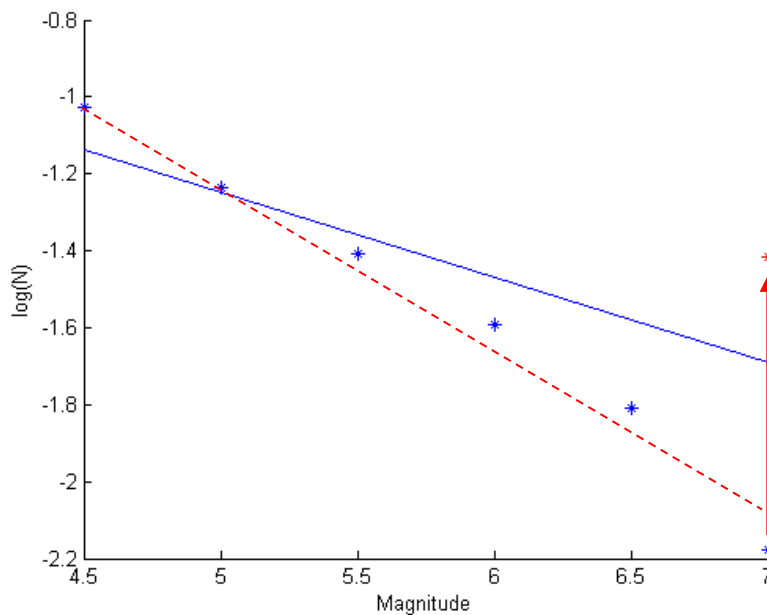


Figure 4.6: Sample Gutenberg-Richter relation of a region where an earthquake of magnitude $>M7$ is overdue, so its rate got increased. This results in a smaller b -value.

The idea is simply to increase the rate of large earthquakes depending on the time since the last occurrence of an event within a certain magnitude bin. Increasing this value and afterwards calculating the Gutenberg-Richter relation leads to a smaller b -value and thus to a higher probability of larger earthquakes. Figure 4.6 shows how such an increase can look like.

This algorithm needs an additional data source. Under the assumption that the b -value variations are heavily dependent on the distribution of faults in an area, these so called fault-related asperities are a proxy of the estimated b -values. Thus, a vector map of faults is needed to appropriately compute this model, with respect to the hybrid methods, only the surface geometry of a fault is needed (two spatial points; start and end point). Depending on the dataset, each fault is subdivided into several segments of 10 – 200 km length. The whole method follows a simple step-by-step procedure for the time-independent modeling like the following.

1. Calculation of regional b -value (see chapter 4.1.3.). Taking completeness into account.
2. Distribution of earthquake dataset over all faults within a certain distance, sorted into magnitude bins of 0.25-steps (alternatively 0.5-steps).

3. Calculation of b -values for each fault segment, the total fault- b -value is then the mean respectively. Taking completeness into account.
4. Spatial smoothing for local b -values.
5. Forecast calculation (see chapter 4.1.3)

With the changes with respect to the time-dependent modeling the method looks like the following:

1. Calculation of regional b -value (see chapter 4.1.3.).
2. Distribution of earthquake dataset over all faults within a certain distance, sorted into magnitude bins of 0.25-steps. Storing both first year of magnitude occurrence and the most recent year.
3. Calculation of earthquake rates/average interevent time based on the year-observations for each magnitude bin.
4. Calculating the lognormal cumulative probability for an earthquake based on average interevent time and time since the last occurrence for the next time period
5. For all faults which are activity since a certain year and at least a certain number of earthquakes in a certain magnitude-space bin, add the lognormal cumulative probability to the annual rate.
6. Calculation of time-dependent b -values for each fault segment, the total fault- b -value is then the mean respectively. Time-independent part takes completeness into account. The final b -value is the mean of the time-independent and the time-dependent b -values.
7. Spatial smoothing for local b -values.
8. Forecast calculation (see chapter 4.1.3)

Steps 1 and 5 – 8 are straight forward following the procedures of chapter 4.1.3. Since the time-dependent procedure is just an expanded version of the time-independent one, the following description uses the step-notation of the time-dependent method. At first it is necessary to calculate a regional b -value as a proxy estimate of seismic activity in the investigated area, following procedures of chapter 4.1.3. Afterwards the fault map is used to distribute the data catalogue of earthquake over all the different faults and their corresponding segments. This is simply done by counting all earthquakes around a fault segment using the distribution radius r . The counted earthquakes are sorted into magnitude bins with steps of e.g. 0.25 starting from a minimum magnitude threshold M_{min} . Especially for the time-dependent version, the first year a certain magnitude bin got occupied is stored as well as the year of the most recent occurrence. Based on the number of earthquakes between the current year and the year of the first occurrence of a certain magnitude, the annual rates and respectively the average interevent times are computed for each fault and magnitude bin.

For the time-dependent version, for each magnitude bin, the lognormal cumulative probability is computed based on the average inter event time \bar{t} , the time of last occurrence and the standard deviation, which was simply assumed to be $1/3 \bar{t}$. For each fault, a fault-related b -value is computed using the according magnitude bins and data completeness estimates. For the time-dependent version, if earthquakes of a certain magnitude bin occurred after a certain year with a certain number, the cumulative lognormal probability is added to the observed earthquake rate to account for a possible upcoming event in the near future.

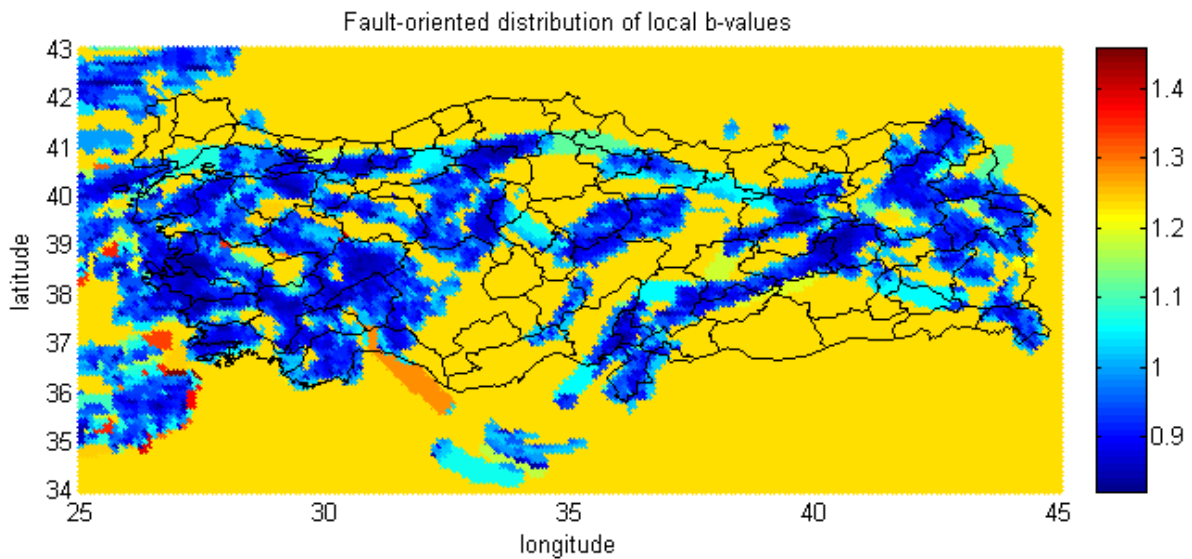


Figure 4.7: Fault-oriented distribution of b -values for Turkey. Color indicates the local b -value.

Finally, after all fault-related b -values have been computed. A smooth b -value map is generated by using a simple spatial grid. For each grid point, a linear spatial weighting of all fault-related b -values within r around the location is performed. For all other locations, the global b -value is used.

Finally, using the either the time-dependent or the time-independent b -values a forecast or future earthquake rate can be computed using known approach from chapter 4.1.3.

Both versions for time-independent and time-dependent forecasting are introduced an applied here, first testing results will be presented in chapter 5. It should be noted that this algorithm is an a priori approach developed by the author.

4.4 Overview and Summary of Coding

After reviewing and reconstructing several features of time-independent and time-dependent approaches it can be clearly seen that both ways are still connected to each other. The computational possibilities of time-independent modeling are smaller than expected. As described above, the range of how to construct such a model is restricted to data-handling, spatial smoothing and rate calculation. In all three areas

the parameter effects are only minor. Thus, the choice of a modeler due to which method he prefers leads has only marginal influence on the result as long as the data and modeling is done appropriately. Nevertheless, covering all three model elements it is possible to provide a complete set of algorithm parts to assemble different models fitted to the current needs.

How these elements are further combined and will be discussed in chapter 5, where they are tested as well. However, in conclusion, time-independent models are nothing else than (how Zechar and Jordan named their own method in 2010) just simply smoothed seismicity, which are fast and straight forward in computation. However, even if these methods are simple, they provide nice a priori estimates of seismic activity and can still be very useful to give a good approach for investigating future earthquake occurrence.

Time-dependent methods in contrast go more into detail, searching for patterns and signals, which indicate an up-to-date change in seismicity. They start to incorporate more than just observations and one statistical formula, with assumptions related to seismic clustering and fault activation or quiescence it is possible to give better estimates of current seismic hazard and not just the mean rates. The codes of the time-dependent methods reconstructed here are still based on statistical observations and are only an excerpt of the possibilities, other approaches use e.g. the application of time-dependent Weibull distributions or alarm-based pattern searching (like the reverse tracing of precursors method).

In the following chapter, the approaches, which have been introduced in detail both for time-independent and time-dependent modeling are tested on their accuracy and general operability. The time-independent methods are reassembled to test how different ways of smoothing and handling of the Gutenberg-Richter relation lead to different results. For the time-dependent methods, it should be tested how they can forecast future seismicity and if their advantages are really good enough to justify their complexity relative to the rather simple time-independent models.

5 Testing

Testing certain approaches is a key tool to verify whether a method works appropriately or not. A method can be regarded as working and also as not working. Such a testing procedure is of course not trivial. To encounter this issue a set of stochastic and probabilistic tests have been developed, which are also used in the RELM project [Schorlemmer et al., 2007] and have been further evaluated and advanced by [Zechar et al., 2010]. Both approaches are regarded here.

To sophisticatedly test models and compare the results, the testing procedure must be applied on common datasets which the models share. Therefore two regions have been chosen to be tested in spatial and temporal scales for retrospective forecasting. Turkey and Italy are well observed regions with both dense and long datasets. Details about the testing range will be given in chapter 5.2.

5.1 Testing Algorithms

The following tests follow in general the descriptions of [Zechar et al., 2010]. In total 3 tests are introduced to find out how well a certain method maps a future observation. The N-test measures how well the total number of earthquakes is forecasted based on a Poisson distribution. In additionally, the S- and M-tests investigate based on a stochastic catalogue modeling how likely the observation is within the forecast. A testing region is defined over the location domain S and the magnitude domain M , both binned e.g. in magnitude steps of 0.25 [e.g. [4.0, 4.25); [4.25, 4.5); etc.] and location discretization in latitude-longitude rectangles of $0.1^\circ \times 0.1^\circ$. Thus, the total forecast Λ can be summarized as

$$\Lambda = \{\lambda(i, j) | i \in M, j \in S\} \quad (5.1)$$

Where i and j represent the bins in space and magnitude, where j can of course consist of two parameters, namely the longitude and latitude values of a certain location. The same way, the observation Ω can be defined as

$$\Omega = \{\omega(i, j) | i \in M, j \in S\} \quad (5.2)$$

Both λ and ω denote the number of earthquakes within a certain magnitude-space bin respectively for the forecast and the observation.

5.1.1 N-Test

The N-Test is used to determine how well a forecast catches the number of observed earthquakes. In general the number of expected earthquakes is just the sum of all events within each magnitude-space bin. Same holds for the number of observed earthquakes.

$$N_{fore} = \sum_{(i,j)} \lambda(i, j) \quad (5.3)$$

$$N_{obs} = \sum_{(i,j)} \omega(i, j) \quad (5.4)$$

Under the assumption of a Poisson process the likelihood can be estimated by checking in which part of the tail of the forecast-related Poisson distribution is. Therefore two Poisson probabilities are calculated:

$$\delta_1 = 1 - F(N_{obs} - 1 | N_{fore}) \quad (5.5a)$$

$$\delta_2 = F(N_{obs} - 2 | N_{fore}) \quad (5.5b)$$

Where F is a right-continuous cumulative Poisson distribution function. Hereby δ_1 the probability of observing at least N_{obs} events and δ_2 denotes the probability of observing at most N_{obs} events. This is considered a two-sided test. For both values the critical region is if one of them becomes very small. For very small values of δ_1 it is an underprediction, vice versa, a very small value for δ_2 is an overprediction.

5.1.2 S-Test & M-Test

Both the M- & S-test refer to the L-test introduced by [Schorlemmer et al., 2007]. The S-test tests the likelihood of the spatial distribution neglecting the magnitudes, and vice versa, the M-test tests the likelihood of the magnitude distribution disregarding the location. Here again a Poisson distribution is used to calculate the likelihood of a forecast, following formula (5.6).

$$\Pr(\omega|\lambda) = \frac{\lambda^\omega}{\omega!} \exp(-\lambda) \quad (5.6)$$

Transforming the joint probability over all bins and applying the natural logarithm the joint log-likelihood can be calculated:

$$L(\Omega|\Lambda) = \sum_{(i,j)} (-\lambda(i, j) + \omega(i, j) \log(\lambda) - \log(\omega!)) \quad (5.7)$$

The joint log-likelihood of equation (5.7) will be negative, the result which is closer to zero is defined as more likely.

To finally check if a forecast is consistent with the observation, it is necessary to calculate a set of simulated catalogues based on the forecasted rates. Therefore a cumulative distribution is constructed by adding up the probabilities of all bins and normalizing the whole distribution. Afterwards a set of random numbers between 0 and 1 is chosen, the length of the set is equal to N_{obs} . Each value of the set is associated to the corresponding bin of the normalized cumulative distribution of the forecast. Afterwards the joint log-likelihood of each simulated catalogue is computed. With multiple simulated catalogues it is possible to compare the likelihoods of the simulated results with the observed likelihood. Hereby two ways can be followed; one is used during the CSEP project [Schorlemmer et al., 2007] which checks if the likelihood of the forecast is in a certain confidence interval of the forecast (often used 95%). The second approach by [Zechar et al., 2010] checks how many simulated catalogues are less likely than the observed one. The forecast is assumed to be consistent, if the log-likelihood of the observed catalogue is larger than most of the simulated ones.

For the M-test the cumulative normalized distribution over all magnitude bins is calculated by

$$\omega^m(i) = \sum_{(j)} \omega(i, j) \quad (5.8a)$$

$$\lambda^m(i) = \sum_{(j)} \lambda(i, j) \quad (5.8b)$$

The quantile score κ introduced by [Zechar et al., 2010] is calculated the following way

$$\kappa = \frac{|\{M_x | M_x \leq M\}|}{|\{M_x\}|} \quad (5.9)$$

Where $|\{M\}|$ is the number of elements in $\{M\}$, where M is the joint log-likelihood of the observed catalogue, and M_x is the joint log-likelihood of the simulated catalogue. The same procedure is used to calculate the quantile score ζ of the S-test, but with a cumulative normalized distribution over all spatial bins.

$$\omega^s(i) = \sum_{(i)} \omega(i, j) \quad (5.8a)$$

$$\lambda^s(i) = \sum_{(i)} \lambda(i, j) \quad (5.8b)$$

$$\zeta = \frac{|\{S_x | S_x \leq S\}|}{|\{S_x\}|} \quad (5.9)$$

A forecast is assumed to be inconsistent if the quantile score, of either the results of M- or the S-test are very small.

To directly compare forecast methods, an additional indicator for both the S- and the M-test is how close the mean likelihood of the simulated catalogue is to the observation. A method is assumed to be better if the likelihood of the simulated catalogue is closer to the observation.

For the testing procedure of this thesis, a spatial binning of $0.1^\circ \times 0.1^\circ$ is used. The magnitude bins are set into steps of 0.25, starting with the lowest completeness magnitude, e.g. $\{[4.0, 4.25); [4.25, 4.5); \dots\}$. The number of stochastic simulated catalogues must be sufficiently high to provide computational stability. Due to computational issues, 10.000 catalogues are computed for the S-test and 30.000 for the M-test. This different numbers of catalogues is related to the number of bins in each test. The number of spatial bins is in most of the tests in the range of 10^4 to 10^5 while the magnitude bins are in the order of 10^1 .

5.2 The Testing Range

To test the methods appropriately a common testing range is used. Each method shares dataset and spatial discretization. The dataset is restricted both by temporal and spatial boundaries. In total, two different regions have been chosen for further testing.

1. Turkey (Marmara Sea Region)
2. Italy (Central Apennine)

Turkey has been chosen due to the known hazard of a possible upcoming M7 earthquake close to Istanbul, and well defined seismic regions like the Northern Anatolian fault. Furthermore the dataset covers about 1000 years of earthquake observations. Italy has this feature as well, several hundred years of earthquake data reaching back until the Romans. A special interest area is the Central Apennine, which lead to devastating events like the well-known 2009 L'Aquila earthquake. Italy is governed by a vast number of different tectonic settings and is therefore an ideal testing area. Details to the data used will be given in the following chapters together with some statistics of earthquake occurrence for retrospective tests and some general remarks of earthquake observation in for different time periods.

5.2.1 Data

Data used in this study originates from several sources and covers different time periods, depending on the data availability and its corresponding completeness. The completeness periods for different magnitude bins are calculated for each region separately. For both regions, the maximum depth for an earthquake is set to be about 30 km, deeper earthquakes are excluded from the dataset.

For Turkey, the major part of data originates from the joint European-Mediterranean earthquake catalogue (EMEC) [Grünthal et al., 2012], which covers most parts of Europe and the Mediterranean for a period since 1000 until 2006. The remaining data from 2007 until 2013 is covered by the Advanced National Seismic System Worldwide Earthquake Catalog [ANSS].

Italy uses also a combined dataset of two sources in total. For the ancient periods from 0 to 2006 a combination of CPTI04 and CPTI11 [Rovida et al., 2011] is used, CPTI11 represents the currently most recent version of the Italian parametric earthquake catalogue, but it does not include events before the year 1000, so this gap was filled by an earlier version, CPTI04. For the years between 2006 and 2013 the Bollettino Sismico Italiano (BSI) earthquake catalog recorded by the Istituto Nazionale di Geofisica e Vulcanologia (INGV) [Gruppo di lavoro BSI, 2002] was added. Declustering lead just for Turkey for significant changes, while for Italy the b-value only slightly changed.

Region	Turkey	Italy
Catalogue	EMEC & ANSS	CPTI04 & CPTI11 & BSI
First Event	10.11.1000	5.2.62
Last Event	12.10.2013	19.9.2013
Lowest magnitude	5.0	4.5
Number of events	3128	2536
b-value	1.10 - 1.17*	1.35

Table 5.1: Overview of catalogue characteristics. *(declustered & clustered)

The ANSS catalogue provides mostly no moment magnitude scales, if another scale occurred, conversions as shown in figure 2.4 are applied to finally use only moment magnitude scales for each testing region, same holds for the case in the other catalogues if no moment magnitude was provided. As a lower cut-off magnitude, M4.5 and M5.0 have been chosen. This value seems to be a good estimate to cover sufficient small data for the Gutenberg-Richter relation and is still relevant enough and complete for most of the regions to estimate hazardous earthquake occurrence.

Magnitude Range	Turkey	Italy
M4.5 – M5.0	1960*	1750
M5.0 – M5.5	1900	1500
M5.5 – M6.0	1750	1250
M6.0 – M6.5	1500	1000
M6.5 – M7.0	1000	1000
>M7	1000	1000

Table 5.2: Overview of regional completeness periods. *(not applied for time-independent methods)

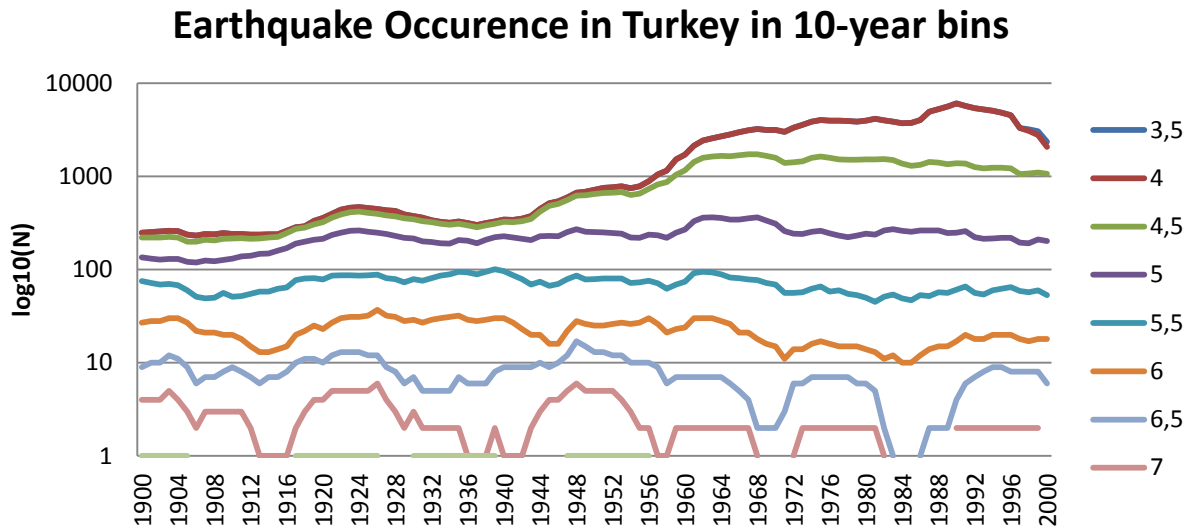


Figure 5.1: 10-year sets of observations of earthquakes in Turkey in bins of $M > 3.5$ to $M > 7.5$. Each point contains the cumulative number of earthquakes of each magnitude bin from the year written on the x-axis and the following 9 years.

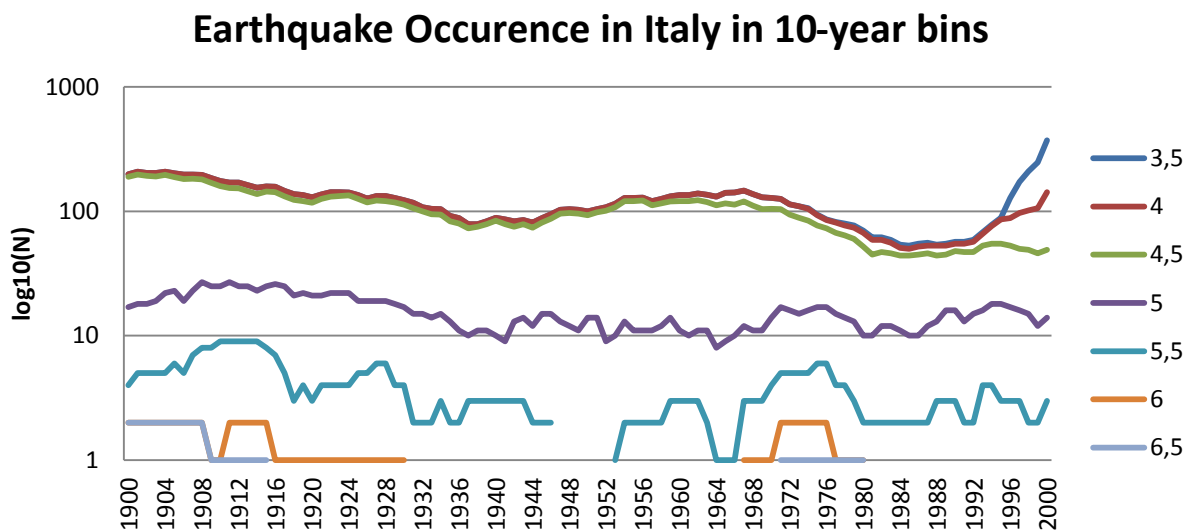


Figure 5.2: 10-year sets of observations of earthquakes in Italy in bins of $M > 3.5$ to $M > 6.5$. Each point contains the cumulative number of earthquakes of each magnitude bin from the year written on the x-axis and the following 9 years.

Another important factor of testing is the decadal occurrence of earthquakes. The testing in the following will be performed in 10-year retrospective tests. Seismicity might vary extremely between different decades. Therefore statistics of earthquake occurrence in 10-year bins have been developed to refer possible failures in testing of the forecasted number of events with variations in seismicity. Figures 5.1 and 5.2 show these statistics for Turkey and Italy respectively

5.3 Test Results – time-independent

The general testing procedure of time-independent methods follows two branches. The first branch picks a certain 10-year time period and tests different values for spatial smoothing to account for variations in the S-Test. After identifying a range of smoothing parameters within the S-Test performs well, this range is additionally tested in up to three more retrospective time periods. The data of the tested time period is removed from the modeling dataset, so that the data used in the test only contains events outside of the testing period. Testing different time periods should check the time-independent nature of the methods, because seismicity might change between different decades and thus might lead to one-sided results if just testing for one period. For example, if the model works well for a certain period it can still happen that it performs badly for another period, so multiple time periods are tested.

5.3.1 Methods & Application on Testing Range

A set of 6 methods has been tested for time-independent mapping purposes. All methods are tested with different smoothing parameters to test spatial forecasting behavior and additionally tested within three retrospective time periods, each of ten years. The time periods have been chosen to be from 1975 – 1984, 1985 – 1994 and 1995 – 2004. For both Turkey and Italy with respect to figures 5.1 and 5.2 these periods represent time intervals with either stronger or weaker seismic activity. The short period of observations of California will be used to identify if the methods work with such small datasets as well. Each test contains the complete dataset excluding the forecasted 10-year period.

No.	Smoothing	GR handling	Parameter	Declustering
1a	Static Gaussian	Regional	Kernel distance	No
1b	Static Gaussian	Regional	Kernel distance	Yes*
2	Dynamic Power-law	Regional	Dynamic range	No
3	Dynamic Gaussian	Regional	Dynamic range	No
4	Static stencil	Regional	Stencil size	No
5	Static Gaussian	Local	Kernel distance GR-smoothing	Yes*
6	Static Gaussian	Local fault-based	Kernel distance	Yes*

Table 5.3: Overview of tested methods within the testing range. (*) Declustering was only applied for the Turkish data.

The time-independent methods composed for this test represent a wide range of different possibilities, testing various smoothing approaches and ideas how to handle the earthquake occurrence rates with the Gutenberg-Richter relation. For the case of a simple static Gaussian smoothing method with regional b-values the effect of declustering is tested in Turkey. Two methods use adaptive smoothing kernels.

Methods 5 and 6 compute local b -values where one additionally uses geographical inferences from fault data. Table 5.3 gives a short overview of the key features of each of these methods.

No.	Turkey	Italy
1a	1000 – 2013*	0 – 2013*
1b	1000 – 2013	n/a
2	1900 – 2013	1750 – 2013
3	1900 – 2013	1750 – 2013
4	1900 – 2013	1750 – 2013
5	1000 – 2013*	n/a
6	1000 – 2013*	n/a

Table 5.4: Overview of data periods for each method, (*) indicate application of completeness

Not all methods are tested at the same level for each region. The main testing range is considered to be Turkey, due to its long period of earthquake observations, its well-developed tectonic features like the North- & East Anatolian faults and the prediction of an upcoming Istanbul earthquake [Parsons, 2004]. Testing range 1, Turkey, will test all features and parameters of the different methods, to identify the best fitting range of parameter values for each approach. This parameter range is afterwards used to minimize the number of necessary tests for testing range 2, Italy. Italy will perform as some kind of verification area of the approaches and their related parameters. Table 5.4 gives the applied overview of testing periods with respect to the different time-independent methods. The calculation of the b -value is independent of these periods, the regional b -values can also be found in table 5.1. The regional b -values used here are calculated on a complete dataset from the onset of each catalogue until its most recent entry. For Turkey, b -values have been computed for the clustered and declustered case, while for Italy almost no difference was observable, so only clustered data was used.

5.3.2 Results

A general phenomenon of the time-independent testing with different 10-year retrospective tests is the extreme variability of seismic activity. While some periods behave within the range of “regular” activity, other decades show a completely different behavior. That is of course in the nature of earthquake occurrence, but not useful for testing purposes. Retrospectively seen, these tests can also be used to determine how much a certain period differs from the observed average, which is in general represented with the time-independent smooth seismicity methods. Thus, in the following, the main focus will be in explaining the likelihood test results of a decade which is assumed to be representative for the general seismic activity. For

Turkey and Italy this period is from 1995 – 2005. Details of the results are focused on this decade, additional information of the results of other periods will be given in advance. The test results of all periods can be found in Appendix C.

At first, a general comparison of all methods was made by using testing range 1, Turkey. One method was additionally tested to compare the effects of declustering and a method (6), which uses local b -value estimates and for which two smoothing parameters were tested, while all other methods have been adjusted by only one parameter. For most of the methods, the smoothing parameter is the smoothing radius around each grid point, in terms of distribution functions the smoothing radius represents the standard deviation. For methods 2 and 3, where adaptive smoothing was used, the smoothing parameter represents the number of event within a circle of variable size must contain. The circle is centered at each grid point and its radius is then the standard deviation of the spatial smoothing distribution. Details about the smoothing algorithms can be found in chapter 4.1.2.

The period from 1995 to 2005 has been chosen to be the starting point of the testing range, because its seismic activity both for Turkey and Italy was relative stable with respect to the historical record. A method is assumed to work correctly if the likelihood estimate of the observation within the forecasting probabilities of a method is larger than the likelihood estimate of arbitrary earthquake catalogues within the forecasting probabilities ($\kappa > 0 \mid \gamma > 0$). The best case would be if the likelihoods of both match exactly ($\kappa = 0.5 \mid \gamma = 0.5$). These values are not given here because they can easily be seen from the plots given in figures 5.3 and 5.4 as long as the red dot, which represents the likelihood of the observation, is either inside the black bar or on the right of it- The black bar shows the 95% quantile of the likelihood distribution of the stochastically computed catalogues. If the red dot is in the middle of the black bar, this result would represent $\kappa = 0.5$ or $\gamma = 0.5$ respectively.

Due to spatial testing, all methods have been able to match the likelihood of the observation appropriately within a certain range of the used smoothing parameters. The magnitude likelihood of the starting period matched almost exactly for most of the methods, except for the methods with local b -value estimates, where these methods overestimated the occurrence of strong earthquakes, while the likelihood was within acceptable ranges. In addition, the test to compare clustered and declustered datasets lead to the result that using a clustered dataset covered the earthquake density better than a declustered one. Similar results are made for the period from 1975 – 1985. The second period from 1985 to 1995 lead to more scattered results. Almost all methods failed the S-Test, and overestimated the M-Test. This was related to the uncommonly calm seismic decade in which neither M7 nor M6.5 events occurred in Turkey, and of course no related aftershocks.

Despite of the relative failures of the local b -value approaches with respect to the other methods, the best fitting smoothing radius for local b -values was calculated to be about 75 km. The other best fitting smoothing parameters are shown in table 5.5 with respect to the testing period.

Testing range 2 – Italy, lead to better results for all periods than testing range 1. Almost all methods passed all tests in all three periods even the local b-value method produced reliable results. This seems to be related to a more “stable” seismic activity in Italy and to a longer and more complete dataset of Italy relative to Turkey. In contradiction to Turkey, most of the methods tended to behave best with rather strong smoothing parameters, while the tests in Turkey lead with relatively small smoothing parameters to good results. Figures 5.5 and 5.6 give examples of how the likelihood behaved based on different smoothing parameters for certain methods applied in testing range 1. Table 5.5 summarizes all results for the best fitting smoothing parameters for the tested methods.

Testing the likelihood of time-independent methods is a good tool to test how well a map of earthquake probabilities represents a certain period of seismicity. The earthquake probability maps which are calculated from such methods are nothing else than the long-term average of e.g. annual seismic activity. In general, these methods compute the earthquake density independent from their magnitude. Thus, due to the completeness of earthquake catalogues the spatial density of earthquakes is overrepresented in regions where earthquakes clustered during the most recent decades. Strong earthquakes come together with fore- and aftershocks of magnitudes which might not be covered in older decades. So locations which had strong events e.g. more than 200 years ago are underrepresented in such density maps because the recording does not contain the clustered activity of smaller magnitudes. That is the reason why no further evaluation of the density maps is given here and another argument that likelihood tests are currently not representative for universal forecast testing but useful to evaluate the seismic activity of certain periods.

Nevertheless, the likelihood tests are a useful tool for evaluation and comparison and will be further applied in this thesis.

Method	Parameter	1995 – 2005		1985 – 1995		1975 – 1985	
		Turkey	Italy	Turkey	Italy	Turkey	Italy
1 st.G	Radius [km]	35	50	>40	50	>40	50
2 d.pl	No. Events [-]	20	10	5	10	5	10
3 d.G	No. Events [-]	25	15	5	10	5	10
4 st.St	Radius [km]	60	150	150	150	70	150
5 st.G-lb	Radius [km]	90	90	90	90	90	90
6 st.G-lb-f	Radius [km]	70	n/a	70	n/a	70	n/a

Table 5.5: Overview of best fitting smoothing parameters. Methods 2 & 3 are adaptive methods for which the minimum number of events within a radius was calculated. The other methods use smoothing radii in km.

S-Test Likelihood Comparison for 1995 - 2005, Turkey

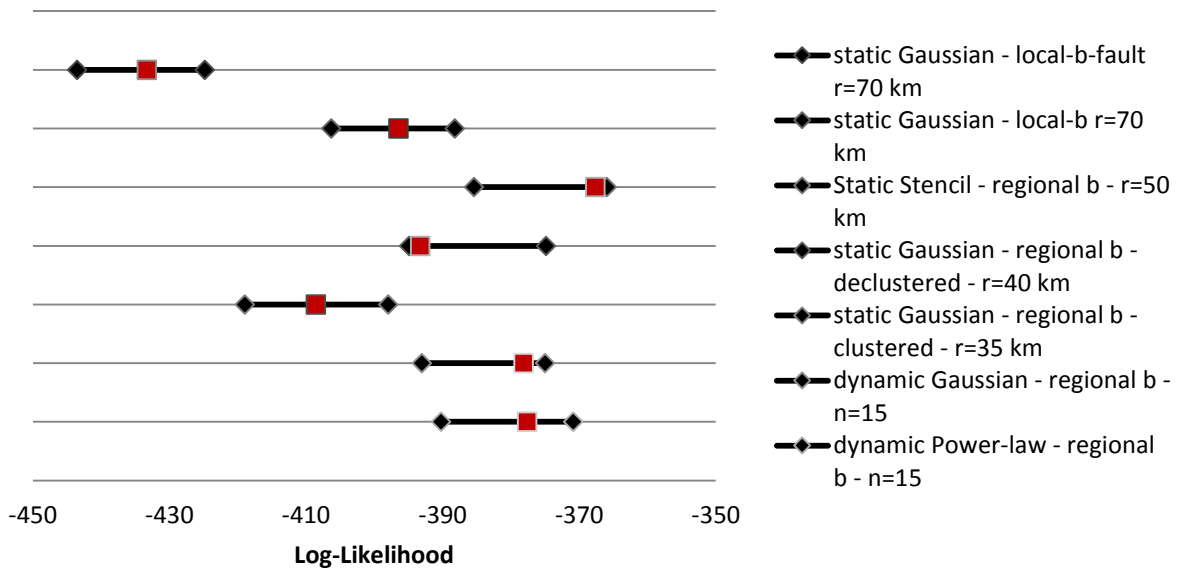


Figure 5.3: Spatial likelihood comparison for the tested methods, where the lines represent the 95% confidence interval of the stochastic earthquake density, and the red point represents the likelihood of the observed events. Applied on Turkey of the period from 1995 to 2005.

M-Test Likelihood Comparison for 1995- 2005, Turkey

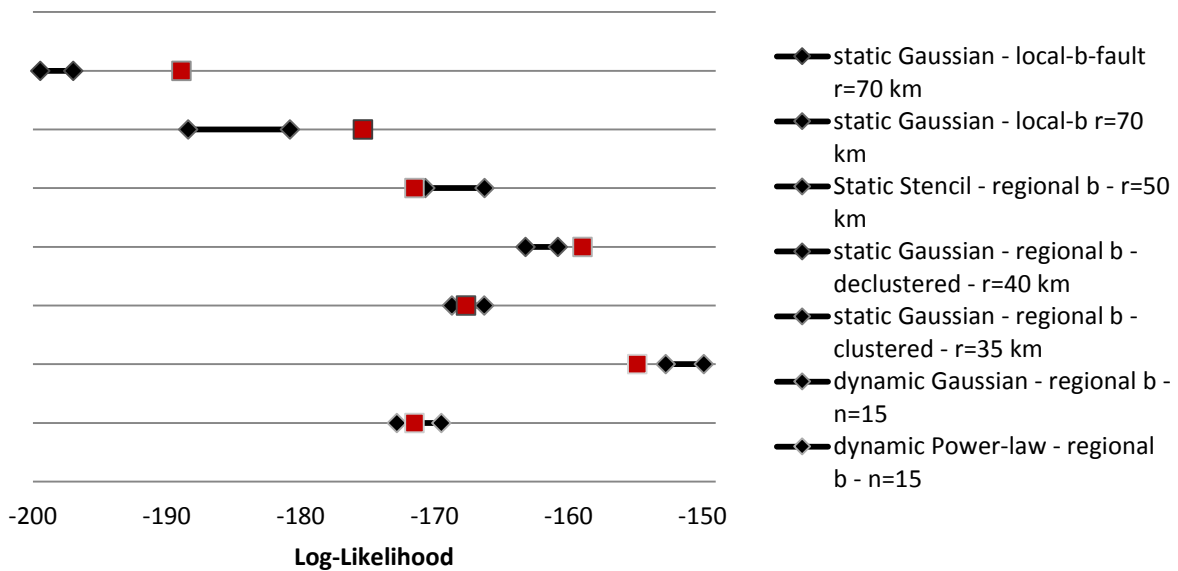


Figure 5.4: Magnitude-based likelihood comparison for the tested methods, where the lines represent the 95% confidence interval of the stochastic earthquake density, and the red point represents the likelihood of the observed events. Applied on Turkey of the period from 1995 to 2005.

S-Test Likelihood Comparison for 1995- 2005, Italy

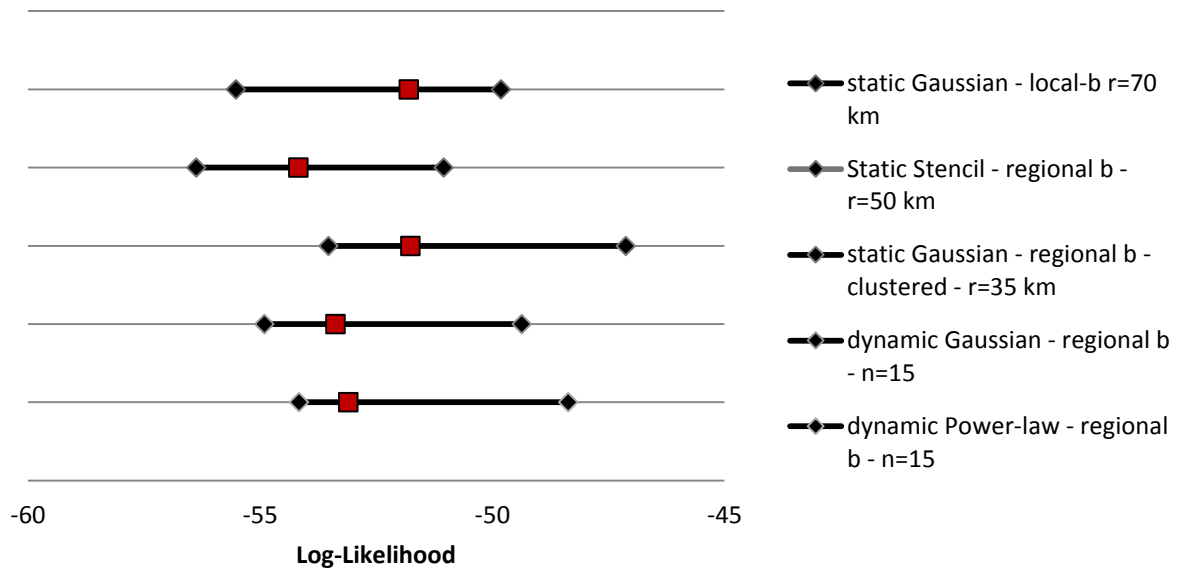


Figure 5.5: Spatial likelihood comparison for the tested methods, where the lines represent the 95% confidence interval of the stochastic earthquake density, and the red point represents the likelihood of the observed events. Applied on Italy of the period from 1995 to 2005.

M-Test Likelihood Comparison for 1995- 2005, Italy

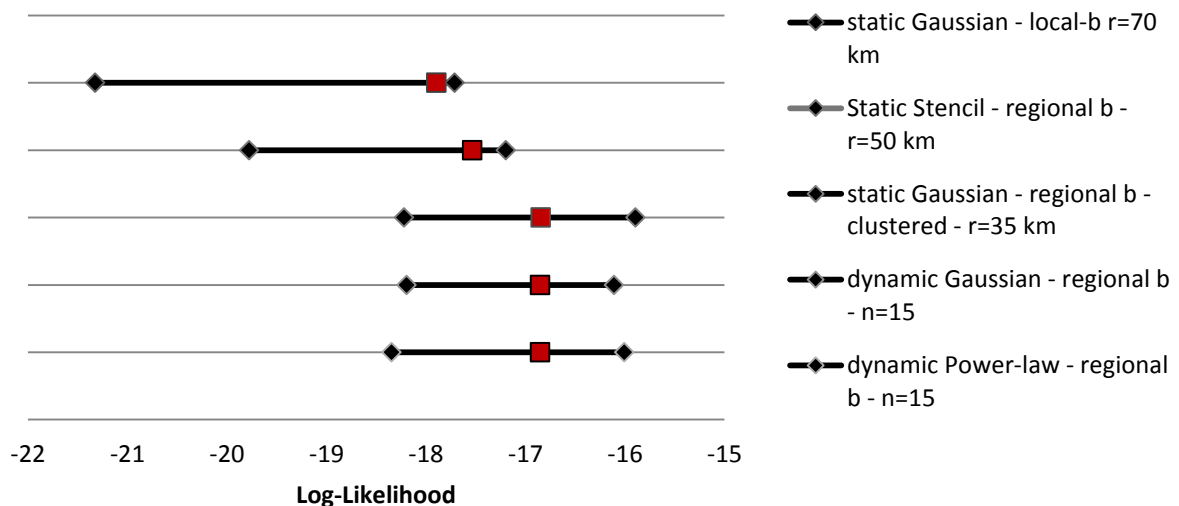


Figure 5.6: Magnitude-based likelihood comparison for the tested methods, where the lines represent the 95% confidence interval of the stochastic earthquake density, and the red point represents the likelihood of the observed events. Applied on Italy of the period from 1995 to 2005.

S-Test for adaptive kernel methods

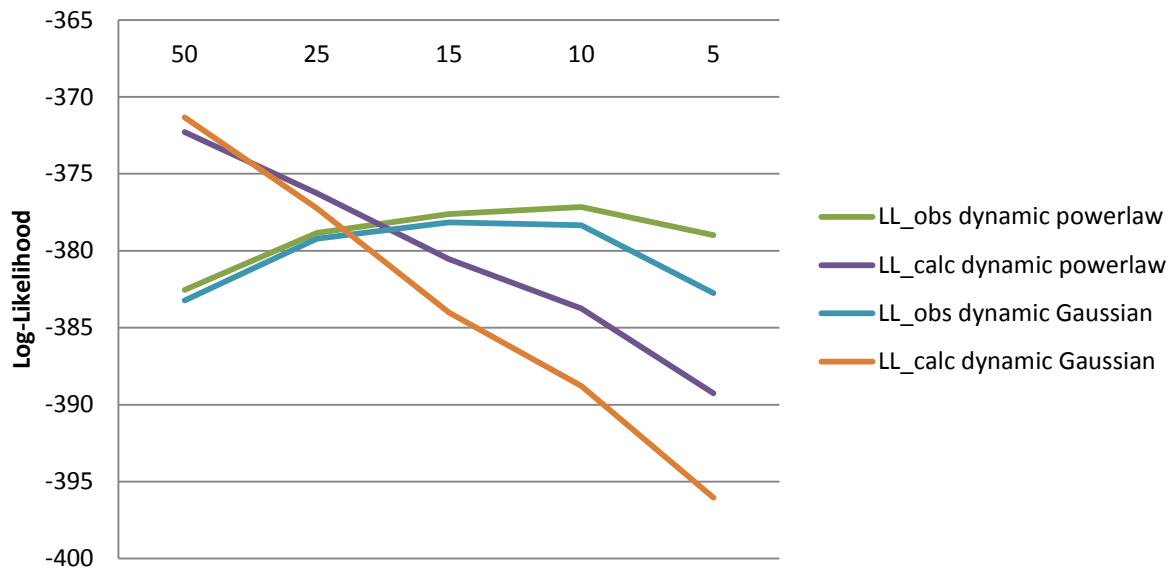


Figure 5.7: Likelihood results for different smoothing parameters of the adaptive smoothing method, applied on Turkey of the period of 1995 – 2005.

S-Test for static Gaussian methods

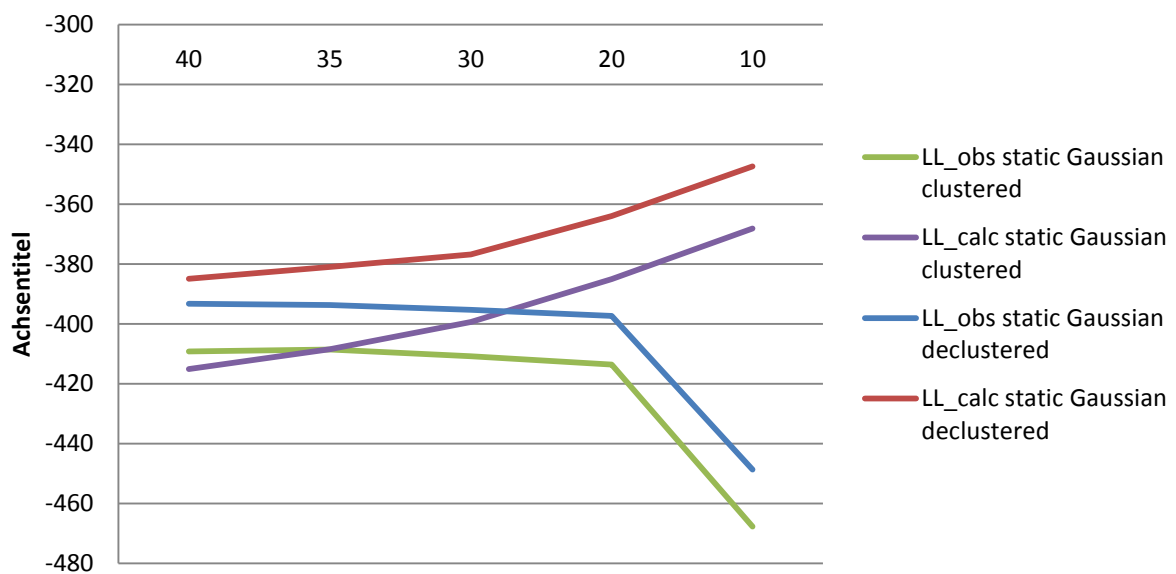


Figure 5.8: Likelihood results for different smoothing parameters of the static Gaussian smoothing with either clustered or declustered datasets, applied on Turkey of the period of 1995 – 2005.

5.4 Test Results – time-dependent

Three methods are tested for time-dependent purposes. The first one, the Pattern Informatics (PI) method is used to identify regions which are more susceptible to future large earthquake than the common average. The epidemic-type-of-aftershock-sequences (ETAS) methods, which has been introduced in chapter 4.2.2 is used to identify aftershock activity and to separate it from the background seismicity. The last method uses time-dependent b -value estimates to identify regions which are close to rupture.

The tests for time-dependent methods are simple with respect to the time-independent approaches. The methods are tested for multiple time periods, which are known for certain activity in a certain region. The PI method and the time-dependent b -value approach are used to identify known large target events, like the 1999 Izmit earthquake in Turkey or the 2009 L'Aquila event in Italy. The ETAS algorithm is evaluated in two ways; one tests the background seismicity the same way like the time-independent methods, while the second one tests the forecasted number of aftershocks after certain large events.

5.4.1 Test Results – Pattern Informatics

The PI method is used to identify locations which are prone for future earthquakes. It assumes that changes in seismicity from the average are precursory signals for future earthquakes for a certain location, so called hotspots. Testing the results of the PI method is based in comparing hotspot locations with the locations of observed earthquakes of a certain period.

Parameter	Turkey	Italy
Minimum magnitude	M5.0	M4.0
Total intensity period	1500 – 1985	1500 – 1985
Reference period	1900 – 1985	1900 – 1985
Learning period	1986 – 1995	1986 – 1995
Change period	1996 – 2013	1996 – 2013
Time increment	6 months	6 months
Spatial resolution	30 x 30 km	30 x 30 km

Table 5.6: Overview parameters for the two testing regions of the PI method.

The method follows in general the description in chapter 4.2.1. Most important parameters to calibrate this approach are the resolution of spatial discretization, the learning and testing periods and the resolution of intensity intervals, which represent the increments of the time intervals. The test was performed for Turkey and Italy with slightly different sets of parameters.

The method uses the most active regions during the total intensity period as proxy information about generally active regions. For Turkey all earthquakes with $M_c \geq 6$

are used for the total intensity map, for Italy all earthquakes with $M_c \geq 5$. For the comparison of the different time increments, the threshold magnitude is set to $M_c - 1$. For the pattern search, the top 50% active regions are used, [Holiday et al., 2005] used the 10% most active regions for Japan and California, this change is reasonable because both the general seismicity is weaker and the dataset in general has a larger magnitude threshold and thus less events to generate the statistic. For identification of these regions a time-independent smooth seismicity approach with an adaptive power-law kernel is applied.

The reference time interval is chosen to be from 1900 to 1985 with time increments of 56 months, both larger and smaller increments have been tested. For smaller increments almost no changes are observable, while the resolution for larger increments gets blurred out. The change interval from which the change in seismicity is observed is chosen to be from 1985 to 1995. The following years from 1996 to 2013 are the testing years, where the earthquakes occurred which will be forecasted with the PI method. The forecast finally consists of a set of cells which observed a strong change in seismicity. An earthquake is assumed to be appropriately forecasted if it occurred inside or close (e.g. ~ 10 km distance) to an indicated cell. As it can be seen from table 5.7 and figures 5.9 and 5.10 the PI method fails almost totally for Italy, including the L'Aquila earthquakes, and reaches a 50% score for Turkey, containing the Izmit event but not the Düzce earthquake. The target earthquakes have been chosen to be $M_c + 0.5$, which represents the mean value suggested from [Holiday et al., 2005].

Region	Observed	In Forecast
Turkey	4	2*
Italy	9	2*

Table 5.7: Results of PI Method testing. *An earthquakes is assumed to be part of the forecast if it was observed at least directly adjacent to an indicated cell.

The failure of the PI method seems to be related to the lack of sufficient data. The change in seismicity which is used as precursory information is better observable for smaller magnitudes. Furthermore is the definition of the top 50% active regions strongly dependent on the dataset and its completeness. A correlation of failure with the date of occurrence of a certain earthquake was not visible,

The results of [Holiday et al., 2005] and [Holiday et al., 2007] are made for Japan and California, two regions with the best developed seismic observations, where even M5 earthquakes occur relatively often. The observation of seismicity changes of M4 or M5 earthquakes in Italy and Turkey over 100 years cannot account for large scale seismicity changes as needed for the PI method. The fact, that the Italian test contains more small events than the test for Turkey is a contradiction because the Turkish test leads to better results, so it is assumed that the incorporation of at least M3 or M2 earthquakes is necessary. In addition the theory to use seismicity changes over years as a general indicator for future earthquakes is questionable. Using

foreshocks as indicators of an upcoming future large earthquake is in general a matter of weeks to hours and also again accounts more for small earthquakes with magnitudes $<M4$. To account for foreshocks as a precursor, it is necessary to increase the temporal resolution in the scale of days together with the resolution of magnitudes in the data. This additionally restricts the dataset on the last couple of decades of observation.

Using information of the most active regions of the past is further more misleading because the change in spatial seismicity cannot occur outside of regions where strong events happened in the past, so seismicity is not allowed to migrate outside of these regions. Another element which should be improved is related to the time increments. To improve the results, the algorithm could be expanded to account for temporal and spatial completeness. Furthermore, the method should be improved in terms of which regions with seismicity changes should be taken into account and not just certain active regions of the past. With a transformation from a location identifier to a daily alarm-based method which incorporates all earthquakes with magnitude $>M2$ without restrictions by past observations it might be possible to increase the success rate.

In conclusion, the PI method does not generate reliable forecasts in its current version, the ration between indicated regions and locations where are forecast was successful was way too high. It could be used as a secondary indicator to observe long-term changes in seismicity but not as an a priori predictor.

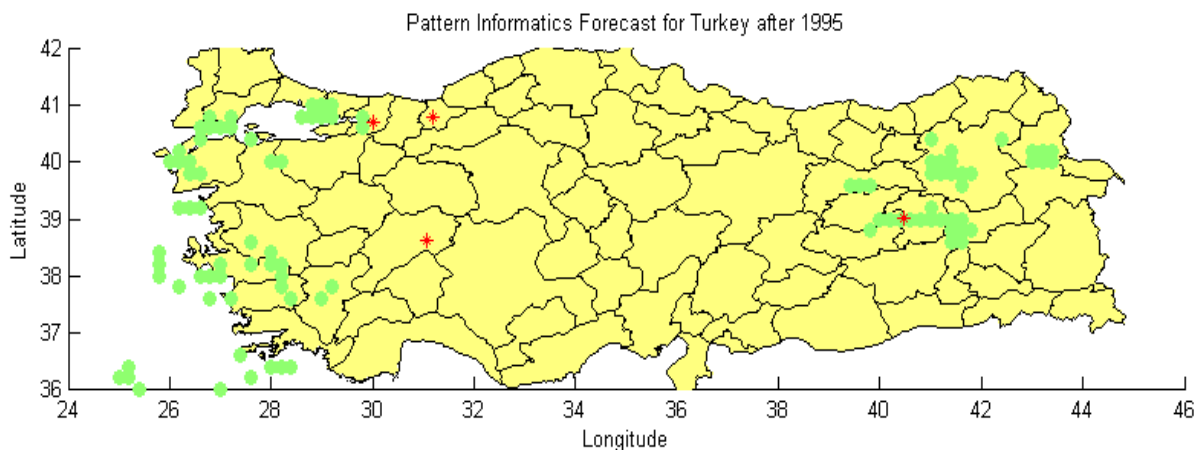


Figure 5.9: Mapping of the PI method for Turkey. The green zones represent hotspot regions for future earthquakes, while the red dots show the observed earthquakes from 1995 to 2013 with magnitude $>M6.5$.

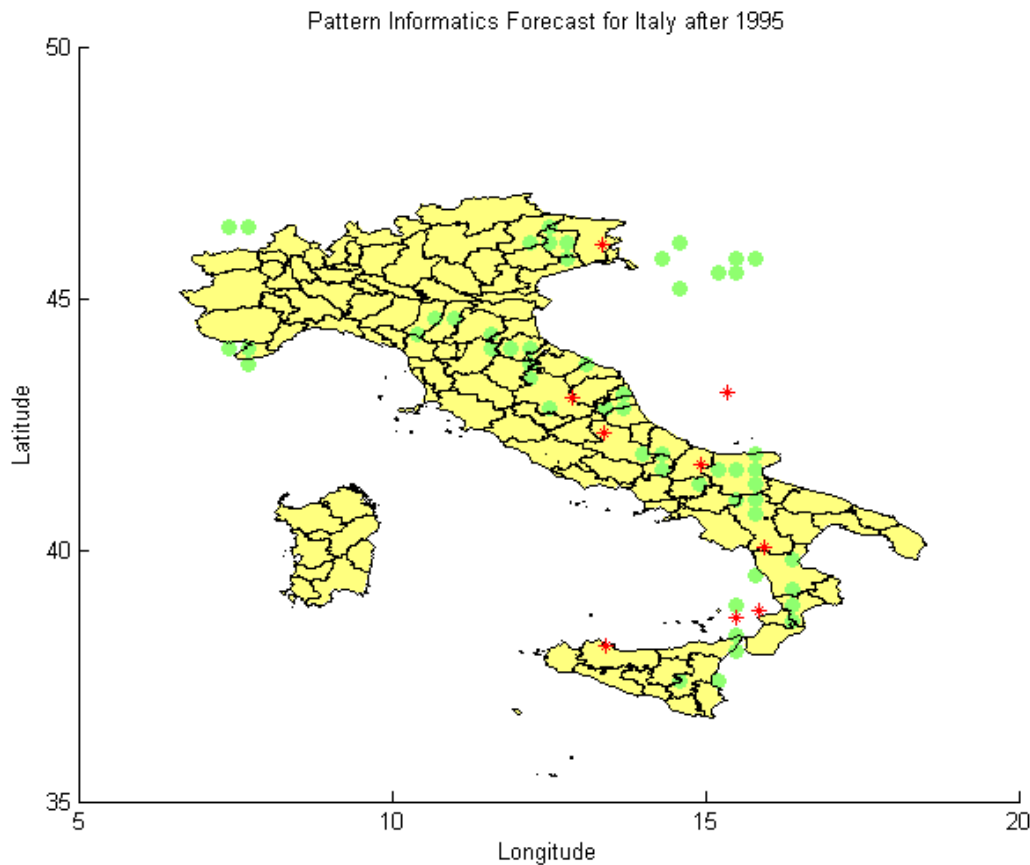


Figure 5.10: Mapping of the PI method for Italy. The green zones represent hotspot regions for future earthquakes, while the red dots show the observed earthquakes from 1995 to 2013 with magnitude >M5.5.

5.4.2 Test Results – Time-dependent b -value

The time-dependent b -value method, based on specific data of fault segments is tested for Turkey. The test basically follows the approach of time-independent testing on the one hand and additionally in comparing time-independent with time-dependent hazard maps.

The model uses the fault data of Turkey from the SHARE fault database of Europe [Basili et al., 2013] and follows the description of chapter 4.3, where it is explained in detail how the time difference since the last event of a certain magnitude at a fault is connected to the average interevent time to generate time-dependent b -values. Thus, a declustered version of the Turkish dataset is used, containing the earthquakes from 1000 to 1995. Therefore the declustering algorithm of [Reasenber, 1985] was applied. The testing period is chosen to be from 1995 to 2005, which includes the Izmit earthquake in 1999 as a testing proxy. The general likelihood of both the time-independent test and the time-dependent is compared to show which approach leads to better estimates of future seismicity. The declustering was used to avoid further overrepresentation of recent decades in the distribution of b -values.

Testing the likelihood of the hazard map itself did not lead to any significant increase of the forecast's quality and is of course due to the finding of the time-independent methods not really necessary, but the hazard map is still consistent with observation within its probability range of time-independent approaches.

Thus, it is more important to test whether the change in local seismicity rates lead to any links of observed earthquakes. The changes in seismicity rates are only marginal taking the absolute values, rates for magnitude 6.5 vary in range of $[2 * 10^{-3}, 10^{-4}]$. However, taking these changes as a priori information to indicate regions where larger earthquakes are more likely to occur, it is significant. Figure 5.11 shows a map of the seismicity changes together with all earthquakes of magnitudes $>M6.0$ from 1990 until 2013. 8 earthquakes occurred within the testing regions, 3 earthquakes happened in areas with higher seismicity (including the Van 2011 event), while 6 events hit a region with either seismicity decrease or even no change in seismicity.

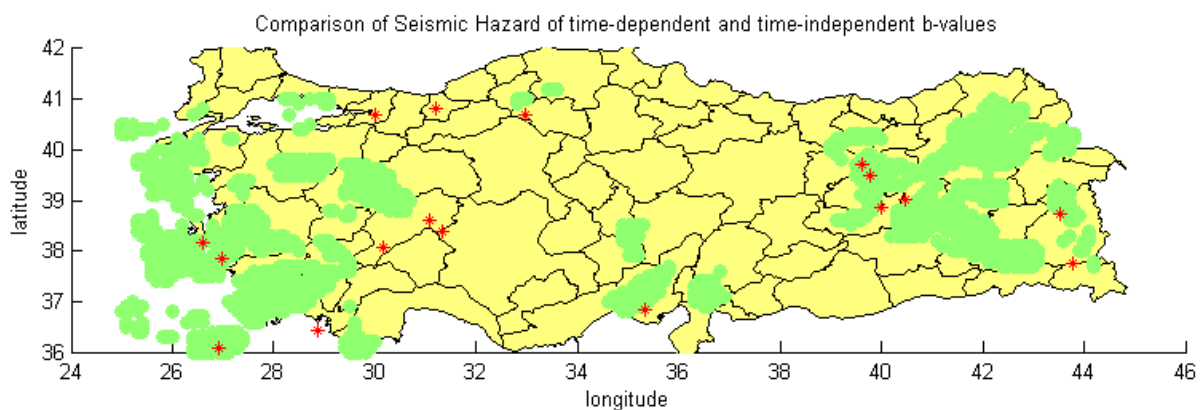


Figure 5.11: Difference of the seismicity rates between the time-dependent and time-independent approaches. The green areas are regions where a change in seismicity rates have been observed and future earthquakes are awaited. Red dots show observed earthquakes between 1995 and 2013.

This result can be seen as a success of this method, even with a success rate of about 50%, but not including the Izmit and Düzce earthquakes of 1999. Nevertheless the method needs improvement. The hazard map still does not indicate any hot spot regions, furthermore the method is restricted to the information of local faults and can only be as good as the fault geometry and resolution. In addition, the method currently uses rather simple assumptions to distribute historical events over the fault data to calculate the b-values. Thus, the algorithm needs a lot more refinement, but as a first attempt to introduce time-dependent b-value calculations, the method can be used as a working alternative to time-independent calculations. Furthermore the ratio between regions which are indicated to be prone to future earthquakes and location where an earthquake was observed is still too high but definitely not worse as the ration of the PI method, which is a more well established and developed approach.

5.4.3 Test Results – Epidemic Type of Aftershock Sequences

The ETAS method separates independent background seismicity from the aftershock seismicity. With this strong element of short-term forecasting a simple separation is applied to test this method in two ways. The first way tests the background seismicity with the same testing procedure as the time-independent methods. The second way investigates the occurrence of aftershocks by reviewing the aftershock activity after the 1999 Izmit and Düzce earthquakes close to the Marmara Sea.

The ETAS algorithm adjusts its parameters on its own based on a stochastic likelihood process. The dataset used, covers all years from 1500 until the onset of the testing period containing all earthquakes with magnitude $>M5$. The data has to be non-declustered because the algorithm itself represents a declustering process by separating aftershock activity from the background seismicity.

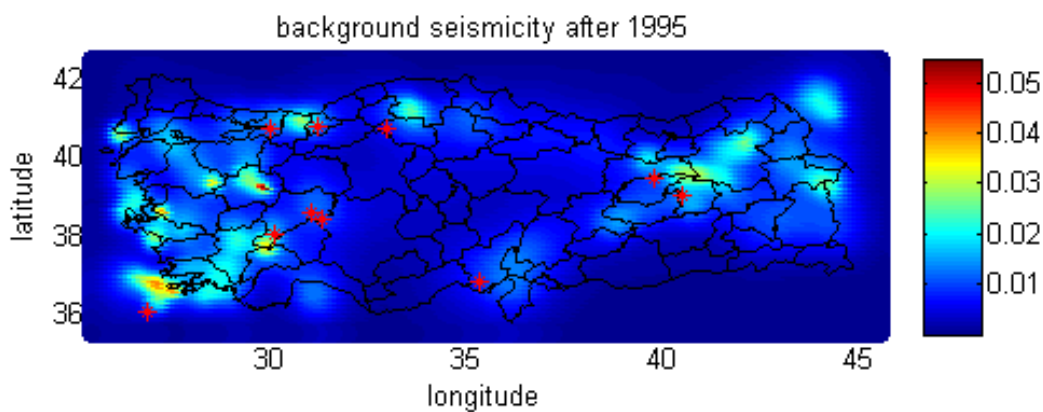


Figure 5.12: Map of forecasted background seismicity after January 1, 1995 in Turkey. Color scale shows the annual earthquake activity of magnitudes $>M4.25$. Red dots indicate earthquakes of magnitude $>M6$ from 1995 to 2005.

In general the stochastic tests both for spatial and magnitude likelihood were very successful, each tested 10-year period from 1985 – 1995, 1990 – 2000, 1995 – 2005 and 2000 – 2010 were forecasted within the probability range of the background seismicity, even for the first period from 1985 – 1995, the ETAS method outperforms most of the time-independent approaches of chapter 5.3. In comparison, the likelihood forecast for the magnitude range was better than the spatial forecast. This was related to the relative over precision and high resolution of the ETAS smoothing algorithm but was still in the range of successful testing.

The results can be seen in figures 5.12 and 5.13. It should be noted that the direct results of the ETAS algorithm calculated annual rates for $M4.25$ earthquakes for the background seismicity, while implementing a magnitude threshold of the dataset of $M5$. A similar scaling law holds for the calculation of aftershock seismicity, where the calculated daily rates fit for $M2.75$ earthquakes.

To test the accuracy of aftershock seismicity, multiple earthquake density maps with pure aftershock content have been calculated and compared to the observed earthquakes within a certain time period. In addition, the aftershock activity of 4

months has been calculated and compared to the observed number of earthquakes. With the application of the above mentioned scaling law the rates fit the observed seismicity very good.

In general the ETAS algorithm works quite well both for independent background seismicity earthquake density maps and for aftershock seismicity. The code used in this thesis should be further improved to avoid the mentioned scaling problem and the incorporation of e.g. fault data for a better spatial resolution of aftershock occurrence should be a useful advancement. Furthermore for the development of a time-dependent earthquake forecast containing independent and aftershock seismicity a complex stochastic model is necessary which currently needs more calculation power than a normal personal computer can offer. Both are task to encounter in the future.

Observation vs. Calculation - 1999 - Izmit M7.1

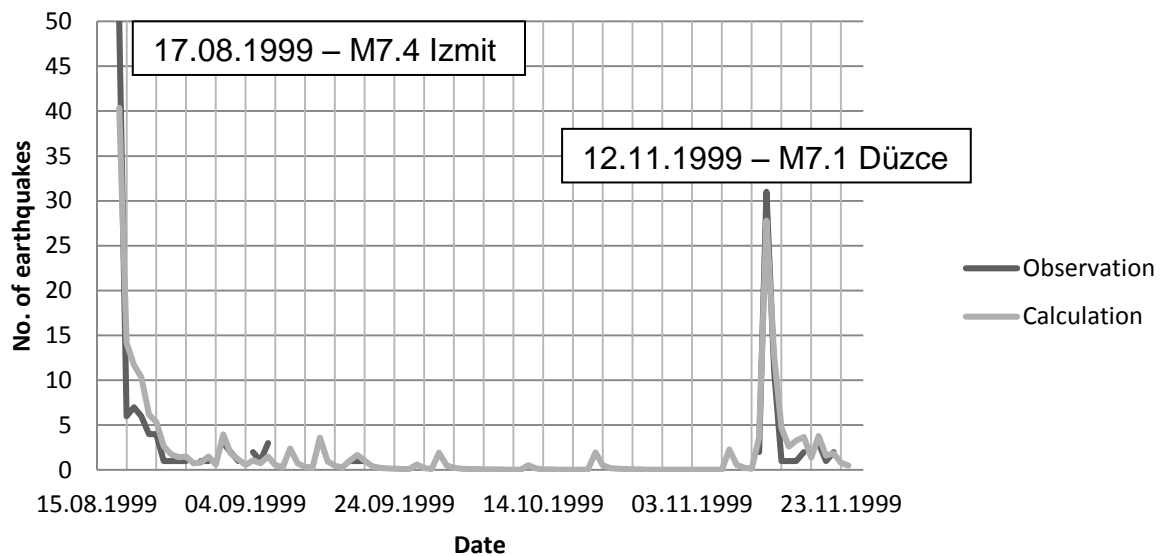


Figure 5.13: Comparison of aftershock seismicity of M4 – M5.5 earthquakes after the 17.08.1999 Izmit earthquake.

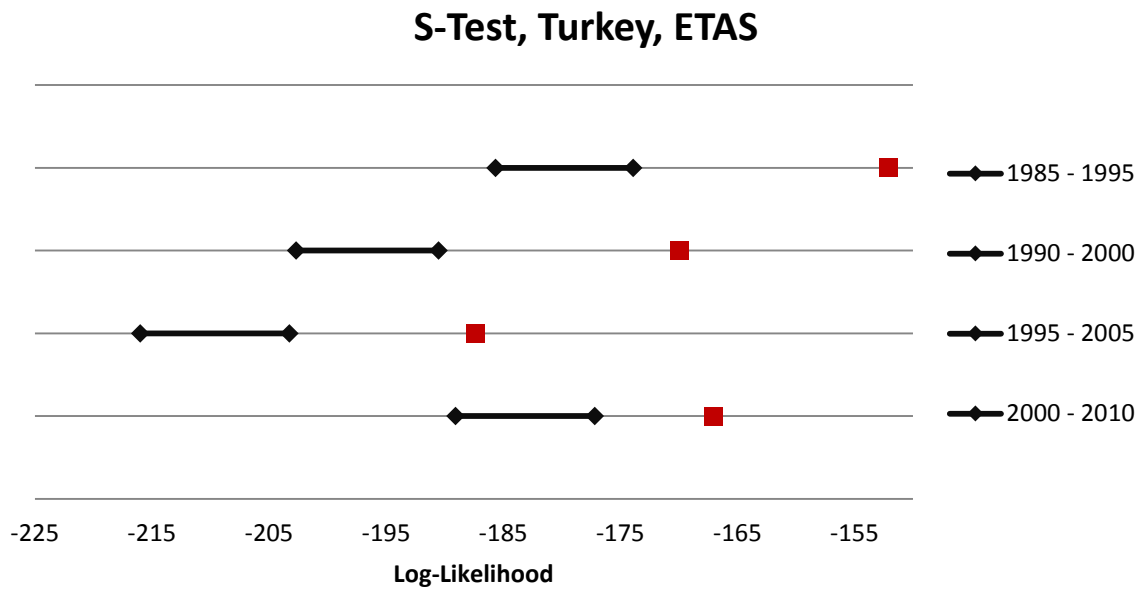


Figure 5.14: Spatial likelihood comparison for the ETAS method, where the lines represent the 95% confidence interval of the stochastic earthquake density, and the red point represents the likelihood of the observed events. Applied on Turkey for different time periods

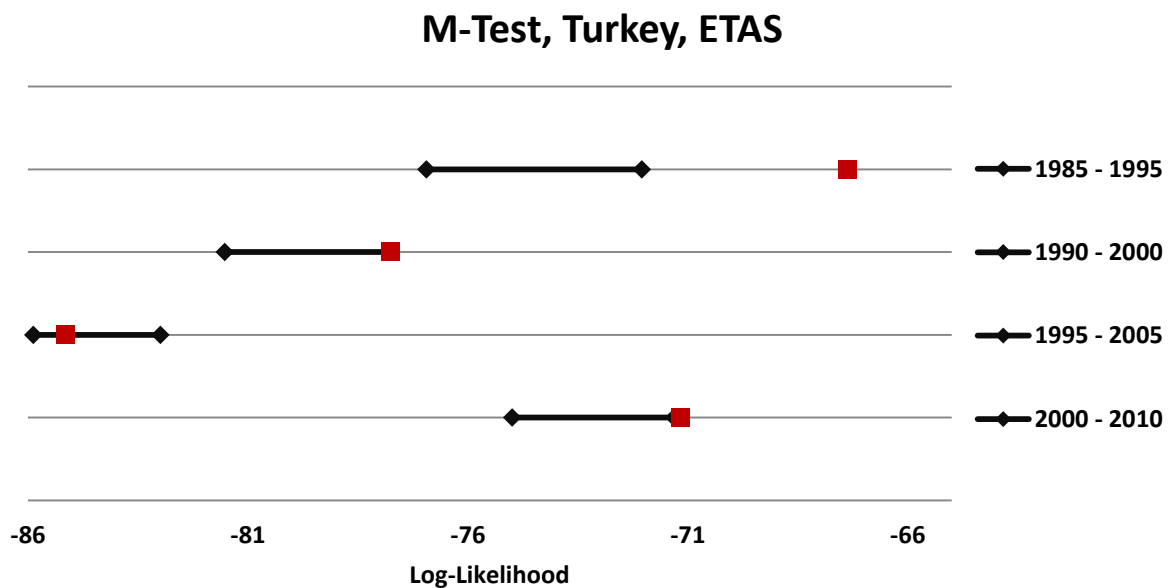
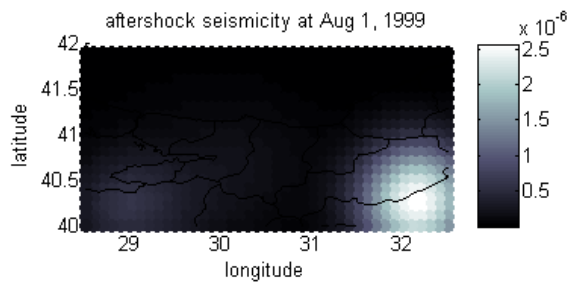


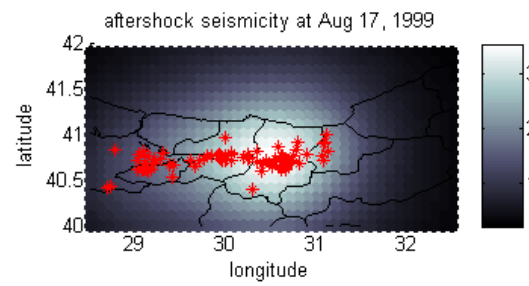
Figure 5.15: Magnitude-based likelihood comparison for the ETAS method, where the lines represent the 95% confidence interval of the stochastic earthquake density, and the red point represents the likelihood of the observed events. Applied on Turkey for different time periods

5 Testing

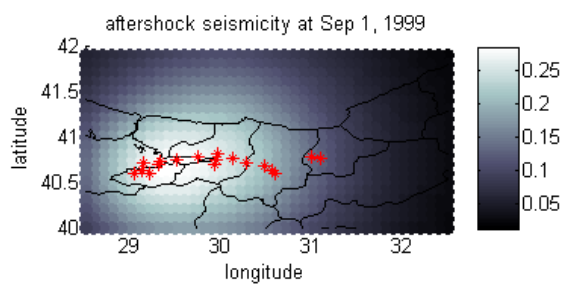
a) observations: 01.08.1999 – 16.08.1999



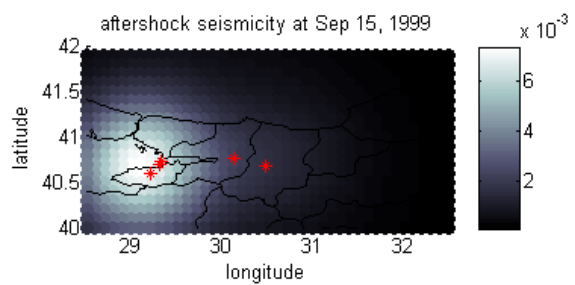
b) Izmit event $M_w = 7.4$
observations: 16.08.1999 – 31.08.1999



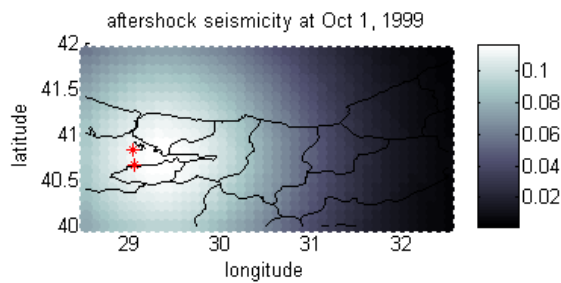
c) observations: 1.09.1999 – 15.09.1999



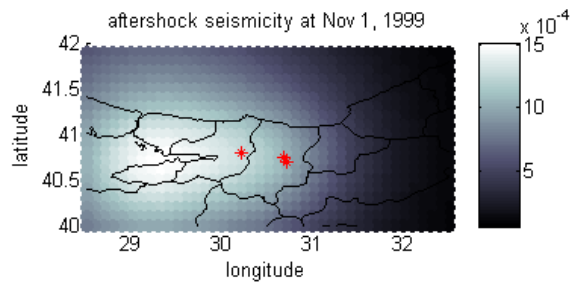
d) observations: 15.09.1999 – 30.09.1999



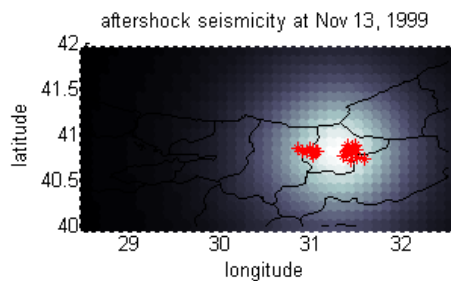
e) observations: 1.10.1999 – 31.10.1999



f) observations: 1.11.1999 – 12.10.1999



g) Düzce event $M_w = 7.1$
observations: 12.11.1999 – 30.11.1999



h) observations: 1.12.1999 – 31.12.1999

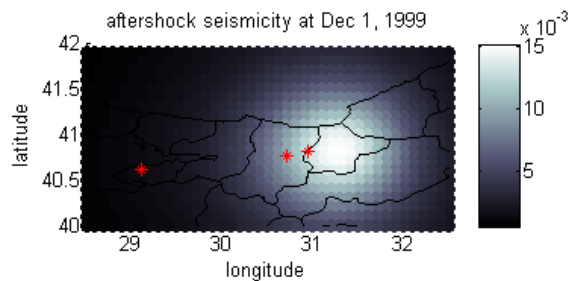


Figure 5.16: Aftershock calculated aftershock activity for the Izmit and Düzce earthquakes. Red dots indicate earthquakes of a certain period after the indicated date. The color scale shows the forecasted daily rate.

5.5 Test Conclusion

Testing earthquake forecasts is a complex task. Both tests and tested methods should be developed and calibrated carefully. Especially the data must be treated well with respect whether a method needs clustered or declustered data and which magnitude threshold is useful and applicable for certain regions and periods.

After testing 6 time-independent and 3 time-dependent approaches, it is obvious that time-independent methods did not reach their initially assumed level of quality. Changes in certain parts of the algorithm generally lead to only minor changes in the overall likelihood, moreover the testing of time-independent methods is rather a test whether the tested period occurred within the range of average seismicity or if the seismicity changed with respect to the long-term average than a real test of the reliability of a forecasting approach. Thus, the period of 1985 – 1995 in Turkey was a quiet time, where no large earthquakes hit the country. Such an activity is far away of the long-term average leading to bad results in likelihood tests. Additionally if earthquakes migrate into a former quiet region, which was not covered by the data catalogue, the likelihood tests fail again.

Nevertheless all time-independent methods tested above are useful for the development of seismic hazard maps, but with relatively small differences according to the different approaches it is advised to use the simpler versions. If for example two methods reach relatively equal results, the method with less complexity and assumptions is preferred. That is why for example approaches with local b -value estimates shouldn't be used for time-independent forecasts. Another struggle of time-independent methods is the overrepresentation of recent decades, but this could either be solved by stochastically filling the dataset with smaller earthquakes as after- and foreshocks of older strong earthquakes or by a significant increase of the completeness magnitude. While the second approach is not advisable, the first would need a thesis on its own to account for all possible parameters.

For time-dependent tests the PI method performed not as good as firstly assumed. This might be related to the data used, containing only larger earthquakes where such necessary changes in seismicity are barely visible. It also shows how hard it is to link future earthquakes with changes in past seismicity. Both the development of foreshocks and quiescence is also more a short-term observation than a long-term, appealing to e.g. month- or even daily-based forecasts instead of annual.

The ETAS algorithm is a complex alternative to classic time-independent forecasts, but lacks in spatial accuracy due to overprecision. One way to solve this would be additional smoothing. The ETAS code used in this thesis additionally needs further scaling of the calculated seismic rates both for the independent background seismicity and the aftershock activity. However with the application of such a scaling law, the results look promising. Future developments should be related to long-term and short-term forecasts incorporating aftershock activity into a stochastic model.

The development of time-dependent Gutenberg-Richter relations is also promising, especially by comparing the final seismic rates with time-independent results to

indicate regions which might be more susceptible for future earthquakes. The current version is still an early development which should be further improved, with respect to spatial handling of earthquakes and the impact of the relation of time since the last event and the average interevent time.

In conclusion, the time-independent methods can cover nicely the long-term average of earthquake activity, but the forecast is only as good as the actual seismicity that occurs within its long-term averages, changes are not covered. Testing these methods is also linked to such seismicity changes and should be further improved. Time-dependent methods are still under development and should be further calibrated. Currently some results look promising, but are still not good enough to give sophisticated time-dependent forecasts.

Aside from that the introduction of the fault-related b -value method both for time-independent and time-dependent approaches, which was developed by the author, shows that even methods, which have been assembled in a relatively short time can compete with well-known methods and algorithms. Thus, the test results do not even differ so much in quality and accuracy. This shows that is in fact no very hard to generate a method that computes some kind of forecast, but to advance the accuracy of the forecast in a way that it significantly outperforms any other method is the real hard task to encounter in the future.

6 Hybrid Method Development

This chapter introduces a newly developed method, the Slip Accumulation Method (SAM) to identify regions of future strong earthquakes. The identification algorithm is based on the spatial distribution of fault slip rates. Firstly, the basic idea is introduced while afterwards the theory behind the method will be explained in more detail. Finally it is shown how this idea is forged into a working algorithm that is able to produce reliable forecasts and hazard maps.

It should be noted that this is a fast sample approach for a hybrid method. Its theoretical and scientific expression might not be as well developed as a method which was created by known research groups or scientists, but will rather be used as an example how to apply and implement additional data and forecasting algorithms to finally use them as indicators for future earthquakes.

6.1 Idea

The basic idea for the development of the hybrid method relates to the analysis of strain accumulation along faults. For data input, a map of faults is used with information of the annually accumulated slip. This data is provided by the SHARE fault database of Europe [Basili et al., 2013] and will be applied on Turkey and Italy in the following description.

The slip accumulation is distributed spatially around each fault with a linear decrease with distance. Between certain earthquakes the slip accumulates and gets finally released during strong events. Therefore data of rupture length and slip is necessary. This is solved with the respective magnitude relations proposed by [Wells and Coppersmith, 1994].

The same way of spatial increase of strain around a fault, the slip is released around the 2D rupture fault line of strong earthquakes. The accumulation of slip is furthermore linked with the general earthquake density above a certain magnitude threshold to avoid accumulation of slip in regions of creep, where the slip is not covered by strong earthquakes. Finally regions with a strong accumulation are assumed to be locations of future large earthquakes.

How well this approach works can be tested by producing maps of accumulated slip until a certain date and comparing them with the next decades of strong earthquake activity, e.g. magnitudes $> M6.5$. There are multiple sources of uncertainty which have to be considered and taken into account during the evaluation of the results.

1. Fault data is incomplete or not correct
2. Linking of earthquake density with strain accumulation is incomplete due to magnitude-dependent temporal completeness
3. Uncertainties of the conversion of rupture length and slip
4. For simplification, all earthquakes are assumed to be strike slip.

However, these uncertainties are considered to be tolerable with respect to the fact that this approach is rather a first test if the idea works in general. Detailed method calibration and development in general needs multiple months or years of work and cannot be covered in this thesis.

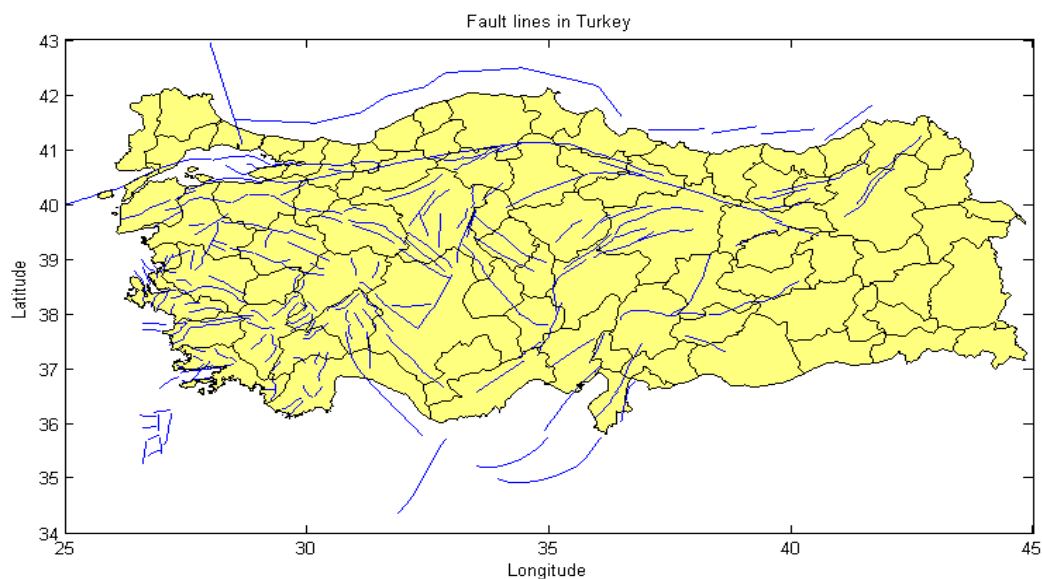


Figure 6.1: Distribution of fault lines in Turkey using fault information of the SHARE fault database [Basili et al., 2013].

6.2 Theory

Basically this hybrid method can be considered to be a renewal method. However, while most of the other renewal methods use purely probabilistic elements, like beta distributions or Weibull distributions [Zhuan et al., 2012], the method introduced here uses direct spatio-temporal loading based on fault-related slip rates. Both can be explained by the elastic rebound theory [Reid, 2010]. This simply means that as longer it has been since the last large earthquake the more probable is the occurrence of a future large earthquake within a certain region.

The theory can be basically divided into two parts. The first one is about how to implement the data provided by historical earthquake catalogues and what kind of data is provided by the fault model. The second one is how to calculate spatial strain accumulation in this method and how it is released afterwards with the help of the introduction of a simple mechanical model.

6.2.1 Data

To assemble a slip-rate method two kinds of data are necessary. The first one covers the faults – the strain source, while the second one covers the earthquake observation – the release by surface slip.

The SHARE fault database provides a lot of information about faults all over Europe, especially important for the method introduced here is the fault's strike angle and its associated slip rate. In addition, the data provides the range of strike angles of the earthquakes that occurred along the fault. It is assumed that the maximum slip of a fault accumulates in an area of about 10 km to both sides of the fault lines. This broad area should cover spatial uncertainties because the faults are often not as distinct as a straight line. The surface expression often follows such a straight line, but earthquakes occur often also kilometers away from there. Each fault is generally divided into several fault segments with common fault parameters. Each segment represents a straight line. Historical catalogues often do not provide information of the strike angle of ancient earthquakes the strike angle range given by the fault database is necessary for the spatial distribution of slip release.

Unfortunately historical catalogues do not provide any information about rupture length and rupture slip. Reasonable of course because there has been no way to measure these scales directly, even most of the magnitudes are just estimates from geology or historical documentation derived from intensity observations. However, there are a couple of relations which can be used to convert magnitude scales into rupture length L , average rupture slip AD and additionally rupture width W . Following the description of [Wells and Coppersmith, 1994] and using the combined version for general focal mechanisms of [Chan et al., 2010] leads to the following relations

$$\log_{10}(L) = -2.44 + 0.59 * M_w \quad (6.1)$$

$$\log_{10}(W) = -1.01 + 0.32 * M_w \quad (6.2)$$

$$\log_{10}(AD) = -4.80 + 0.69 * M_w \quad (6.3)$$

There exist several alternatives of conversion functions and of course the differentiation by earthquake type and focal mechanism. However for the sake of simplicity the above stated relations are used.

Combining information of both data sources provides enough data to calculate the spatial accumulation of fault slip and its release.

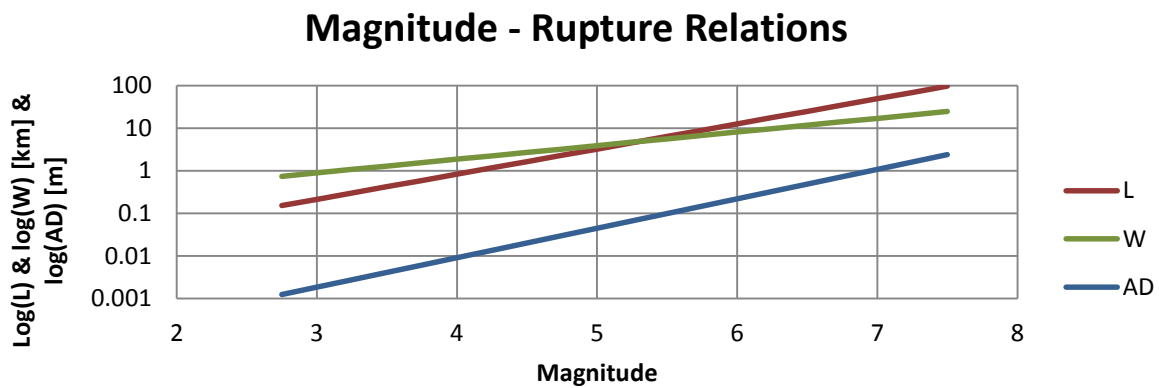


Figure 6.2: Relations of magnitude scales to rupture parameters for general focal mechanisms, following [Chan et al., 2010].

6.2.2 Slip accumulation and release

The accumulation of slip follows a linear distribution function by distance from a fault. Same holds for the release of slip, where the spatial distribution follows the same linear function. That a linear distribution of slip release and accumulation is reasonable can be explained by a simple mechanical projection using a framework model with linear shear line loads which represent the tectonic load on the fault. The slip location is associated with a shear joint in the center of the framework, between two bars which represent two different plates.

The bend line is shown in figure 6.4 where it can be easily seen that the distribution of slip can be simplified by a linear function for the area close to the slip source. Due to the uncertainty of the narrow field of seismic slip, a minimum distance of 10 km is assumed where the spatial slip remains unchanged with respect to the distance from the source.

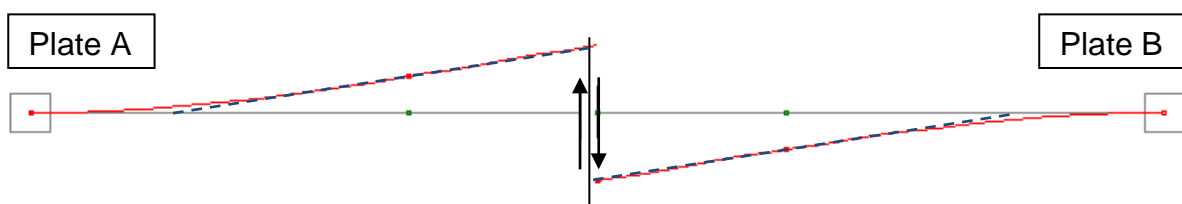


Figure 6.3: Simple mechanical model of fault slip between two plates. Arrows indicate slip direction for each plate respectively. The red lines denote the bending of bars/plates under the tectonic load. The blue dashed lines show the simplified linear distance function.

This simplified description holds true only for purely strike slip faults and earthquakes. However, for the method introduced here all faults and earthquakes are assumed to be strike slip. Furthermore this is only a two dimensional projection which does not take any three dimensional features into account.

6.3 The Slip Accumulation Method (SAM)

The slip accumulation method, which uses the above introduced idea and theory, can be seen as an indicator method similar to the PI method of chapter 4.2.1. However, instead of using statistics as the main part of the algorithm an accumulation and release model is introduced to identify regions with high probabilities for future earthquakes. It uses information from historical earthquake catalogues as well as data from fault models like the SHARE fault database.

It uses multiple spatial smoothing techniques as well as stochastic elements to account for several data uncertainties and incompleteness. In general the method can be summarized with the following step-by-step procedure.

1. Spatial discretization
2. Calculation of earthquake density
3. Spatial distribution of slip rates
4. Calculation of rupture parameters
5. Slip accumulation
6. Slip release
7. Slip smoothing

While steps 1 – 4 are time-independent, steps 5 and 6 are calculated for each time step separately. Step 7 is the final step to produce a map of smooth accumulated slip distribution, which is used as an indicator of regions for future earthquakes.

The general description of this procedure is given in chapter 6.3.1 while the calibration of the different model parameters is shown in chapter 6.3.2.

6.3.1 Method description

At first the whole region for which the method is applied is divided into boxes of 10 x 10 km, afterwards the relative earthquake density is calculated. This is necessary to link the earthquake density with the slip rates to differ from regions with creep from regions with strong friction and large earthquakes. Alternatively this can be also done by calculating fault-related local b-value distributions.

The relative earthquake density is calculated using an adaptive smooth seismicity approach with a power-law kernel. Details about this method are given in chapter 4.1.2. Only earthquakes with magnitude above a certain magnitude threshold M_{min} are used.

Each location i has a certain relative event density $\tilde{\lambda}$ which is calculated the following way

$$\tilde{\lambda}(i) = \frac{\lambda(i)}{\sum_i \lambda(i)} \tag{6.4}$$

$$\bar{\lambda}(i) = \frac{\tilde{\lambda}(i)}{\tilde{\lambda}_{max}} \quad \tilde{\lambda}(i) < 0.25 * \tilde{\lambda}_{max} \quad (6.5a)$$

$$\bar{\lambda}(i) = \frac{\tilde{\lambda}(i)}{\tilde{\lambda}_{max}} \quad \tilde{\lambda}(i) \geq 0.25 * \tilde{\lambda}_{max} \quad (6.5b)$$

Where λ is the event density of location i , calculated based on a smooth seismicity method as described above and $\tilde{\lambda}_{max}$ is the maximum value of the normalized event density of the whole region. The restriction to the 25% maximum normalized value is related to avoid local peaks of seismic activity.

The next step covers the distribution of slip rates.

$$s_{min}(i, f) = s_{min}(f) * \min\left(1, \frac{\Delta}{d(i, f)}\right) * \min\left(1, \frac{\bar{\lambda}(i)}{3 * \bar{\lambda}}\right) \quad (6.6a)$$

$$s_{max}(i, f) = s_{max}(f) * \min\left(1, \frac{\Delta}{d(i, f)}\right) * \min\left(1, \frac{\bar{\lambda}(i)}{3 * \bar{\lambda}}\right) \quad (6.6b)$$

Where $s_{min}(f)$ and $s_{max}(f)$ are the minimum and maximum slip rates of fault f respectively. Δ is the spatial correlation parameter of the faults and $d(i, f)$ is the closest distance between location i and the closest segment of fault f . $\bar{\lambda}(i)$ is derived by formulas (6.5a) and (6.5b) and $\bar{\lambda}$ is the mean of all $\bar{\lambda}$. Finally the local maximum and minimum slip rate is the maximum of all fault contributions respectively.

$$s_{min}(i) = \max_f(s_{min}(i, f)) \quad (6.7a)$$

$$s_{max}(i) = \max_f(s_{max}(i, f)) \quad (6.7b)$$

Rupture length, width and average slip is then computed for each earthquake in the historical catalogue with a magnitude above M_{min} . Only earthquakes within 50 km distance from a fault are used and associated with its closest fault segment from which the earthquake gets a strike angle assigned, which is randomly chosen between the maximum and minimum strike angle of the associated fault.

The following has to be repeated for each time increment Δt . The slip accumulates at each location depending on the time since the last time step. The slip rate $s_r(i)$ is randomly chosen between $s_{min}(i)$ and $s_{max}(i)$. Thus, the slip state $s(i, t)$ can be expressed the following way

$$s(i, t_j) = s(i, t_{j-1}) + s_r(i) \Delta t \quad (6.8)$$

Where Δt is the time difference between t_{j-1} and t_j . As initial condition the time of the first entry of the earthquake dataset is assumed to be t_0 and the initial slip is

estimated to be $s(i, t = t_0) = 0$. Under the condition of using several hundred years of earthquake observation it is assumed that the seismic cycle, leading to earthquakes with magnitude $< M8$, is fulfilled even with natural initial conditions as long as the period since the onset of the data until the first date of forecasting is sufficiently large.

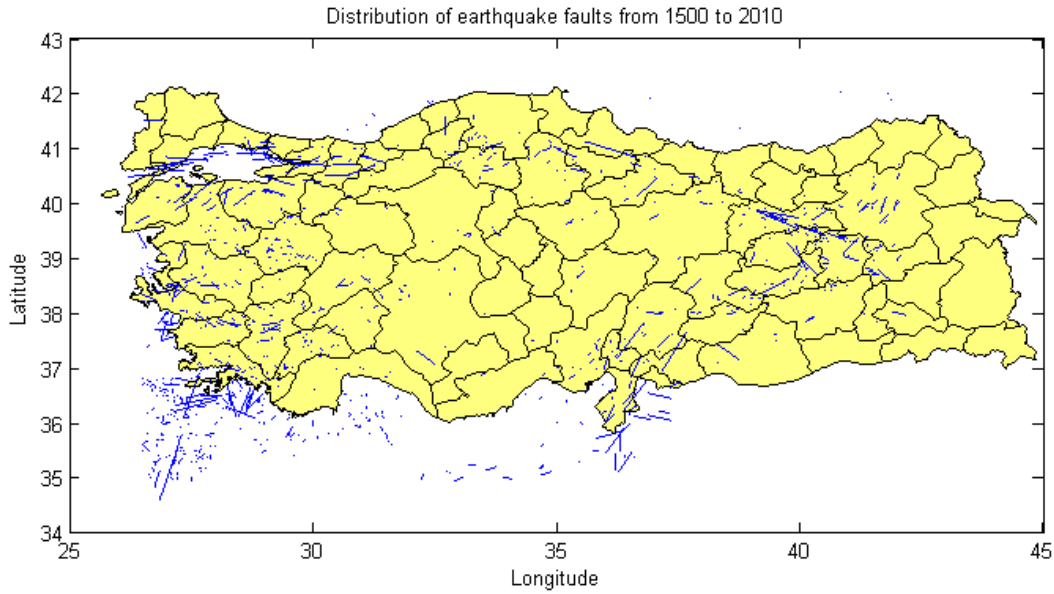


Figure 6.4: Distribution of earthquake rupture faults from 1500 to 2010.

The release of slip is governed by two levels. The first level is the direct slip release close to the earthquake fault, the second one is the indirect slip release related to the clustering of weaker earthquakes before and after a large event, which also release a certain level of slip. While the first level of slip release is directly controlled by the rupture parameters, it is assumed that about 1% of the direct slip is released in the second level. To determine spatial extent of slip of the first level maximum value of rupture length L or rupture width W is used; $\Delta = \max(L, W)$. The second level uses two times the extent of the first level. Formulas 6.9 and 6.10 show the release of slip for the first and second level respectively.

$$s(i, t_j) = s(i, t_{j-1}) - s(e) * \min\left(1, \frac{\Delta}{d(i,e)}\right) \quad d(i, e) \leq 4\Delta \quad (6.9)$$

$$s(i, t_j) = s(i, t_{j-1}) - 0.01 * s(e) * \min\left(1, \frac{\Delta}{d(i,e)}\right) \quad d(i, e) \leq 8\Delta \quad (6.10)$$

Where $s(e)$ is the slip of earthquake e and $d(i, e)$ is the minimum distance between the location i and the earthquake e 's fault line. A map of the earthquake rupture faults is shown in figure 6.4. To finally compute the map of the current slip state the whole region is again smoothed with a static power-law kernel.

6.3.2 Calibration

The method introduced here was tested for Turkey, therefore a complete set of model parameters have been estimated. As a minimum magnitude threshold $M_{min} = 6$ is assumed to account for completeness for a dataset starting in the year 1000. This threshold is only used for the relative earthquake density which is linked to the slip rate calculation. The general threshold for the total time-dependent calculation of slip is assumed to be $M_{min} = 4$, because smaller earthquakes create slip that can be neglected. The adaptive kernel smoothing is assumed to use at least 15 earthquakes around each location. For the static smoothing for the final map of current slip a static kernel distance of 25 km is applied

The correlation distance of the spatial extent of earthquake slip is assumed to be a maximum of 10 km. The starting year of the calculation is set to 1000 and each time step is from one earthquake to the next one afterwards. Figure 6.5 shows the slip rates in [mm] for Turkey and Italy respectively.

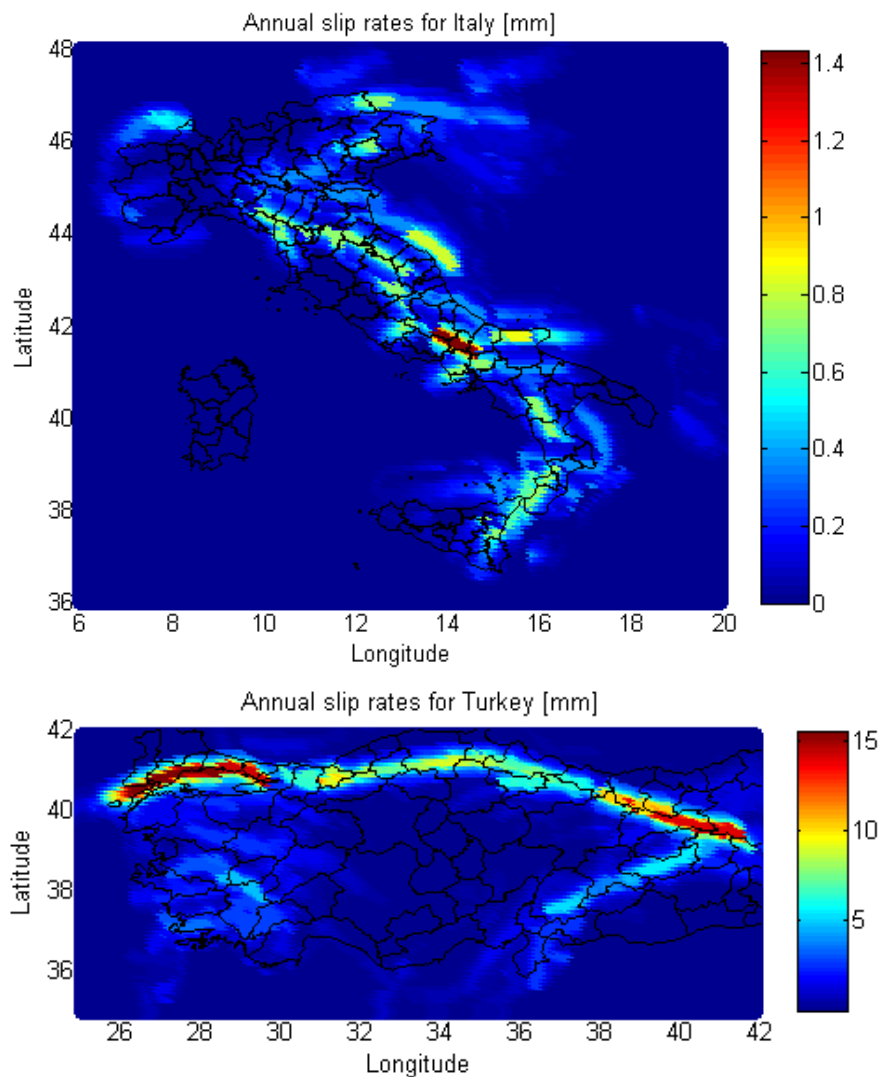
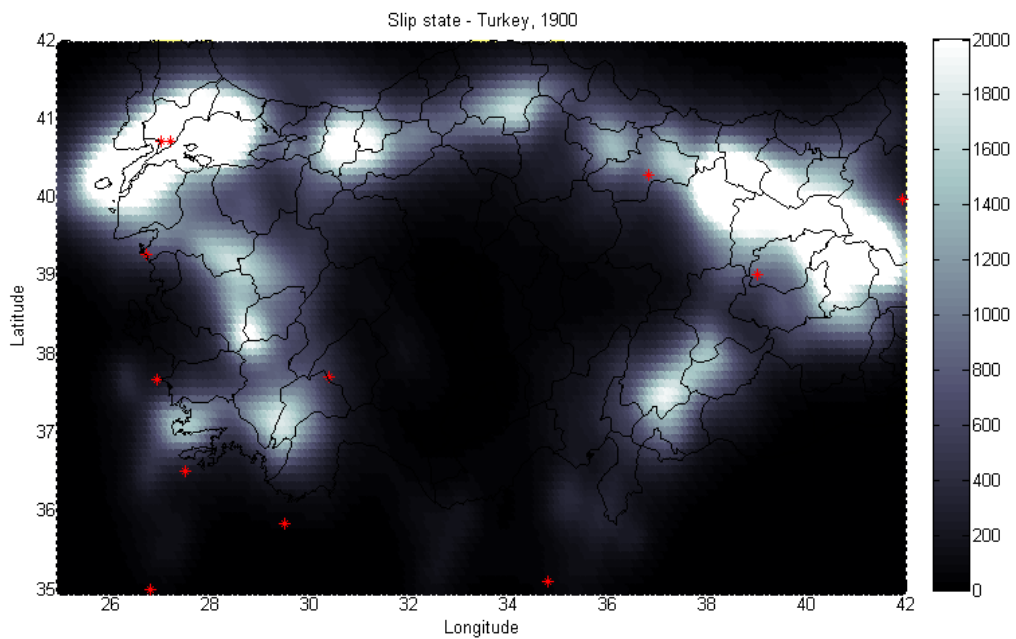


Figure 6.5: Annual slip rates of Italy and Turkey in [mm].

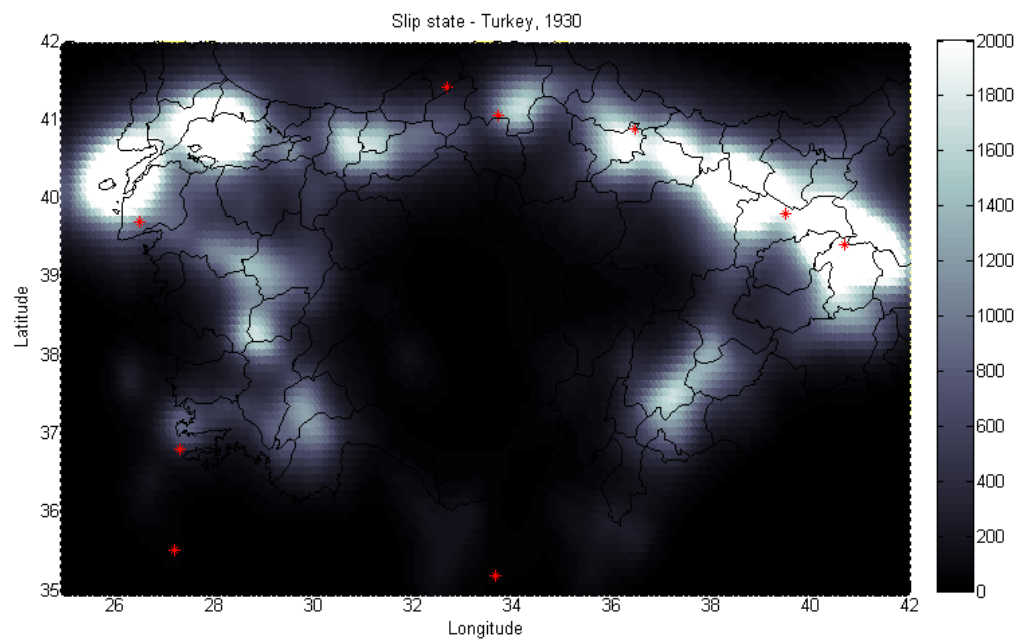
6.4 Results

The method was simply tested by comparing the map of current slip with the occurrence of earthquakes with magnitude $>M6.5$ during the following 20-30 years. Starting from 1900, the years 1930, 1950 and 1990 have been chosen, because the following years always contained several strong earthquakes throughout whole of Turkey. These maps are shown in figure 6.6.

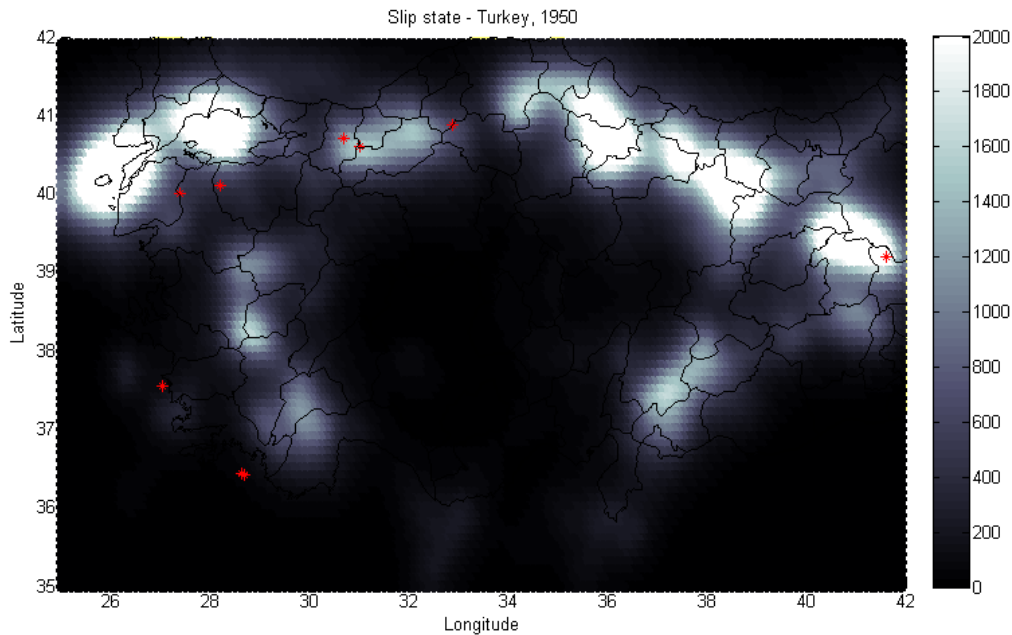
a) 1900 – 1930



b) 1930 – 1950



c) 1950 – 1990



d) 1990 – 2013

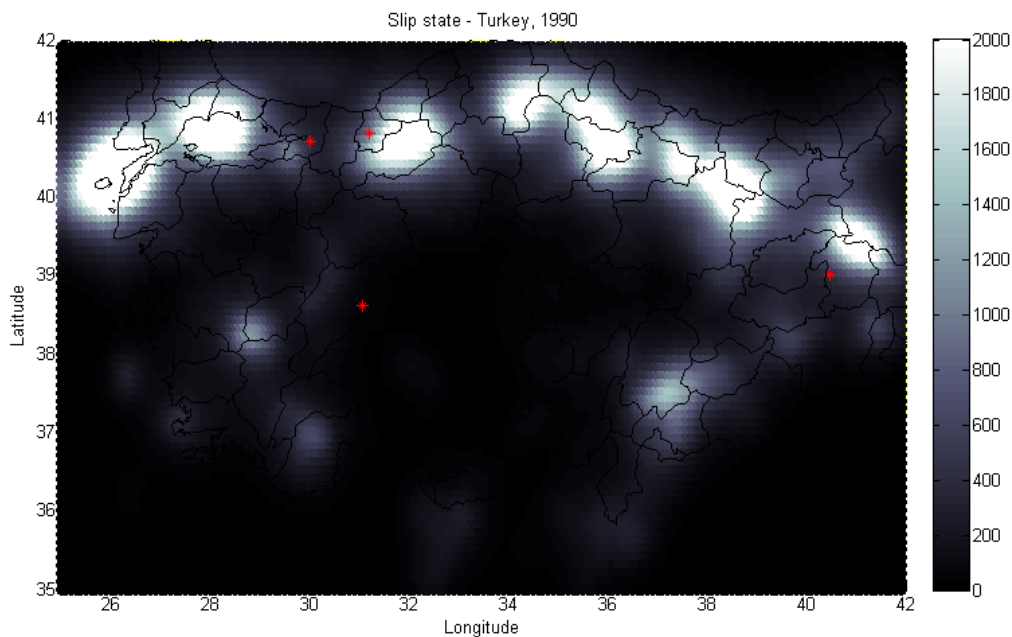


Figure 6.6: Four maps of accumulated slip in Turkey. Color scale is shown in millimeters. Red dots indicate earthquakes of $M \geq 6.5$ during the denoted period.

Regions with a strongly accumulated slip are called high hazard regions. Following the interpretation of figure 6.6 most earthquakes during the denoted period occurred within or close to regions where the current slip accumulated strongly. In the first period a total of 12 earthquakes have been observed, 8 occurred within or close to high hazard regions, two events were very close to the regions, while the remaining earthquakes occurred outside of any indicated location. The remaining periods show

similar results. Table 6.1 summarizes this testing procedure. The rate of success is simply the number of direct forecasts over the observed earthquakes. Earthquakes which occurred close to the forecast count as a 50% success

In conclusion, this method is assumed to be highly promising. With a success rate of about 75% it leads to better results as e.g. the Pattern Informatics approach. Similar results have been accomplished during a test for Italy (see figure 6.7 and table 6.2). Nevertheless it needs a lot of further development to increase the spatial resolution and to avoid further uncertainties.

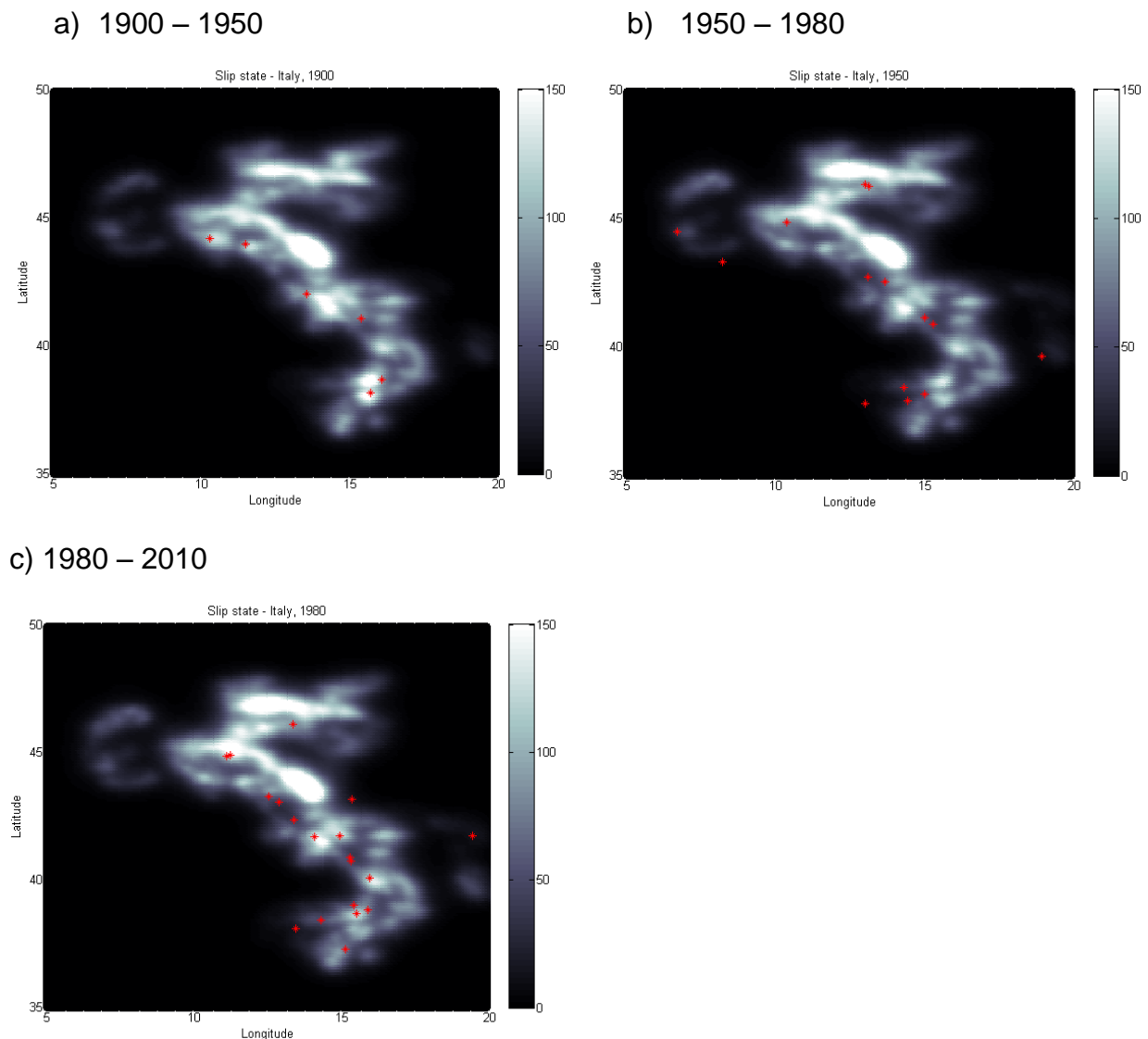


Figure 6.7: Four maps of accumulated slip in Italy. Color scale is shown in millimeters. Red dots indicate earthquakes of $M \geq 5.5$ during the denoted period.

By comparing the slip states of Turkey and Italy, the total amount of accumulated slip is about more than 10 times larger in Turkey. In some sense reasonable to the fact that the tectonics of Italy doesn't provide as strong earthquakes as Turkey due to fault size and slip rates, but the difference seems still too large.

There are several elements which should be improved for future development. First of all, the spatial extent of slip rates should be further investigated in detail and the data should be further checked. There are a lot of regions where the observed released slip is a lot higher than the accumulated and vice versa. In addition, the slip release should be extended to more complex focal mechanisms combined with a more sophisticated conversion from magnitude to rupture parameters. Thus, it should be reasonable to advance the method to three dimensions. To finally compute sophisticated forecasting maps an algorithm should be created which compares the general slip accumulation of a location with its current state, because currently locations with high slip rates are overrepresented in the map of current slip. In addition, calculating a precise indicator of at which amount of accumulated slip a fault ruptured should be determined. In general the spatial distribution of slip should be increased, because currently almost all regions have a certain amount of slip and so the ability to rupture, but the accumulation region doesn't match always the regions where the release takes place depending on the earthquake's epicenter, so the ration between regions of indicated slip and locations of earthquake occurrence is still too high. Thus, the correlation with earthquake location and slip accumulation should be further advanced.

Period	Observed	In Forecast	Close to Forecast	Not in the Forecast	Rate of Success
1900 – 1930	12	8	2	2	83.3%
1930 – 1950	9	6	1	2	72.2%
1950 – 1990	8	6	1	1	87.5%
1990 – 2013	4	3	0	1	75.0%

Table 6.1: Results of Slip Accumulation Method testing procedure for Turkey for earthquakes with magnitudes of $M \geq 6.5$

Period	Observed	In Forecast	Close to Forecast	Not in the Forecast	Rate of Success
1900 – 1950	6	6	0	0	100%
1950 – 1980	14	9	3	2	75%
1980 – 2010	19	14	3	2	81.6%

Table 6.2: Results of Slip Accumulation Method testing procedure for Italy for earthquakes with magnitudes of $M \geq 5.5$

7 Case Studies

After assembling, constructing, developing and finally testing of several forecasting methods this chapter introduces several state-of-the-art forecasts for Italy and Turkey using the approaches introduced above. Using earthquake data up to November 2013 will lead to a forecast for the next 30 years. Therefore time-independent and time-dependent seismic hazard maps are computed together with maps which indicate high hazard regions.

7.1 Time-independent Forecast

For the time-independent forecast, three hazard maps are computed and afterwards superpositioned to give a combined time-independent forecast map. The first map is based on the adaptive smooth seismicity approach with a power-law kernel, which lead to the best results among the adaptive kernels. The second map uses a static Gaussian kernel with a regional b-value, while the third map uses also a static Gaussian kernel but local fault-related b-values. Fault-related b-values are also computed for the time-dependent case. Furthermore the background seismicity result of the ETAS approach is also calculated.

Figures 7.1 and 7.2 show the general time-independent earthquake probability maps, which are superpositions of multiple smooth time-independent forecasting approaches for magnitudes $>M5$ and $>M7$ respectively. The time-independent hazard analysis is based on a 30 year calculation using both clustered and declustered datasets depending on the method. The superposition should lead to a better stability. Nevertheless the recent activity since 1960 is still visible in the map. The different methods use all data until November 1st 2013.

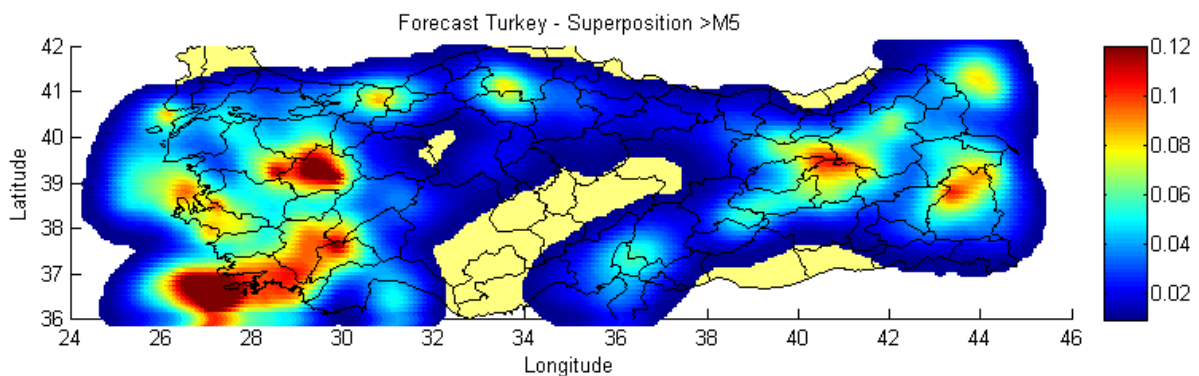


Figure 7.1: Time-independent seismicity map for $M_w \geq 5$ based on 4 different time-independent forecasting approaches.

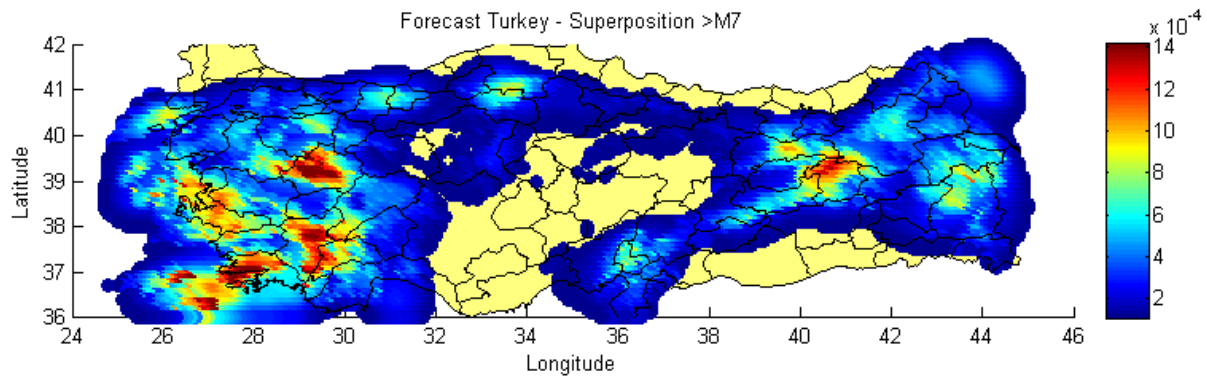


Figure 7.2: Time-independent seismicity map for $M_w \geq 7$ based on 4 different time-independent forecasting approaches.

To avoid local peaks, the color axis of each map has an upper cut-off value of about 66% of the maximum value. Both maps follow the simple principle that future earthquakes occur in regions where earthquakes happened in the past. Due to the nature of their algorithm, most of the time-independent methods do not differ between local earthquake density and earthquake strength, regions with a strong seismicity during periods with a good observation completeness (speaking of the last 50 years) are overestimated in these maps while regions with strong earthquake during the past but without representation by smaller events are underestimated. This issue is a matter of earthquake clustering and completeness which cannot be solved by classical declustering or completeness approaches, because it would need to reduce the number of small earthquakes during complete period, while the number of small earthquakes should be increased during incomplete periods, this is further discussed in chapter 5.

At least for the seismic activity of the last decades these maps sum up the general event density without neglecting important regions, even if the estimate is quantitatively incorrect.

7.2 Time-dependent Forecast

For time-dependent forecasting, the fault-related time-dependent b-value method is used together with its time-independent brother for comparison and the slip accumulation method. Firstly, a comparison of the time-independent and time-dependent b-value calculations will indicate fault segments which are overdue, following the idea of a seismic cycle. The comparison shows the difference between the rates of earthquakes with magnitudes $>M7$ of the time-independent to the time-dependent calculation.

The second time-dependent approach shows the level of accumulated slip throughout Turkey. This method simply indicates regions where a large amount of seismic slip is present and should be released in the future. However as described in chapter 6.4, the general spatial result has a low resolution and should be reviewed

carefully. Thus, the lower cut-off slip was set to be 30 cm while the upper cut-off slip is about 2m to neglect local variations and to remain small slip areas visible. The maximum calculated slip is about 5m, which seems way too high and is referred to spatial uncertainties in the distribution of slip accumulation and release. Clearly visible in the accumulated slip is the gap which was produced by the 1999 Izmit and Düzce events.

Nevertheless both time-dependent maps give a nice overview of how methods which should indicate technically the same thing differ so much.

While the first one indicates areas where the observation of strong earthquakes is above the average interevent time, the other one indicates physically where the potential of a future earthquake is given by accumulated seismic slip.

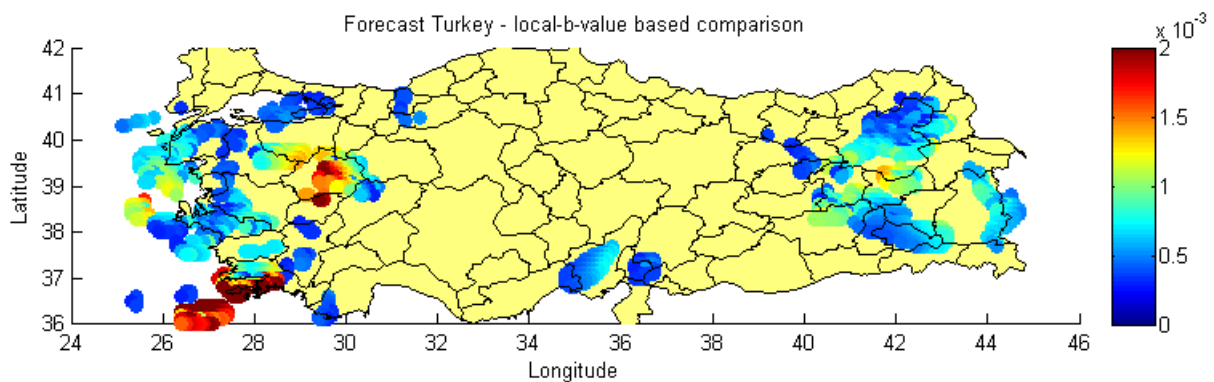


Figure 7.3: Direct comparison of earthquake rates within a 30-year forecast for earthquake $>M7$. Only regions where the average interevent time is already passed are indicated.

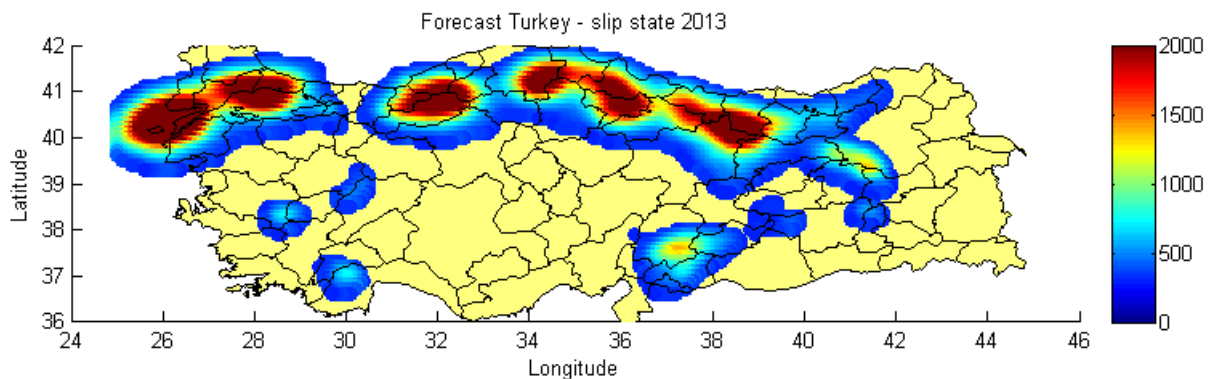


Figure 7.4: Slip state of the faults of Turkey where the slip is above 30 cm.

7.3 Summarized Forecast

Reviewing the time-independent maps it is obvious that south western Turkey should receive a future with a large number of both medium and large earthquakes just based on the data which was dominated by the last decades. Regions where certain large events hit the local population like the Izmit area and the central part of the North Anatolian Fault are shown as regions of stronger future seismicity than

neighboring areas. In contradiction the time-dependent calculation of slip accumulation shows hazard for almost the whole area of the North Anatolian Fault. The south western region is not even covered completely with accumulated slip. Two explanations can be used to solve this paradox. On the one hand the data used to calculate slip might not cover this region appropriately. On the other hand the hazard calculated in the time-independent approach does not take care of the time difference since the last event, it just uses the past event density, so the slip seems to be released which might infer that future large earthquakes should not be awaited in south western Turkey during the next thirty years. So the real value of time-independent earthquake density maps due to forecasting is questionable.

Comparing the two time-dependent indicator maps it can be seen that several regions of the forecasted locations overlap. Figure 7.5 shows exactly where both time-dependent forecasts correlate. Following the overlapping regions, both the Marmara Sea, the center of western Turkey and the eastern end of the East Anatolian Fault are assumed to have a high chance to be regions where future $>M7$ earthquakes might be located. Especially the forecast for the Marmara Sea region is consistent to the forecast of [Parsons et al., 2004]

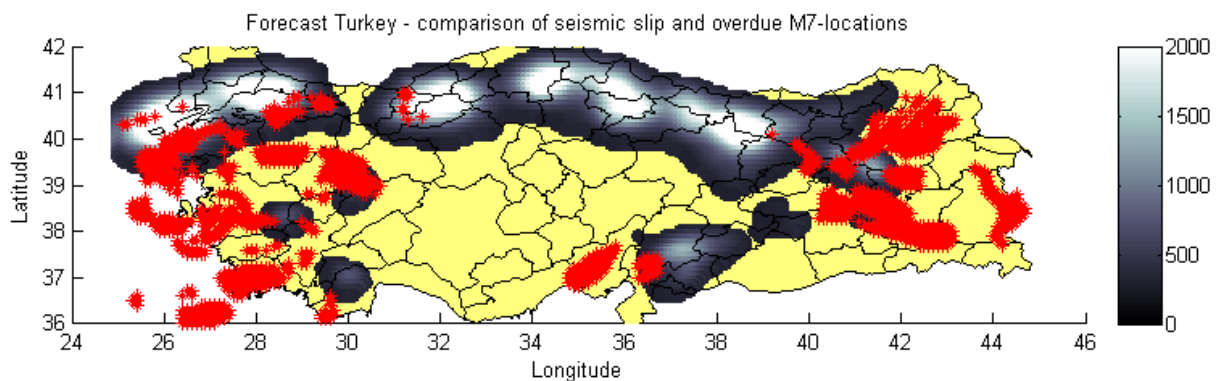


Figure 7.5: Direct comparison of the regions where the occurrence of earthquakes with magnitudes $>M7$ is statistically overdue and regions where seismic slip accumulated.

In conclusion, it can be seen that real forecasts are hard to compute. Both the time-independent and time-dependent approaches lack in spatial accuracy and are in most of the cases inconsistent. Both the general concept of earthquake forecasting and the method to test forecasts should be reviewed carefully. While the time-independent forecasts denote regions with past events, the time-dependent forecast indicates regions where something changed by time, but to understand these changes and to sum them all up appropriately more data in better resolution is necessary. Nevertheless it is possible to give a forecast within wide ranges. While the time-independent forecast maps can be used to compute the general risk of earthquakes based on the last decades independent of the magnitude, the time-dependent approaches encounter the direct probability of future large earthquakes. Thus, it is more important to understand the results of time-dependent analysis whilst comparing them with the general risk indicated by time-independent analysis.

8 Conclusion

After reviewing about 20 different earthquake forecasting approaches, reconstruction and development of almost a dozen algorithms and running hundreds of tests, this chapter summarizes the findings of this review and analysis of state-of-the-art in earthquake forecasting based on computer algorithms.

Furthermore it is important to note the distinction between predictions and forecasts and importantly the speaking in general of forecasts during this thesis and not of predictions. Finally a short outlook of future developments is given.

8.1 A brief Summary of Earthquake Forecasting

Calculating an earthquake forecast is a more complex struggle than it might look at first sight. Calling it a “common practice” for more than two decades, time-independent forecasting uses rather simple statistics to compute estimates of future seismicity, but calling it a sophisticated forecast would be totally misleading.

After testing and developing a toolbox to assemble different version of the same thing it is obvious that time-independent forecasting reached its limits. A typical method of that kind takes the locations of former earthquakes, draws a circle around it and uses the past earthquake density as the value for the color scale. Even after incorporating declustering algorithms, spatially varying Gutenberg-Richter relations and adaptive spatial smoothing algorithms the different approaches differ only in a marginal range. Furthermore the testing procedures of these methods lack in precision. Computing stochastic catalogues based on the earthquake forecasts and comparing their likelihood with the likelihood of observed earthquakes does of course show how strongly a method’s result correlate with the observation, but this also shows how strongly the observation correlates with the long-term average of seismicity.

A time-independent forecast is useful by determining the hazard from regions where the seismicity remains relatively stable for long time periods. Thus, if the task is to calculate a general seismic hazard a time-independent method is the right choice, but which method should be used or which combination of smoothing and Gutenberg-Richter handling is rather a matter of research preferences, but it shall be noted that most of these approaches lead to a overrepresentation of the seismic activity of recent decades, this issue is related to seismic clustering and data completeness and explained in chapter 7.1. An overview and general toolbox for such a task was developed during this thesis. A description of the toolbox can be found in Appendix D where both the readme and the content of the main file is given. However, to account for an up-to-date forecast with indication of daily hazards a time-independent method would be the wrong way. Instead, time-dependent

methods have been developed. Covering all different approaches which have been developed during the last 15 years would be a work of a lifetime, so two sample methods have been chosen together with a development by the author to introduce this certain kind of forecasting model.

Using changes in seismicity, the Pattern Informatics approach tries to indicate regions with future earthquakes, but the testing lead to rather unsatisfying results. After applying the method to both Italy and Turkey the forecasting ability is rather questionable with a success rate of less than 50%. Reasons for this failure are explained in chapter 5.4.1, but it also shows how hard it is to indicate future seismicity.

Another way to account for future earthquakes is to restrict the forecast on a certain kind of earthquakes. The Epidemic-type of Earthquakes Sequences method separates the independent background seismicity, which is a result of tectonics, from the aftershock seismicity, which is triggered by former earthquakes. This approach leads to well-developed results by generating a time-independent forecast with the same quality of resolution like any other time-independent method but additionally calculates a forecast for directly triggered aftershock seismicity, which nicely covers the observed activity. Such a method can be used for daily or hour-based forecasts for example to indicate the amount of future aftershock seismicity after large events. Even the knowledge of the amount of triggered earthquake hazard can save lives and deaths due to aftershocks e.g. of the 2009 L'Aquila and 1999 Izmit earthquakes might have been avoided.

The third approach of time-dependent forecasting was a development of the author, which compares the average interevent time with the time since the last earthquake at certain locations to change the b -value of the Gutenberg-Richter relation with either decrease or increase of the hazard of certain locations. Such locations could be, like tested above, the known faults in the tested region. Due to the fact that the changes in absolute rates are minor, the direct changes of time-independent and time-dependent b -values are computed. This simple method lead to a success rate of more than 50% and could be further improved. This relatively good result is a nice way to show how incorporating secondary information like the location of faults improves the power of an algorithm. Furthermore, this approach shows how relatively simple it is to develop a time-dependent forecasting algorithm which is able to compete with well-known and internationally published methods. Thus, the results of the time-dependent b -value method are not worse than e.g. the results of the PI method. Nevertheless this method should be further tested and advanced.

With the incorporation of more information the third category of earthquake forecasting is introduced. Hybrid methods use more data than just historical earthquake observations and of course apply physical laws and algorithms to bring more science into a range of methods where statistics seemed to be the only tool up to now. Of course there have been a lot of different and very complex methods developed during the last decade, often applied with a lot of computing power and a team of researchers behind it. Thus, the reconstruction and computation of such an

existing method would have been out of range for this thesis, furthermore the data used is often not as easy to access as historical earthquake data.

That is the reason why it was necessary to use what was on the table. The SHARE fault database of Europe provides slip rates for all known faults in Europe, so a method of slip accumulation has been developed to show how the development, calibration and testing of a hybrid method can take place.

With the simple idea of accumulation and release of slip along faults it was possible to indicate the regions of future earthquakes. After testing the method for different time periods, more than 75% of the observed earthquakes with magnitudes above 6.5 occurred in regions where slip has been accumulated. However, it should be taken into account that the indicated locations covered a wide part of the testing region. Nevertheless, this method was developed within a couple of weeks and it already achieved relatively good result, combining these facts is quite remarkable. Testing and further advancing is strongly advised.

After this brief summary of the developments and achievements of this thesis it can be easily seen that the whole science of earthquake forecasting is still under strong development. Researchers around the world are struggling with the creation of sophisticated forecasts. While some approaches already reached their limits and work well within certain, sometimes quite narrow, boundaries, or are under development and quite promising for the future, other methods are totally misleading following wrong assumptions and ideas.

Thus it is important to distinguish between a method of high value and potential and methods which might look nice and work well for a certain period and location but are totally not useful for general application.

8.2 Forecasting vs. Prediction

After spending a lot of time debating the potential of earthquake forecasting, earthquake prediction is even harder. Calculating the boundaries of space and time of future earthquakes to compute a forecast is sometimes possible within certain ranges. However, to directly create a prediction that at a certain date at a certain location will a certain earthquake happen sounds almost impossible.

For decades, a lot of world leading scientists are debating the matter whether earthquake prediction is possible or not. With the onset of the science of seismology and investigating the occurrence of earthquakes it was tried to predict earthquakes. Almost every prediction failed, because observed precursors of past earthquakes happened only once at a certain time and so weren't real precursors at all, or the model of prediction was so overfitted to a certain case that it even cannot predict anything else. Or the observation of special phenomena turned out to be misleading as well. The very small number of successful predictions has been more luck than knowledge.

Understanding earthquakes well enough to develop predictive methods is a goal from which science is currently far away. Processes of rupture, tectonic loading,

accumulation of stress, strain, etc. are not well enough understood to compute a real prediction.

The current state of science allows only to give estimates of future seismicity. As long as the science in the matter of earthquake occurrence is more an estimate than real knowledge it is impossible to give a direct prediction. Every approach to say anything about the future is also just an estimate as long the theory of its algorithm is just an estimate. However, an estimate is not a bad thing, it is simply a solution within boundaries and within these boundaries it is possible to give at least an indirect prediction with boundaries, a so-called forecast.

Thus the future of earthquake prediction is rather a future in earthquake forecasting, because science is still too far away to compute a sophisticated prediction.

8.3 Future Developments

Thus, the future of earthquake forecasting is the area of hybrid methods, where theories and observations from nature and from physics are linked with earthquake statistics. One of these approaches has been introduced in this thesis with quite promising results.

There are also a lot of other methods, from which a couple are listed in the method catalogue of appendix A, which incorporate theories like the Coulomb stress change to increase the forecast accuracy. Developing such methods is the future of earthquake science due to forecasting. The limits of purely statistical time-independent forecasts are reached. During the last five years a lot of promising models have been developed, but which have been unfortunately too complex to reconstruct and test during this thesis. Not only are the methods themselves under development. The testing procedures to calculate their accuracy have to be improved. Another interesting task for the future would be a stochastic "filling procedure" which adds random fore- and aftershocks to historical catalogues to avoid the above mentioned overrepresentation of recent decades due to magnitude completeness instead of increasing the magnitude threshold.

Due to the developments of this thesis, the catalogue of forecasting methods can help to find the right method to solve the current task. The author also plans to expand the current version of the catalogue in the future with new entries of upcoming models. Furthermore it gives a good overview of what have been developed so far for future comparisons and of course it can be used to choose the right method for a certain task an earthquake scientist might encounter.

Furthermore the toolbox of time-independent smooth seismicity methods should help to easily assemble useful methods for projects in the area of general seismic hazard. Finally the two methods developed by the author can be used for further developments and as inspiration for other methods. Of course the level of development of both of the methods is not as high as it might be from a large research group, but they are still good starting points for more well-developed versions.

8.4 Closing Words

Finally this whole thesis is meant to be a short overview of the vast range of earthquake forecasting and prediction. The focus to call the results rather a forecast than a prediction is explained in chapter 8.2. Each method which has been introduced, computed and tested here gives at least a short insight of what is possible. Of course all methods, especially the big well-developed approaches like the Pattern Informatics, the ETAS method or the development of the two author-methods, are worth a Master thesis on their own, so each restriction to certain tests and boundaries in parameter choice came from the decision to cover as much as possible without losing the whole task out of view.

The case study in chapter 7 is not meant as an official forecast or even a prediction, but it should give a short introduction of how it can look like to apply a method for a time period where its results are unknown. During retrospective tests it is easy to cheat by overfitting the method to the current state of observation, but calculating a forecast for a result that is unknown is another very interesting task. In a couple of years some of the above given forecasts will come true, however, others might never happen.

Maybe in a couple of years most of the methods introduced in this thesis are totally outdated or proved to be wrong, while others may lead to a perfect forecasting procedure.

All this together proves at least that earthquake forecasting and prediction is one of the most interesting fields in geoscience, highly debated with an incredible importance for mankind, especially for everyone who lives in a city where strong seismicity is not far away.

Acknowledgements

After more than half a year of hard work, I want to thank my family who made it even possible to study a second degree and also many thanks to my friends for all the support during that time and of course their patience during my endless talks of earthquakes and faults.

Furthermore I want to thank Dr. James Daniell and Dr. Matthias Hackl for their time, advice and support, many thanks also to Prof. Hans-Peter Bunge and Prof. Heiner Igel for their time and support.

And thanks to all the people who gave me words of cheer during times when stress took too much of my life.

Figures

Figure 2.1: A simple cartoonish summary of the main mechanisms and interactions of the earth's surface and its inside and atmosphere. From [Chen and Scawthorn, 2003].....	5
Figure 2.2: Geometry of a fault used to define movement direction of the fault. From [Stein and Wysession, 2003].....	8
Figure 2.3: Spherical projection of the focal mechanisms. Dark quadrants represent compression, while white ones are for tension. From [Stein and Wysession, 2003]	8
Figure 2.4: Direct comparison of different magnitude scales relative to the moment magnitude. From [Chen and Scawthron, 2003]	10
Figure 2.5: Sample map for seismic zonation for Italy with indicated earthquake distribution, after [Burkhard and Grünthal, 2009].	15
Figure 3.1: Coulomb stress changes after the 1992 earthquake sequence (Joshua Tree, Landers, Big Bear) in California. From [King et al., 1994]	29
Figure 3.2: Overview of a sample entry of the method catalogue, with descriptions for each catalogue parameter	32
Figure 4.1: A declustered earthquake dataset of turkey from 1990 until 2010. The blue line denotes the original data while the red line indicates the declustered data. Details about the data itself is given in chapter 5.....	36
Figure 4.2: From [Rhoades, 2013], a radial cross section through a donut distribution for different κ values (here k). For $\kappa=1$ the donut distribution takes the shape of a standard bivariate Gaussian distribution.	37
Figure 4.3: Smoothing distance solved for each grid cell. The color indicates the radius of a circle around each grid point with at least k events inside. The minimum value was set to 0.5 km. a) shows the map for $k=10$ and b) for $k=100$	39
Figure 4.4: Different results for smoothed seismic density for Turkey. a) is a static radial stencil $S=5$, b) an adaptive Gaussian kernel, c) an adaptive power-law kernel, d) an adaptive donut kernel with $\kappa=2$. b)-d) used all the same $k=10$ (minimum events around each location). The color code shows the relative density of events per grid cell, the absolute value should not be taken into account.....	40
Figure 4.5: Results for an ETAS-analysis of the Marmara Sea region. Top: background seismicity based on a 1000 year dataset for earthquakes with magnitudes $M>4$. Bottom: aftershock seismicity of the same dataset, the color denotes the earthquake activity in annual rates. For the aftershock seismicity, the annual rate is a theoretical extrapolation of the calculated daily rates.	47
Figure 4.6: Sample Gutenberg-Richter relation of a region where an earthquake of magnitude $>M7$ is overdue, so its rate got increased. This results in a smaller b -value.	49
Figure 4.7: Fault-oriented distribution of b -values for Turkey. Color indicates the local b -value.	51

Figure 5.1: 10-year sets of observations of earthquakes in Turkey in bins of $M > 3.5$ to $M > 7.5$. Each point contains the cumulative number of earthquakes of each magnitude bin from the year written on the x-axis and the following 9 years.....	58
Figure 5.2: 10-year sets of observations of earthquakes in Italy in bins of $M > 3.5$ to $M > 6.5$. Each point contains the cumulative number of earthquakes of each magnitude bin from the year written on the x-axis and the following 9 years.....	58
Figure 5.3: Spatial likelihood comparison for the tested methods, where the lines represent the 95% confidence interval of the stochastic earthquake density, and the red point represents the likelihood of the observed events. Applied on Turkey of the period from 1995 to 2005.....	63
Figure 5.4: Magnitude-based likelihood comparison for the tested methods, where the lines represent the 95% confidence interval of the stochastic earthquake density, and the red point represents the likelihood of the observed events. Applied on Turkey of the period from 1995 to 2005.....	63
Figure 5.5: Spatial likelihood comparison for the tested methods, where the lines represent the 95% confidence interval of the stochastic earthquake density, and the red point represents the likelihood of the observed events. Applied on Italy of the period from 1995 to 2005.....	64
Figure 5.6: Magnitude-based likelihood comparison for the tested methods, where the lines represent the 95% confidence interval of the stochastic earthquake density, and the red point represents the likelihood of the observed events. Applied on Italy of the period from 1995 to 2005.....	64
Figure 5.7: Likelihood results for different smoothing parameters of the adaptive smoothing method, applied on Turkey of the period of 1995 – 2005.....	65
Figure 5.8: Likelihood results for different smoothing parameters of the static Gaussian smoothing with either clustered or declustered datasets, applied on Turkey of the period of 1995 – 2005.....	65
Figure 5.9: Mapping of the PI method for Turkey. The green zones represent hotspot regions for future earthquakes, while the red dots show the observed earthquakes from 1995 to 2013 with magnitude $> M6.5$	68
Figure 5.10: Mapping of the PI method for Italy. The green zones represent hotspot regions for future earthquakes, while the red dots show the observed earthquakes from 1995 to 2013 with magnitude $> M5.5$	69
Figure 5.11: Difference of the seismicity rates between the time-dependent and time-independent approaches. The green areas are regions where a change in seismicity rates have been observed and future earthquakes are awaited. Red dots show observed earthquakes between 1995 and 2013.	70
Figure 5.12: Map of forecasted background seismicity after January 1, 1995 in Turkey. Color scale shows the annual earthquake activity of magnitudes $> M4.25$. Red dots indicate earthquakes of magnitude $> M6$ from 1995 to 2005.....	71
Figure 5.13: Comparison of aftershock seismicity of $M4 - M5.5$ earthquakes after the 17.08.1999 Izmit earthquake.	72

Figure 5.14: Spatial likelihood comparison for the ETAS method, where the lines represent the 95% confidence interval of the stochastic earthquake density, and the red point represents the likelihood of the observed events. Applied on Turkey for different time periods73

Figure 5.15: Magnitude-based likelihood comparison for the ETAS method, where the lines represent the 95% confidence interval of the stochastic earthquake density, and the red point represents the likelihood of the observed events. Applied on Turkey for different time periods73

Figure 5.16: Aftershock calculated aftershock activity for the Izmit and Düzce earthquakes. Red dots indicate earthquakes of a certain period after the indicated date. The color scale shows the forecasted daily rate.74

Figure 6.1: Distribution of fault lines in Turkey using fault information of the SHARE fault database [Basili et al., 2013].78

Figure 6.2: Relations of magnitude scales to rupture parameters for general focal mechanisms, following [Chan et al., 2010].80

Figure 6.3: Simple mechanical model of fault slip between two plates. Arrows indicate slip direction for each plate respectively. The red lines denote the bending of bars/plates under the tectonic load. The blue dashed lines show the simplified linear distance function.....80

Figure 6.4: Distribution of earthquake rupture faults from 1500 to 2010.83

Figure 6.5: Annual slip rates of Italy and Turkey in [mm].84

Figure 6.6: Four maps of accumulated slip in Turkey. Color scale is shown in millimeters. Red dots indicate earthquakes of $M \geq 6.5$ during the denoted period...86

Figure 6.7: Four maps of accumulated slip in Italy. Color scale is shown in millimeters. Red dots indicate earthquakes of $M \geq 5.5$ during the denoted period...87

Figure 7.1: Time-independent seismicity map for $M_w \geq 5$ based on 4 different time-independent forecasting approaches.....89

Figure 7.2: Time-independent seismicity map for $M_w \geq 7$ based on 4 different time-independent forecasting approaches.....90

Figure 7.3: Direct comparison of earthquake rates within a 30-year forecast for earthquake $>M7$. Only regions where the average interevent time is already passed are indicated.91

Figure 7.4: Slip state of the faults of Turkey where the slip is above 30 cm.91

Figure 7.5: Direct comparison of the regions where the occurrence of earthquakes with magnitudes $>M7$ is statistically overdue and regions where seismic slip accumulated.92

Tables

Table 2.1: Overview of temporal and spatial dimensions due to earthquake forecasting.	14
Table 5.1: Overview of catalogue characteristics. *(declustered & clustered).....	57
Table 5.2: Overview of regional completeness periods. *(not applied for time-independent methods).....	57
Table 5.3: Overview of tested methods within the testing range. (*) Declustering was only applied for the Turkish data.	59
Table 5.4: Overview of data periods for each method, (*) indicate application of completeness	60
Table 5.5: Overview of best fitting smoothing parameters. Methods 2 & 3 are adaptive methods for which the minimum number of events within a radius was calculated. The other methods use smoothing radii in km.	62
Table 5.6: Overview parameters for the two testing regions of the PI method.....	66
Table 5.7: Results of PI Method testing. *An earthquakes is assumed to be part of the forecast if it was observed at least directly adjacent to an indicated cell.	67
Table 6.1: Results of Slip Accumulation Method testing procedure for Turkey for earthquakes with magnitudes of $M \geq 6.5$	88
Table 6.2: Results of Slip Accumulation Method testing procedure for Italy for earthquakes with magnitudes of $M \geq 5.5$	88

Literature

- [1] Akinci, A., (2010): *HAZGRIDX: earthquake forecasting Model for $M_L \geq 5.0$ earthquakes in Italy based on spatially smoothed seismicity*, Annals of Geophysics, 53, 3; doi: 10.4401 / ag-4811
- [2] ANSS - Advanced National Seismic System - <http://www.ncedc.org/anss/catalog-search.html>
- [3] Van Aalsburg, J., J. B. Rundle, L. B. Grant, P. B. Rundle, G. Yakovlev, D. L. Turcotte, etc., (2010): *Space- and Time-Dependent Probabilities for Earthquake Fault System from Numerical Simulations: Feasibility Study and First Results*, Pure Applied Geophysics, 167, 697 - 977, doi: 10.1007/s00024-010-0091-3
- [4] Basili, R., V. Kastelic, M. B. Demircioglu, D. Garcia Moreno, E. S. Nemser, P. Petricca, S. P. Sboras, G. M. Besana-Ostman, J. Cabral, T. Camelbeeck, R. Caputo, L. Danciu, H. Domac H., J. Fonseca, J. García-Mayordomo, D. Giardini, B. Glavatovic, L. Gulen, Y. Ince, S. Pavlides, K. Sesetyan, G. Tarabusi G., M. M. Tiberti, M. Utkucu, G. Valensise, K. Vanneste, S. Vilanova, J. Wössner, (2013) – *The European Database of Seismogenic Faults (EDSF) compiled in the framework of the Project SHARE*.<http://diss.rm.ingv.it/share-edsf/>, doi: 10.6092/INGV.IT-SHARE-EDSF.
- [5] Bird, P., Z. Liu, (2007): *Seismic Hazard Inferred from Tectonics: California*, Seismological Research Letters Volume 78, 37-48, 2007
- [6] Burkhard M., .G. Grünthal. (2009): *Seismic source zone characterization for the seismic hazard assessment project PEGASOS by Expert Group 2 (EG1b)*, Swiss Journal of Geosciences 102, issue 1, 149 – 189
- [7] Chan, C.-H., M. Sorensen, D. Stromeyer, G. Grünthal, O. Heidbach, A. Hakimhashemi, F. Catalli, (2010): *Forecasting Italian seismicity through a spatio-temporal physical model: importance of considering time-dependency and reliability of the forecast*, Annals of Geophysics, 53, 3, 129-140; doi: 10.4401 / ag-4761
- [8] Chen, W.-F. and C. Scawthorn (2003): *Earthquake Engineering Handbook*, CRC Press LLC
- [9] Cocco, M., S. Hainzl, F. Catalli, B. Enescu, A. Lombardi, J. Wiemer (2010): *Sensitivity study of forecasted aftershock seismicity based on Coulomb stress calculation and rate- and state-dependent frictional response*, Journal of Geophysical Research, Vol. 115, B05307, doi: 10.1029/2009JB006838

- [10] Console, R., M. Murru, F. Catalli, G. Falcone, (2007): *Real Time Forecasts through an Earthquake Clustering Model Constrained by the Rate-and-State Constitutive Law: Comparison with a Purely Stochastic ETAS Model*, Seismological Research Letters, Volume 78-1, 49-56
- [11] Dieterich J. (1994): *A constitutive law for rate of earthquake production and its application to earthquake clustering*, Journal of Geophysical Research, Vol 99, No B2, 2601-2618
- [12] Falcone, G., R. Console, M. Murru (2010): *Short-term and long-term earthquake occurrence models for Italy: ETES, ERS and LTST*, Annals of Geophysics, 53, 3, 41-50; doi: 10.4401 / ag-4761
- [13] Freed, A. M. (2005): *Earthquake Triggering by Static, Dynamic and Postseismic Stress Transfer*, Annual Review Earth Planetary Science, 33, 335-367
- [14] Gardner, J. K., and L. Knopfoff, (1974): *Is the sequence of earthquakes in Southern California, with aftershocks removed, Poissonian?*, Bulletin of Seismological Society of America, 64(5), 1363-1367
- [15] Gerstenberger, M., S. Wiemer, L. Jones, (2004): *Real-time Forecasts of Tomorrow's Earthquakes in California: a Mapping Tool*, U.S. Geological Survey, Open-File Report 2004-1390
- [16] Gruppo di lavoro BSI (2002), *Bollettino sismico italiano 2002-2009*, Istituto Nazionale di Geofisica e Vulcanologia, Bologna, <http://bollettinosismico.rm.ing.it/>
- [17] Gulia, L., S. Wiemer, D. Schorlemmer (2010): *Asperity-based earthquake likelihood models for Italy*, Annals of Geophysics, 53, 3; doi: 10.4401 / ag-4843
- [18] Gutenberg, B. and C. F. Richter, (1956): *Magnitude and energy of earthquakes*, Annals of Geophysics, vol. 9, pp. 1-15
- [19] Grünthal, G., R. Wahlström, (2012): *The European-Mediterranean Earthquake Catalogue (EMEC) for the last millennium*, Journal of Seismology, 16, 3, 535-570, doi: 10.1007/s10950-012-9302-y
- [20] Hiemer, S., Q. Wang, D. D. Jackson, Y. Y. Kagan, J. Woessner, J. D. Zechar, S. Wiemer, (2013): *A Stochastic Forecast of California Earthquakes Based on Fault Slip and Smoothed Seismicity*, Bulletin of the Seismological Society of America, Vol. 103, No 2A, pp. 799-810; doi: 10.1785/0120120168
- [21] Holiday, J. R., K. Z. Nanjo, K. F. Tiampo, J. B. Rundle, D. L. Turcotte (2005): *Earthquake Forecasting and its verification*, Nonlinear Processes in Geophysics, 12, 965-977, SRef-ID: 1607-7946/npg/2005-12-965

- [22] Holiday, J. R., C.-C. Chen, K. F. Tiampo, J. B. Rundle, D. L. Turcotte, A. Donnellan (2007): *A RELM Earthquake Forecast Based on Pattern Informatics*, Seismological Research Letters Volume 78, 87-93
- [23] Hough, S., (2010): *Predicting the Unpredictable – The Tumultuous Science of Earthquake Prediction*, Princeton University Press, ISBN: 9780691138169
- [24] Kenneth, P., K. P. Burnham, D.R. Anderson, (2002): *Model selection and multimodel inference: A practical information – Theoretic Approach*, Springer, New York
- [25] King, G., R. Stein, J. Lin (1994): *Static Stress Changes and the Triggering of Earthquakes*, Bulletin of Seismological Society of America, Vol. 84, No 3, 935-953, 1994
- [26] Lombardi, A. M., W. Marzocchi (2010): *The ETAS model for daily forecasting of Italian seismicity in the CSEP experiment*, Annals of Geophysics, 53, 3; doi: 10.4401 / ag-4848
- [27] Nanjo, K. Z., (2010): *Earthquake forecast models for Italy based on the RI algorithm*, Annals of Geophysics, 53, 3; doi: 10.4401 / ag-4810
- [28] Ogata, Y., (1988): *Statistical Models for Earthquake Occurrence and Residual Analysis for Point Processes*, Journal of the American Statistical Association, Vol. 83, No. 401, pp. 9-27
- [29] Ogata, Y., (1998): *Space-time point-process models for earthquake occurrence*, Annual Institution of Statistical Mathematics, Vol. 50, No. 2, pp. 379-402
- [30] Omori, F., (1894): *On the after-shocks of earthquakes*, Journal of the College of Science, Imperial University of Tokyo, vol. 7, pp. 111-200
- [31] Parsons, T., (2004): *Recalculated probability of $M \geq 7$ earthquakes beneath the Sea of Marmara, Turkey*, Journal of Geophysical Research, Vol. 109, doi: 10.1029/2003JB002667, 2004
- [32] Reid, H., (1910): *The Mechanics of the Earthquake, The California Earthquake of April 18, 1906*, Report of the State Investigation Commission, Vol. 2, Carnegie Institution of Washington, Washington D.C., pp. 16-28
- [33] Reasenberg, P., (1985): *Second-order moment of central California seismicity, 1969-82*, Journal of Geophysical Research, 90, 5479-5495
- [34] Rhoades, D. A., (2007): *Application of the EEPAS Model to Forecasting Earthquakes of Moderate Magnitude in Southern California*, Seismological Research Letters Volume 78, 110-115
- [35] Rhoades, D. A., (2013): *Alternative distributions for location in the EEPAS model and their effects on model performance and future earthquake hazard in Canterbury*, GNS Science Report 2013/08, 14 p.

- [36] Richter, C.F. (1935): *An Instrumental Earthquake Scale* , Bulletin of Seismological Society of America, 25, pp. 1-32
- [37] Rovida, A., R. Camassi, P. Gasperini and M. Stucchi (eds.), (2011): *CPTI11, the 2011 version of the Parametric Catalogue of Italian Earthquakes*. Milano, Bologna, <http://emidius.mi.ingv.it/CPTI>, DOI: 10.6092/INGV.IT-CPTI11
- [38] Rundle, J. B., W. Klein, K. F. Tiampo, S. J. Gross, (2000): *Linear pattern dynamics in nonlinear threshold system*, Phys. Rev. E., 61. Pp. 2418-2432
- [39] Schorlemmer, D., M. C. Gerstenberger, S. Wiemer, D. D. Jackson, D. A. Rhoades, (2007): *Earthquake likelihood model testing*, Seismological Research Letters, 78, 30-36
- [40] Shebalin, P., V. Keilis-Borok, A. Gabrielov, I. Zaliapin, D. L. Turcotte (2006): *Short-term earthquake prediction by reverse analysis of lithosphere dynamics*, Tectonophysics 413, 63-75, doi: 10.1016/j.tecto.2005.10.033
- [41] Shebalin, P, C. Narteau, M. Holscheider, D. Schorlemmer (2011): *Short-Term Earthquake Forecasting Using Early Aftershock Statistics*, Bulletin of Seismological Society of America, Vol. 101, No. 1, pp. 297-312, doi: 10.1785/0120100119
- [42] Stein, S. and M. Wyssession (2003): *An Introduction to Seismology, Earthquakes and Earth Structures*, Blackwell Publishing.
- [43] Suen, C., Caroline, D. Lo, F. Li (2010): EPiC: *Earthquake Prediction in California*, Stanford University – Computer Learning Project
- [44] Utsu, T. (1961): *A statistical study of the occurrence of aftershocks*, Geophysical Magazine 30, 521-605
- [45] Van Stiphout, T., J. Zhuang, and D. Marsan (2012): *Seismicity declustering*, Community Online Resource for Statistical Seismicity Analysis, doi:10.5078/corssa-52382934. Available at <http://www.corssa.org>.
- [46] Werner, M., J. D. Zechar, W. Marzocchi, S. Wiemer (2010a): *Retrospective evaluation of the five-year and ten-year CSEP-Italy earthquake forecasts*, Annals of Geophysics, 53, 3, doi: 10.4401 / ag-4840
- [47] Werner, M. J., A. Helmstetter, D. D. Jackson, Y. Y. Kagan, S. Wilmer (2010b): *Adaptively smoothed seismicity earthquake forecasts for Italy* , Annals of Geophysics, 53, 3, 2010; doi: 10.4401 / ag-4839
- [48] Wells D. L., K. J. Coppersmith (1994): *New Empirical Relationships among Magnitude, Rupture Length, Rupture Width, Rupture Area, and Surface Displacement*, Bulletin of Seismological Society of America, Vol. 84, No. 4, pp. 974-1002
- [49] Zechar, J. D., T. H. Jordan (2010): *Simple Smoothed Seismicity earthquake forecasts for Italy*, Annals of Geophysics, 53, 3, doi: 10.4401 / ag-4845

- [50] Zechar, J. D., M. C. Gerstenberger, D. A. Rhoades, (2010): *Likelihood-Based Tests for Evaluating Space-Rate-Magnitude Earthquake Forecasts*, Bulletin of the Seismological Society of America, Vol. 100, No. 3, pp. 1184-1195, doi: 10.1785/0120090192
- [51] Zechar, J.D., D. Schorlemmer, M. J. Werner, M. C. Gerstenberger, D. A. Rhoades, T.H. Jordan (2013): *Regional Earthquake Likelihood Models I: First-Order Results*, Bulletin of the Seismological Society of America, Vol. 103, No. 2A, pp. 787-798, doi: 10.1785/0120120186
- [52] Zhuang, J., Y. Ogata, D. Vere-Jones, (2002): *Stochastic Declustering of Space-Time Earthquake Occurrence*, Journal of The American Statistical Association, Vol. 97, No. 458, pp. 369-380
- [53] Zhuang, J., (2011): *Next-day earthquake forecasts for the Japan region generated by the ETAS model*, Earth Planets Space, 63, pp. 207-216
- [54] Zhuang, J., D. Harte, M.J. Werner, S. Hainzl, and S. Zhou (2012): *Basic models of seismicity: temporal models*, Community Online Resource for Statistical Seismicity Analysis, doi: 10.5078/corssa-79905851. Available at <http://www.corssa.org>.

Remark: Program used: MATLAB R2012a, version 7.14.0.739 Natick, Massachusetts: The MathWorks Inc.,

Appendix A: Method Catalogue

Time-independent methods

RI-Algorithm (relative intensity)

Author & related publication:

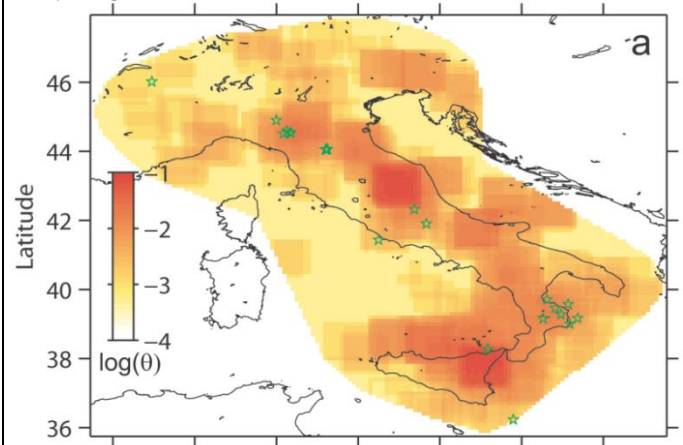
¹K. Z. Nanjo – *Earthquake forecast models for Italy based on the RI algorithm*, *Annals of Geophysics*, 53, 3, 2010; doi: 10.4401 / ag-4810

Description:

The RI algorithm uses the fundamental assumption that future events are more likely to occur in areas with higher seismic activity during the past. The algorithm presented here is progressed development of a former alarm-based version of this method, advanced to become a smoothed seismicity model, which uses a simple counting system to calculate the number of future earthquake in a certain region for specified magnitude bins. The smoothing algorithm is based on a simple stencil smoothing by using the Moore neighborhood of each grid cell.

The method was applied during the CSEP project and used for regions in Italy and Japan. Current results for the Italy analysis showed that the RI-algorithm underestimates the number of future events while spatial and likelihood testing of the model lead relatively well results. [3].

Sample Figure:



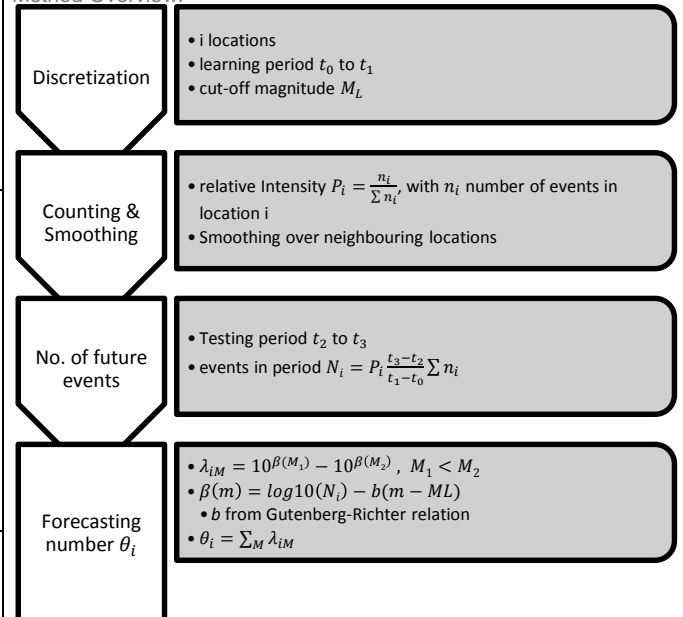
From [1]: RI-based retrospective forecast map, for a period from Apr. 16, 2005 to Mar. 31, 2009 for $4 \leq M \leq 9$ events. Θ denotes the cumulative forecast number (see description). The green stars denote real events in the stated magnitude range which really happened during this period.

Regions & Catalogues:

Italy: Catalogo della Sismicit  Italiana (used: 1985 – 2002), Bollettino Sismic Italiano (since 2005)

Japan: Japan Metrological Agency earthquake catalogue (since 1965)

Method Overview:



Input Parameters:

- Location
- Time
- Magnitude

Model Parameters:

- Smoothing
- b-value

Further publications:

²K. Z. Nanjo – *Earthquake forecast for the CSEP Japan experiment based on the RI algorithm*, *Earth Planets Space*, 63, 261-274, 2011

³J. M. Werner, J. D. Zechar, W. Marzocchi, S. Wiemer - *Retrospective evaluation of the five-year and ten-year CSEP-Italy earthquake forecasts*, *Annals of Geophysics*, 53, 3, 2010; doi: 10.4401 / ag-4840

EPiC (Earthquake Prediction in California)

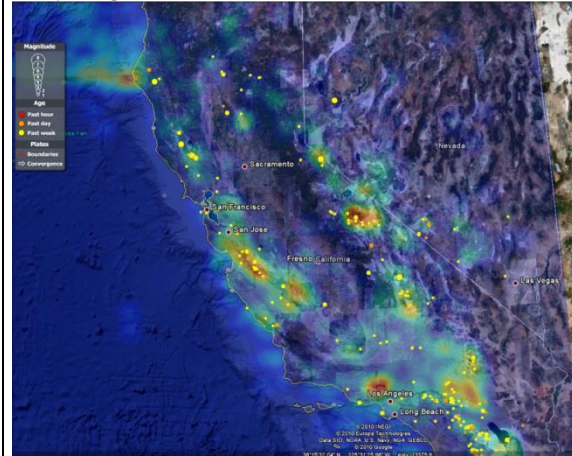
Author & related publication:

¹C. Suen Caroline, D. Lo, F. Li – EPiC: Earthquake Prediction in California, Stanford University – Computer Learning Project

Description:

This method was developed by Stanford students in the area of computer learning algorithms. This is no “professional” method, but still useful due to its attempts in smoothing and earthquake density maps. It uses a simple Poisson model for spatial smoothing. Furthermore a Fourier Analysis was applied to find periodic patterns in time. Finally one can derive a general form of earthquake densities from these calculations. Due to the method overview there is only the Poisson model presented.

Sample Figure:

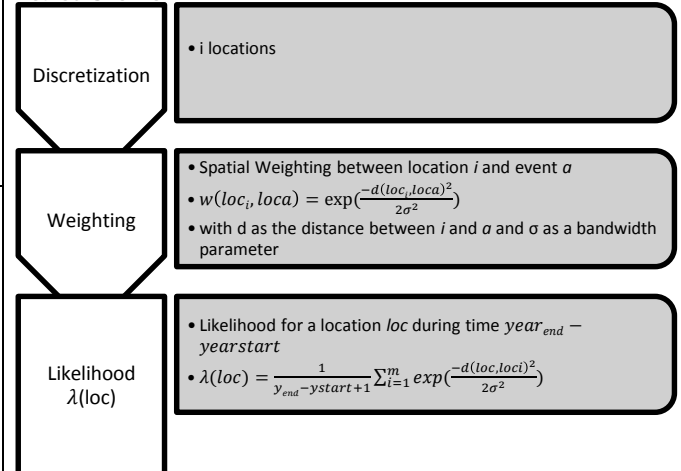


From [1]: Earthquake density derived with the Poisson model, with indicated recent events (yellow points) in California.

Regions & Catalogues:

California: National Geophysical Data Center, Northern and Southern California Earthquake Data Center (used since 1970)

Method Overview:



Input Parameters:

– Location

Model Parameters:

– Bandwidth σ

Further publications:

ALM (Asperity Likelihood Model)

Author & related publication:

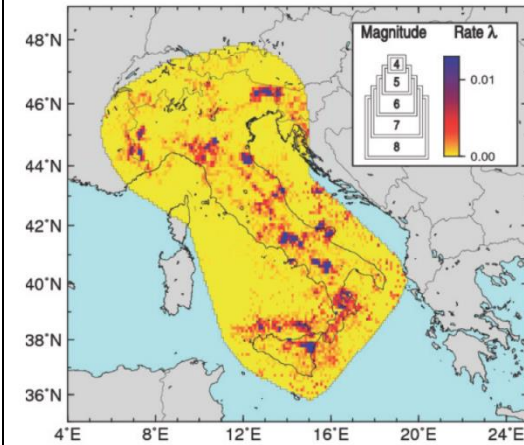
¹L. Gulia, S. Wiemer, D. Schorlemmer – *Asperity-based earthquake likelihood models for Italy*, *Annals of Geophysics*, 53, 3, 2010; doi: 10.4401 / ag-4843

Description:

The ALM assumes that small variations in the b-value influence the forecasting of future seismicity significantly. This method was applied during the CSEP project for Italy and the RELM project for California. The core of this algorithm calculates local and regional b-values and the corresponding a-values. Applying the Gutenberg-Richter relation with these values leads to a time-independent forecast. Two different approaches were applied, while the first one uses the assumption of a global b-value as a proxy, the second one uses a seismic zonation with a set of b-values depending on the local focal mechanism. This relation between b-value and focal mechanism proved for multiple regions around the world.

Due to the tests of the CSEP method, the ALM results lacked in general likelihood, especially in spatial variations. The second approach additionally underestimated the total number of events during the testing period [3]. Due to the tests of the RELM project ALM lacks only in the spatial likelihood and works well for the general likelihood of forecast [4].

Sample Figure:

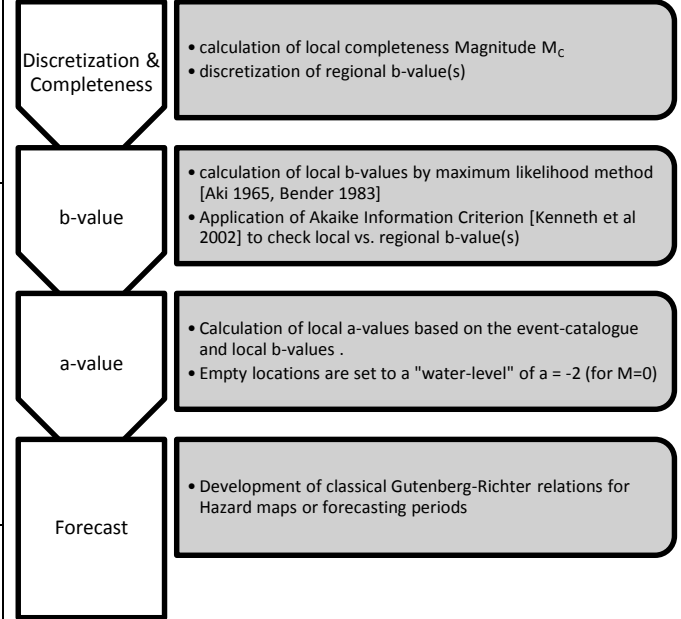


From [1]: 5-year forecast rates for the ALM method based on a regional b-value proxy for a period from 2009 to 2014 based on a standard Gutenberg-Richter relation algorithm.

Regions & Catalogues:

Italy: Catalogo della Sismicità Italiana (used: 1985 – 2002), Bollettino Sismic Italiano (since 2005)
California: Advanced National Seismic System (used: 1984 – 2005)

Method Overview:



Input Parameters:

- Location
- Time
- Magnitude

Model Parameters:

- Seismic Zonation
- Regional b-value(s)

Further publications:

²D. Schorlemmer D., M.C. Gerstenberger, S. Wiemer, D. D. Jackson, D. A. Rhoades – *Earthquake likelihood model testing*, *Seismological Research Letters* Volume 78, 17-29, 2007

³J. M. Werner, J. D. Zechar, W. Marzocchi, S. Wiemer - *Retrospective evaluation of the five-year and ten-year CSEP-Italy earthquake forecasts*, *Annals of Geophysics*, 53, 3, 2010; doi: 10.4401 / ag-4840

⁴J.D. Zechar, D. Schorlemmer, M. J. Werner, M. C. Gerstenberger, D. A. Rhoades, T.H. Jordan – *Regional Earthquake Likelihood Models I: First-Order Results*, *Bulletin of the Seismological Society of America*, Vol. 103, No. 2A, pp. 787-798, April 2013, doi: 10.1785/0120120186

HAZGRIDX

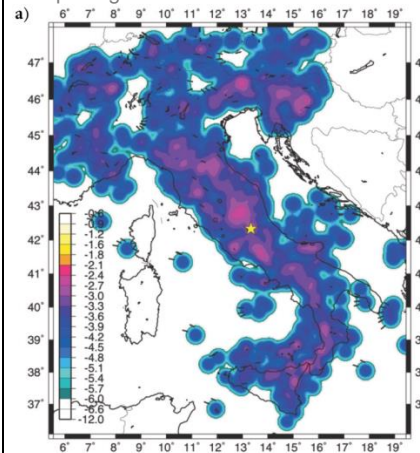
Author & related publication:

¹A. Akinci – *HAZGRIDX: earthquake forecasting Model for $M_L \geq 5.0$ earthquakes in Italy based on spatially smoothed seismicity*, Annals of Geophysics, 53, 3, 2010; doi: 10.4401 / ag-4811

Description:

HAZGRIDX was developed for the CSEP project in Italy based on a seismic smoothing approach. It uses a two-dimensional Gaussian function to smooth declustered earthquake data. Due to smoothing a 15-km correlation distance was applied based on assumption of the regional fault geometry. In addition, a constant b-value was assumed for the testing area. A large dataset of more than 2000 years was applied using time completeness intervals for different Italian territories based on the results of the MSP Working Group [2004]. During the testing process of the CSEP project the HAZGRIDX method underestimated the total number of events during the testing period, but behaved well for spatial and temporal likelihood. The bad results of the event number might be related to the conversion of M_w to M_L .

Sample Figure:

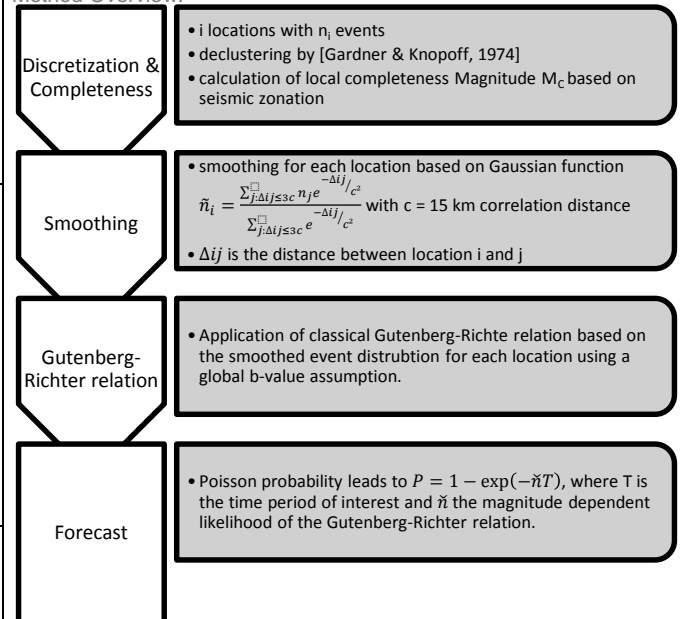


From [1]: 5-year forecast rates using HAZGRIDX and a 15 km correlation distance. Numbers indicate the number of $M_L \geq 5$ events. The yellow star indicates the Apr. 6, 2009 L'Aquila earthquake.

Regions & Catalogues:

Italy: Catalogo Parametrico del Terremoti Italiani (217 B.C – 2003)

Method Overview:



Input Parameters:

- Location
- Time
- Magnitude

Model Parameters:

- b-value
- Smoothing

Further publications:

²J. M. Werner, J. D. Zechar, W. Marzocchi, S. Wiemer - *Retrospective evaluation of the five-year and ten-year CSEP-Italy earthquake forecasts*, Annals of Geophysics, 53, 3, 2010; doi: 10.4401 / ag-4840

ASS (Adaptively Smoothed Seismicity)*

Author & related publication:

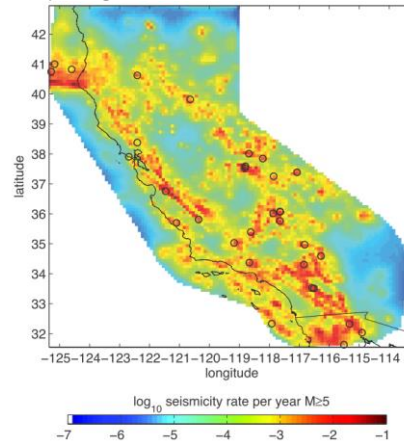
¹M. J. Werner, A. Helmstetter, D. D. Jackson, Y. Y. Kagan, S. Wilmer – *Adaptively smoothed seismicity earthquake forecasts for Italy*, *Annals of Geophysics*, 53, 3, 2010; doi: 10.4401 / ag-4839

Description:

The ASS method is a complex smoothing method, which applies an isotropic adaptive kernel to the earthquake distribution of a declustered event catalogue. The fact that the event catalogue is declustered is an essential assumption. Its first application was during the RELM project for California and it got further used during the CSEP project in Italy. During the first testing in California further adjustments lead to the continuous application of a adaptive power-law kernel instead of a Gaussian kernel. Additional adjustable parameters are related to the overall smoothing intensity depending on the used dataset and its event density.

The results of the RELM showed that the ASS method has been the most accurate under all tested methods [4]. Due to the CSEP project, the ASS method was again under the most accurate ones, but lacked slightly in the spatial locations of the forecast. The model seems to be not smooth enough and underestimates quiet regions which might become active in the future [3].

Sample Figure:



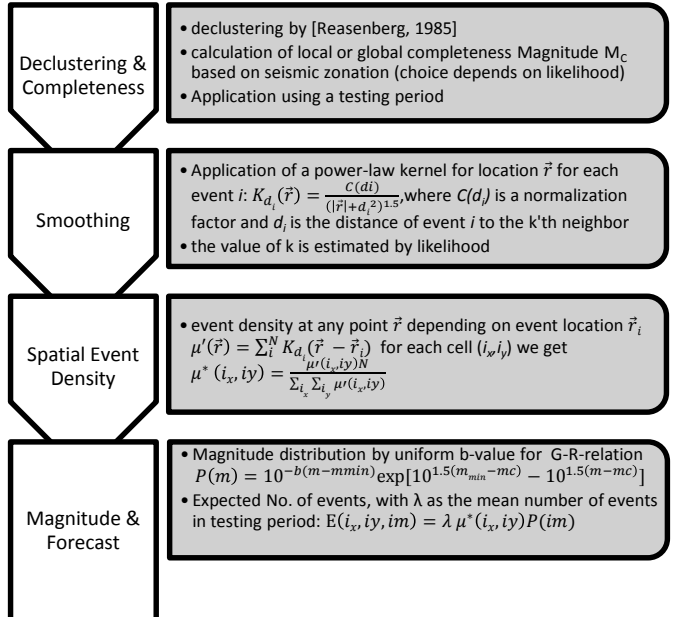
From [2]: Forecasted seismicity rate for $M > 4.95$ events per year in each cell. A power-law kernel was applied to smooth the location, including microseismicity of events with $M \geq 2$ from 1981 to 2005. The black circles indicate $M \geq 5$ events between 1996 and 2005.

Regions & Catalogues:

Italy: Catalogo della Sismicità Italiana (used: 1985 – 2002), Bollettino Sismic Italiano (since 2005), : Catalogo Parametrico del Terremoti Italiani (1901 – 2003)

California: Advanced National Seismic System (used: 1981 – 2005)

Method Overview:



Input Parameters:

- Location
- Time
- Magnitude

Model Parameters:

- b-value
- Smoothing
- Declustering

Further publications:

²A. Helmstetter, Y. Y. Kagan, D. D. Jackson – *High-resolution Time-independent Grid-based Forecast for $M \geq 5$ Earthquakes in California*, *Seismological Research Letters* Volume 78, No.1, 2007

³J. M. Werner, J. D. Zechar, W. Marzocchi, S. Wiemer - *Retrospective evaluation of the five-year and ten-year CSEP-Italy earthquake forecasts*, *Annals of Geophysics*, 53, 3, 2010; doi: 10.4401 / ag-4840

⁴J.D. Zechar, D. Schorlemmer, M. J. Werner, M. C. Gerstenberger, D. A. Rhoades, T.H. Jordan – *Regional Earthquake Likelihood Models I: First-Order Results*, *Bulletin of the Seismological Society of America*, Vol. 103, No. 2A, pp. 787-798, April 2013, doi: 10.1785/0120120186

PEGASOS-EG1b	
<p>Author & related publication: ¹M. Burkhard, .G. Grünthal.– <i>Seismic source zone characterization for the seismic hazard assessment project PEGASOS by Expert Group 2 (EG1b)</i>, Swiss Journal of Geosciences 102, issue 1, 149 – 189, 2009</p>	
<p>Description:</p> <p>This approach is not a method in a classical sense. It was part of a larger project called PEGASOS which was addicted to the seismic hazard of four nuclear power plants in Switzerland. The results of PEGASOS EG1b consist of an in-depth analysis of seismic zonation within the study region. It evaluated seismic recurrence for each zone by calculating recurrence parameters of a tapered Gutenberg-Richter recurrence relationship based on a declustered earthquake catalogue between 1946 and 2000. As a model results a set of b-values was computed together with a distribution of possible maximum magnitudes for each seismic source zone.</p>	<p>Sample Figure:</p> <p>From [1]: Visualization of the small scale zonation for the testing region with indicated large scale tectonic provinces.</p>
<p>Regions & Catalogues:</p> <p>Switzerland (and adjacent regions): ECOS catalogue (used 1946 – 2000)</p>	<p>Method Overview:</p> <div style="display: flex; flex-direction: column; align-items: flex-start;"> <div style="display: flex; align-items: center; margin-bottom: 10px;"> <div style="border: 1px solid black; padding: 5px; margin-right: 10px;">Declustering & Completeness</div> <div style="border: 1px solid black; padding: 5px; background-color: #f0f0f0;"> <ul style="list-style-type: none"> Setup of the Virtual California fault model Adjustment of elastic dislocations to model fault elements Identification and adjustment of model parameters </div> </div> <div style="display: flex; align-items: center; margin-bottom: 10px;"> <div style="border: 1px solid black; padding: 5px; margin-right: 10px;">Zonation</div> <div style="border: 1px solid black; padding: 5px; background-color: #f0f0f0;"> <ul style="list-style-type: none"> Whole region is divided into seismic source zones based on the regional tectonic settings </div> </div> <div style="display: flex; align-items: center;"> <div style="border: 1px solid black; padding: 5px; margin-right: 10px;">Source Parameters</div> <div style="border: 1px solid black; padding: 5px; background-color: #f0f0f0;"> <ul style="list-style-type: none"> Reoccurrence parameters are determined for a tapered Gutenberg-Richter relation based on the maximum likelihood principle. </div> </div> </div>
<p>Input Parameters:</p> <ul style="list-style-type: none"> – Location – Magnitude – Time 	<p>Model Parameters:</p> <ul style="list-style-type: none"> – Zonation
<p>Further publications: ²Coppersmith, K. J., Youngs, R. R. & Sprecher, C. 2008: <i>Methodology and main results of seismic source characterization for the PEGASOS Project</i>, Switzerland. Swiss Journal of Geosciences 102, issue 1, 2009</p>	

Simple Smoothed Seismicity (Triple-S)

Author & related publication:

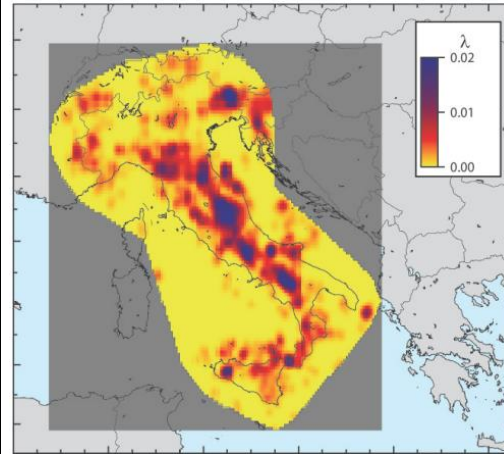
¹J. D. Zechar, T. H. Jordan– *Simple Smoothed Seismicity earthquake forecasts for Italy*, Annals of Geophysics, 53, 3, 2010; doi: 10.4401 / ag-4845

Description:

The Triple-S method is a simple approach to generate time-independent forecasts, which assumes that increasing the accuracy of the parameters of simple methods is sufficient to increase the general forecast accuracy instead of increase the method complexity. In this sense, the Triple-S only consists of an appropriate smoothing algorithm, which takes special care of the near field of smoothing when counting the number of events within each spatial bin. In advance, it uses the area skill score testing procedure to find the most accurate smoothing lengthscale. The normalized smoothed seismicity is finally applied to an untapered Gutenberg-Richter relation to generate the final forecast.

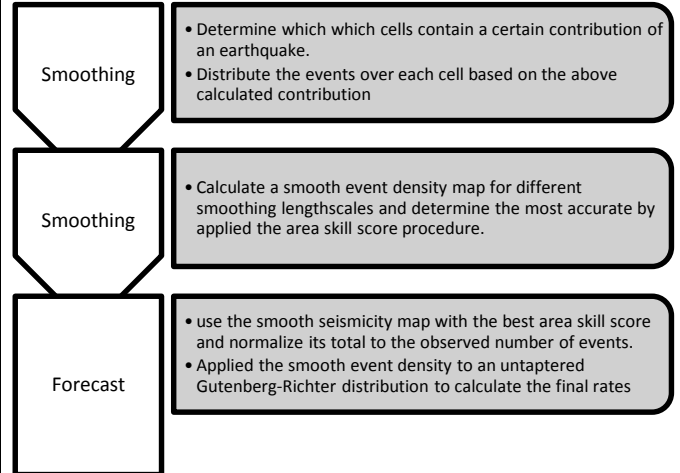
Due to the results of the CSEP testing center, the Triple-S method behaved well in general, but tends to underestimate the total number of forecasted events.

Sample Figure:



From [1]: Forecasted seismicity based on the CPTI catalogue for Italy from 1901 to 2006 with a smoothing lengthscale of 10 km.

Method Overview:



Regions & Catalogues:

Italy: Catalogo della Sismicità Italiana (used: 1985 – 2002), Catalogo Parametrico del Terremoti Italiani (1901 – 2003), Earthquake Catalogue of Switzerland (2003 – 2005)

Input Parameters:

- Location
- Time
- Magnitude

Model Parameters:

- b-value
- Smoothing

Further publications:

²J. M. Werner, J. D. Zechar, W. Marzocchi, S. Wiemer - *Retrospective evaluation of the five-year and ten-year CSEP-Italy earthquake forecasts*, Annals of Geophysics, 53, 3, 2010; doi: 10.4401 / ag-4840

Time-dependent methods

PI method (Pattern Informatics)

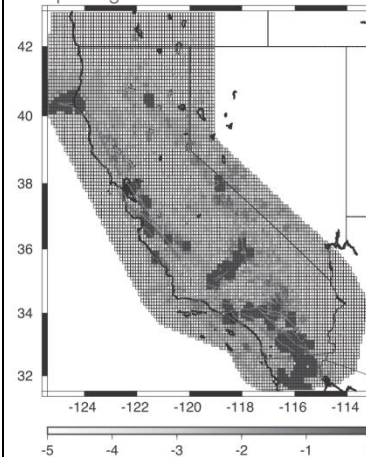
Author & related publication:

¹J. R. Holiday, C.-C. Chen, K. F. Tiampo, J. B. Rundle, D. L. Turcotte, A. Donnellan – *A RELM Earthquake Forecast Based on Pattern Informatics*, *Seismological Research Letters* Volume 78, 87-93, 2007

Description:

The Pattern Informatics method analyzes changes in seismicity rates. These rates are computed for seismic active areas. If a certain threshold in seismic activity is reached the occurrence of a future event is assumed within the testing period. For identifying the seismic active zones a map based on the relative intensity approach is used. The seismic event catalogue is afterwards divided into multiple periods for which the rates are computed. This leads to so called pixel probabilities for which a Gutenberg-Richter relation is applied to finally end up with a forecasting map. During the RELM project the PI method generated relatively good results except for the spatial likelihood. Anyway the PI method received the second best score in the testing range.

Sample Figure:

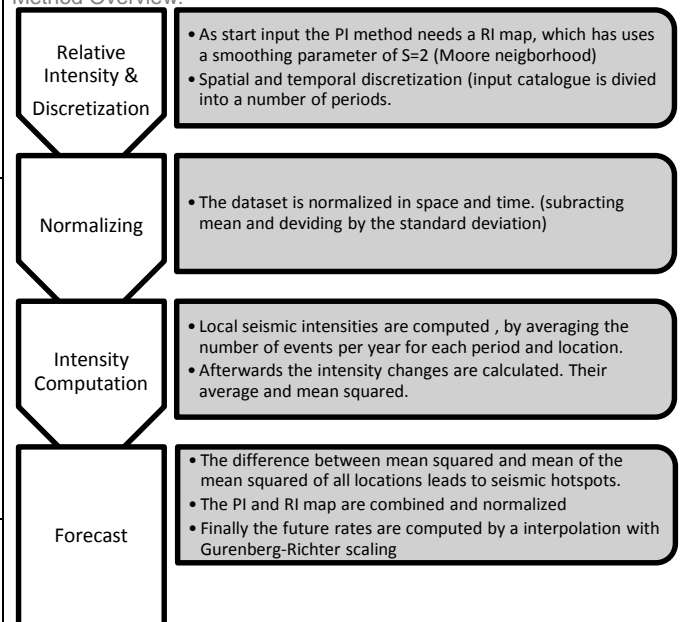


From [1]: Forecastmap, composite of PI method and a RI map. Color map indicates the logarithmic rate of earthquakes per year.

Regions & Catalogues:

California: Advanced National Seismic System (used: 1950 – 2005)

Method Overview:



Input Parameters:

- Location
- Time
- Magnitude

Model Parameters:

- Intensity map
- Time periods

Further publications:

²J. R. Holiday, K. Z Nanjo, K. F. Tiampo, J. B: Rundle, D. L. Turcotte – *Earthquake Forecasting and its verification*, *Nonlinear Processes in Geophysics*, 12, 965-977, 2005, SRef-ID: 1607-7946/npg/2005-12-965

⁴J.D. Zechar, D. Schorlemmer, M. J. Werner, M. C. Gerstenberger, D. A. Rhoades, T.H. Jordan – *Regional Earthquake Likelihood Models I: First-Order Results*, *Bulletin of the Seismological Society of America*, Vol. 103, No. 2A, pp. 787-798, April 2013, doi: 10.1785/0120120186

Reverse-Tracing of Precursors (RTP)

Author & related publication:

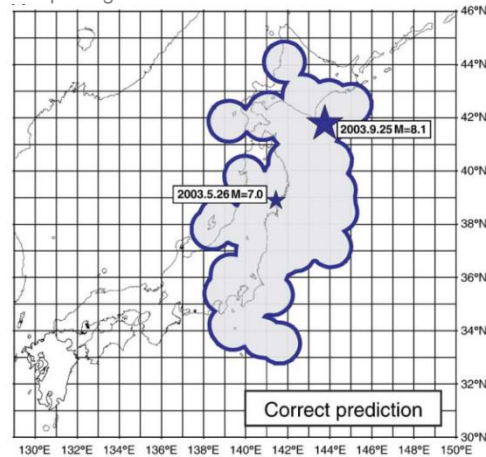
¹P. Shebalin, V. Keilis-Borok, A. Gabrielov, I. Zaliapin, D. L. Turcotte – *Short-term earthquake prediction by reverse analysis of lithosphere dynamics*, *Tectonophysics* 413 (2006), 63-75, doi: 10.1016/j.tecto.2005.10.033

Description:

The RTP method uses short-term spatial and temporal patterns as precursors for short-term earthquake prediction. It searches for these patterns, called precursory chains, to identify future locations of target earthquakes. In this sense, it is a highly time-dependent method using multiple pattern functions and threshold values to identify regions of future seismicity. It was successfully applied during a first testing range in Japan, California, Italy and the Eastern Mediterranean. [1]

After multiple evaluations of different testing ranges with the RTP method, it has been proven that it does not work as well as supposed. The success rate of the forecast is around 25%, containing missed events and failed predictions. Please note that some failed predictions were only about a couple of kilometers, because the target earthquakes were slightly outside the predicted regions. [3]

Sample Figure:



From [1]: Sample figure for an correct prediction in Japan using the RPT method. The indicated area represents the calculated location for the target earthquakes. The stars show the real locations of the actual events.

Regions & Catalogues:

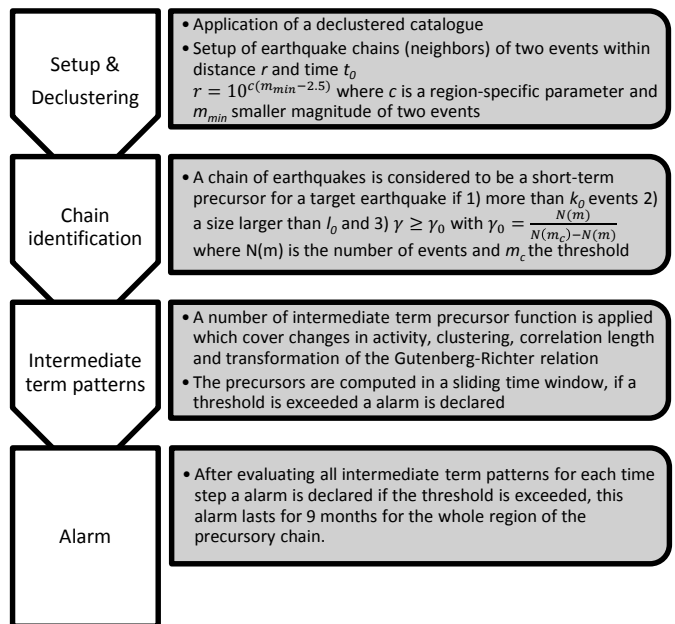
California: ANSS/CNSS Worldwide Earthquake Catalogue (1965 – 2003)

Japan: see above

Italy: see above

Eastern Mediterranean: see above

Method Overview:



Input Parameters:

- Location
- Time
- Magnitude

Model Parameters:

- Threshold values

Further publications:

²J. D. Zechar, J. Zhuang – *Risk and return: evaluating reverse tracing of precursors earthquake predictions*, *International Geophysical Journal* 2010, doi: 10.1111/j.1365-246X.2010.04666.x

³J.D. Zechar, dissertation – *Methods for evaluating earthquake predictions*, 2008

Epidemic-type Aftershock Sequence (ETAS)

Author & related publication:

¹A. M. Lombardi, W. Marzocchi – *The ETAS model for daily forecasting of Italian seismicity in the CSEP experiment*, *Annals of Geophysics*, 53, 3, 2010; doi: 10.4401 / ag-4848

Description:

The epidemic-type aftershock sequence (ETAS) model is a time-dependent short-term forecasting model, which uses just observed earthquake data. The ‘epidemic’ type indicates that each earthquake is a potential triggering event for subsequent events. It combines a calculated background seismicity rate with the magnitude-dependent ability of each aftershock to perturb the rate of earthquake production. The model itself consists of multiple stochastic elements from Omori’s law of aftershock occurrence to Gutenberg-Richter relations. The ETAS formula can be decomposed into the background seismicity rate and the aftershock related activity, which is again decomposed in normal distributions for time and space and the general magnitude-depending ability to produce a certain number of aftershocks. The parameters have to be fitted for each application area by a log-likelihood approach. [1]

The ETAS model can be advanced by adding an ETAS-derived declustering procedure as an additional branching process. The final rate of occurrences is a superposition of both steps. [2]

Regions & Catalogues:

Italy: Bollettino Sismico Italiano (2005 - 2009)

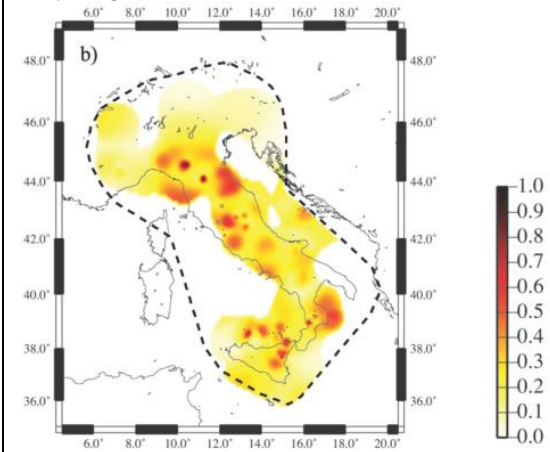
Input Parameters:

- Location
- Magnitude
- Time

Model Parameters:

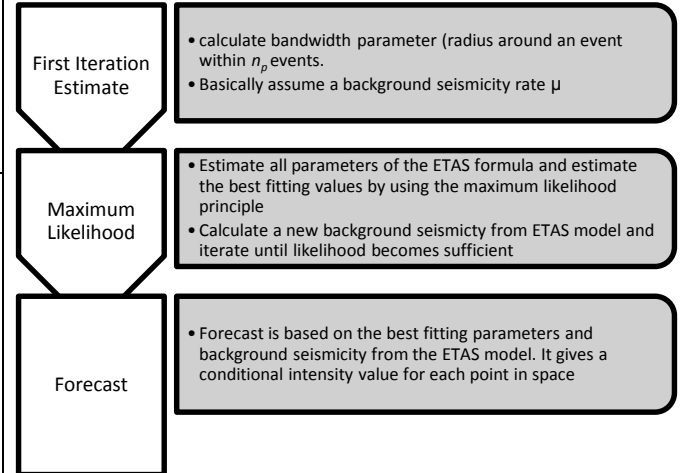
- Multiple ETAS parameters

Sample Figure:



From [1]: Map of the ratio between the triggered seismicity rate and the total seismic rate during the period of April 16, 2005 and June 1, 2009.

Method Overview:



Further publications:

²A. M. Lombardi, W. Marzocchi – *A double-branching model applied to long-term forecasting of Italian seismicity ($M_L \geq 5.0$) within the CSEP project*, 53, 3, 2010; doi: 10.4401 / ag-4762

Every Earthquake a Precursor According to Scale (EEPAS)

Author & related publication:

¹D. A. Rhoades – *Application of the EEPAS Model to Forecasting Earthquakes of Moderate Magnitude in Southern California*, Seismological Research Letters, Volume 78, 110-115, 2007

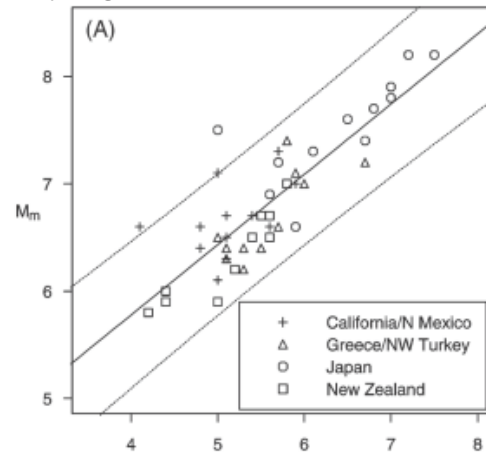
Description:

The EEPAS model is a long-range forecasting method that uses precursory minor earthquake to forecast the major ones. It uses preliminary information about precursory relations of precursor magnitude to mainshock magnitude, time scale and space occupied by all precursory earthquakes, mainshocks and aftershocks.

The procedure and appearance of it is similar to the ETAS model but uses instead of likelihood estimates the above mentioned preliminary examined relations. The model results depend on the quality of the preliminary investigations and the target magnitude scales for which the precursor events should be used.

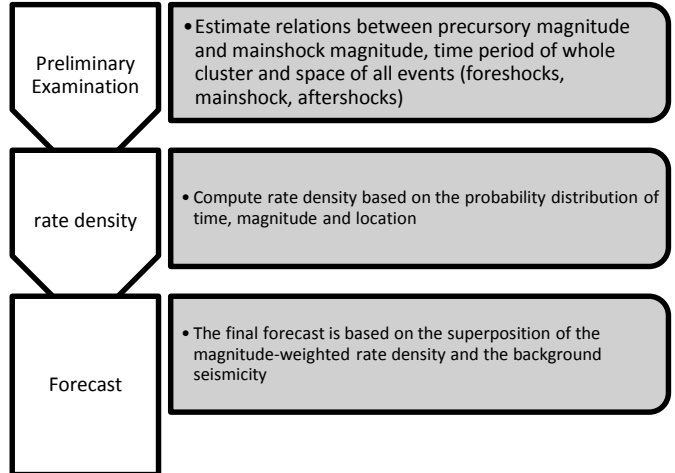
[1]

Sample Figure:



From [1]: Predictive relation of mainshock magnitude relative to precursor magnitude.

Method Overview:



Regions & Catalogues:

California: ANSS Earthquake Catalogue (1932 – 2004)

Japan: Catalogue of Japan Meteorological Agency (1965 – 2009)

Input Parameters:

- Location
- Magnitude
- Time

Model Parameters:

- EEPAS related precursory examination

Further publications:

²D. A. Rhoades – *Application of the long-range forecasting model to earthquakes in Japan mainland testing region*, Earth Planets Space, 63, 197-206, 2011, doi: 10.5047/eps.2010.08.002

Epidemic-Rate-Strain (ERS)

Author & related publication:

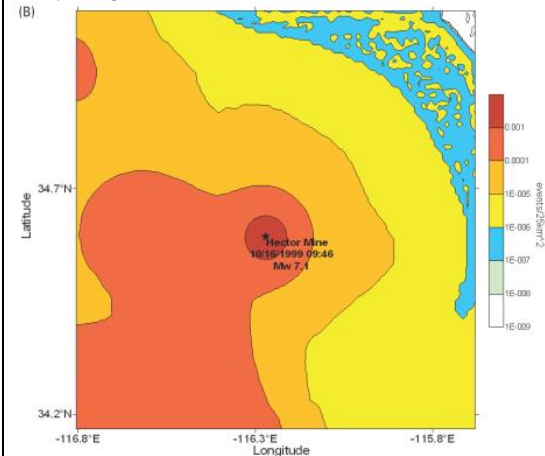
¹R. Console, M. Murru, F. Catalli, G. Falcone – *Real Time Forecasts through an Earthquake Clustering Model Constrained by the Rate-and-State Constitutive Law: Comparison with a Purely Stochastic ETAS Model*, Seismological Research Letters, Volume 78-1, 49-56, 2007

Description:

The Epidemic-Rate-Strain (ERS) Model is a close to real-time forecasting model, which is basically related to the ETAS model. Instead of purely stochastic parameters, the ERS incorporates the concept of the rate-and-state friction theory with two free parameters, which additionally increases the computation speed, because standard ETAS models need at least 4-5 free parameters (often more). It simplifies the purely stochastic model by using a empirically generated stress change parameters.

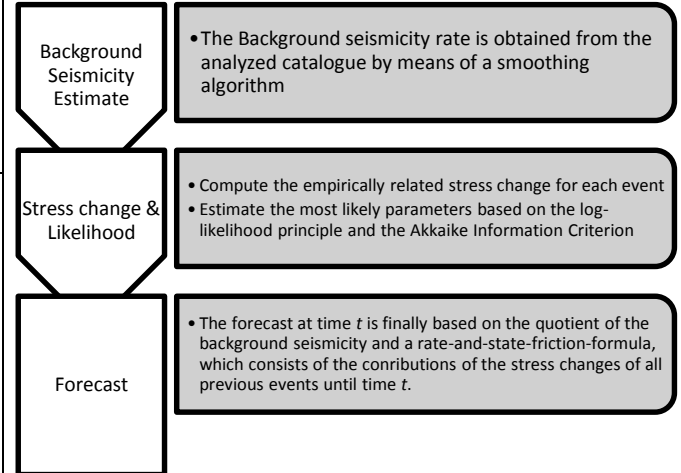
The parameters are estimated based on the log-Likelihood principle. Within a direct comparison to a purely stochastic ETAS model the ERS didn't lead to better results. This seems to be related to the more rigid behavior of the algorithm. [1]

Sample Figure:



From [1]: Occurrence-rate density for $m \geq 4$ earthquakes surrounding the epicenter of the Hector Mine earthquake of October 16, 1999. The occurrence rate was calculated directly for the conditions after the main shock.

Method Overview:



Regions & Catalogues:

California: ANSS Earthquake Catalogue (1984 – 2004)

Italy: INGV Catalogue (1987 – 2009)

Input Parameters:

- Location
- Magnitude
- Time

Model Parameters:

- Multiple ERS parameters

Further publications:

²G. Falcone, R. Console, M. Murru– *Short-term and long-term earthquake occurrence models for Italy: ETES, ERS and LTST*, Annals of Geophysics, 53, 3, 41-50, 2010, doi: 10.4401/ag-4760

Short-term Aftershock Probabilities (StAP)*

Author & related publication:

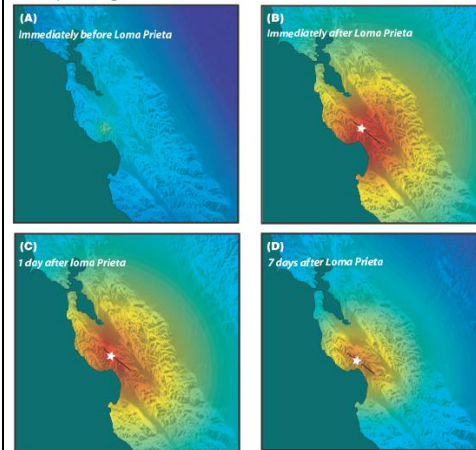
¹M. Gerstenberger, S. Wiemer, L. Jones – *Real-time Forecasts of Tomorrow's Earthquakes in California: a Mapping Tool*, U.S. Geological Survey, Open-File Report 2004-1390

Description:

The model of short-term aftershock probabilities was developed to calculate subsequent events after strong mainshocks for the following days. It combines basic occurrence laws like the Gutenberg-Richter relation and the modified Omori-law to define a time-dependent earthquake probability by taking combined aftershock sequences into account. A special focus is set to the spatial distribution which is calculated based on a leveled smoothing algorithm which uses rupture length and aftershock distribution. [1]

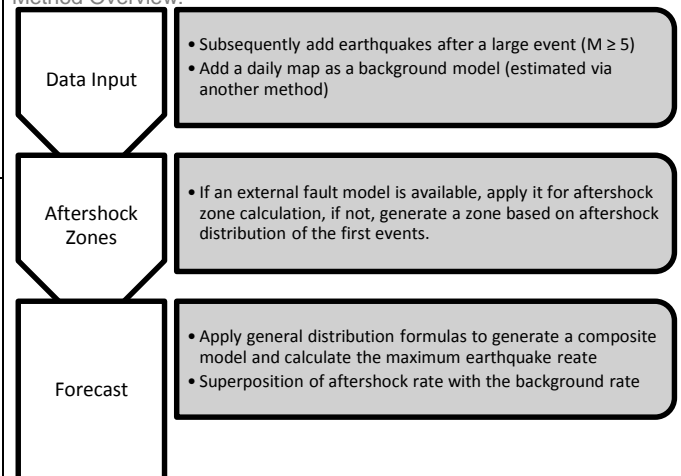
The method was running for several years to estimate earthquake probabilities after large events in California. Please note that this method does not generate long-term forecasting maps, it is totally focused on aftershock probabilities. [2]

Sample Figure:



From [2]: Short-time hazard snap shots for the Loma Prieta earthquake in California with Mw 6.9 from October 17, 1989, in time steps from immediately before the event until 7 days after the earthquake.

Method Overview:



Regions & Catalogues:

California: California Integrated Seismic Network

Input Parameters:

- Location
- Magnitude
- Time

Model Parameters:

- StAP parameters
- Rupture length
- Fault model (if available)

Further publications:

²M. Gerstenberg, L. Jones, S. Wiemer– *Short-term Aftershock Probabilities: Case Studies in California*, Seismological Research Letters, Vol. 78 No. 1, 66-77, 2007, doi: 10.5047/eps.2010.08.002

Early Aftershock Statistics (EAST)

Author & related publication:

¹P. Shebalin, C. Narteau, M. Holschneider, D. Schorlemmer.– *Short-Term Earthquake Forecasting Using Early Aftershock Statistics*, Bulletin of the Seismological Society of America, Vol. 101, No. 1, 2011, 297 - 312, doi: 10.1785/0120100119

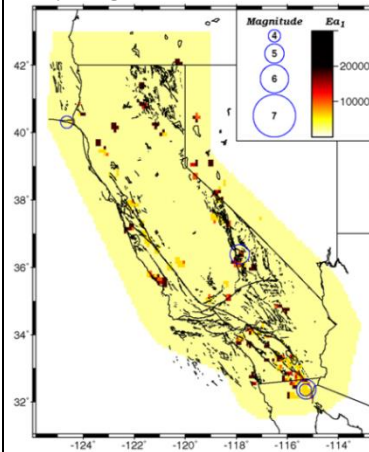
Description:

The EAST method is a short-term prediction method, designed to detect locations which are more prone to moderate or large earthquakes within an active fault zone. Its main hypothesis assumes that the time delay before the onset of the aftershock decay is anticorrelated with the level of stress in the seismogenic crust.

It uses the mean of elapsed time between long-term aftershocks and short-term aftershocks to the mainshock. Calculating their relation between, after reaching a certain threshold in the number of aftershocks in each time bin, generates a short term alarm value. The size of the relation between the mean elapsed times denotes which places are more vulnerable to subsequent target events during the next time step.

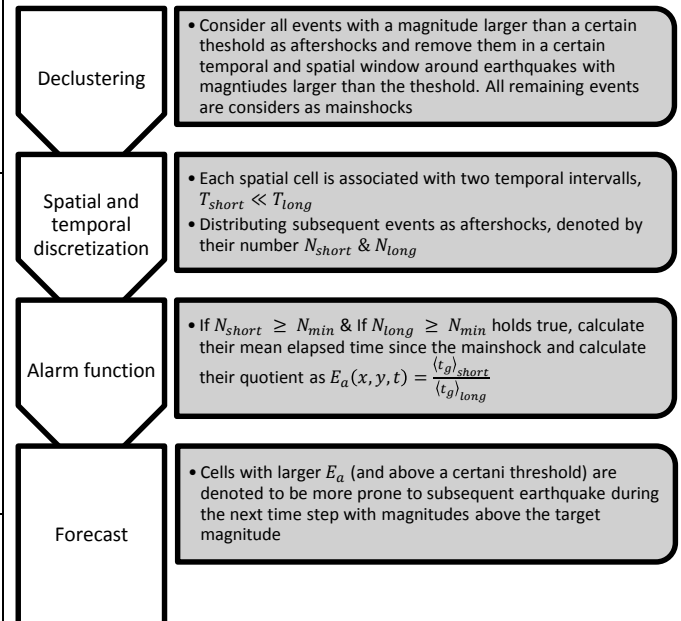
Based on first case studies of Californian earthquakes the method showed promising results.

Sample Figure:



From [1]: EAST forecast map for the period from July 1 – Sept. 30 2009 in California, Circles denote observed earthquakes during the forecasting period.

Method Overview:



Regions & Catalogues:

California: ANSS earthquake Catalogue (1960 – 2008)

Input Parameters:

- Location
- Time
- Magnitude

Model Parameters:

- Declustering parameters

Further publications:

Hybrid Methods

Fault Slip and Smoothed Seismicity (FSSS)*

Author & related publication:

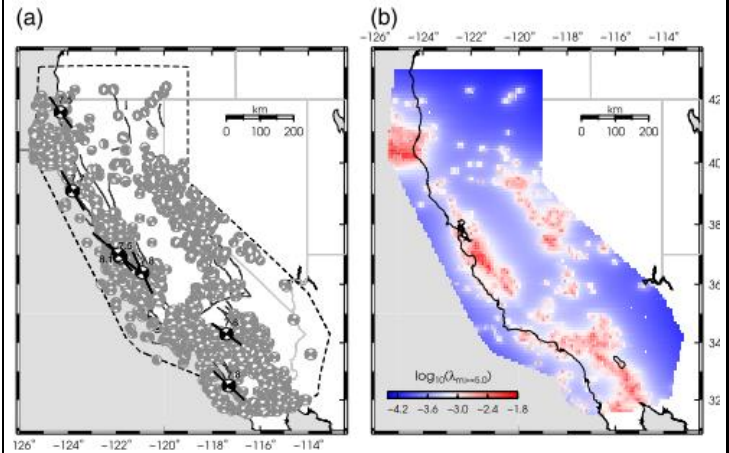
¹S. Hiemer, Q. Wang, D. D. Jackson, Y. Y. Kagan, J. Woessner, J. D. Zechar, S. Wiemer – *A Stochastic Forecast of California Earthquakes Based on Fault Slip and Smoothed Seismicity*, Bulletin of the Seismological Society of America, Vol. 103, No 2A, pp. 799-810, April 2013 doi: 10.1785/0120120168

Description:

The FSSS model is a stochastic earthquake source model for intermediate and long-term forecasts. It consists of two pairs of finally combined density maps. Each pair consists of two types of maps. The first type is a classical smoothed probability density map while the second one is a map of smoothed focal mechanisms. The first pair is made of the data of the historic earthquake catalogue which therefore must also contain information about the focal mechanisms. The second map is constructed by a transformation of the 3D-geometry of a recent fault map to some kind of density map.

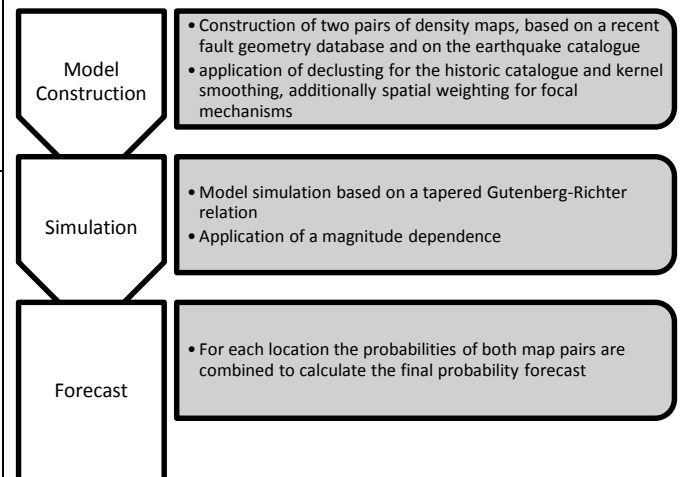
Via merging both maps with a magnitude-dependent weighting procedure and a tapered Gutenberg-Richter model it is possible to determine future areas of earthquakes.

Sample Figure:



From [1]: Two map views of the model result of 2000 earthquakes. (a) Each epicenter is denoted by its focal mechanism. (b) Cumulative forecast map with a total rate of 4.5 events per year with magnitude > 5.

Method Overview:



Regions & Catalogues:

California: Catalog of Wang et al. 2009 (1800 – 2007, extended to 2009), Uniform California Earthquake Rupture Forecast and Southern California Earthquake Center Community Fault Model

Input Parameters:

- Location, Time
- Magnitude
- Focal Mechanism
- Fault database

Model Parameters:

- Smoothing
- Fault transformation

Further publications:

HSM (Hybrid Seismicity Method)*

Author & related publication:

¹C.-H. Chan, M. Sorensen, D. Stromeyer, G. Grünthal, O. Heidbach, A. Hakimhashemi, F. Catalli – *Forecasting Italian seismicity through a spatio-temporal physical model: importance of considering time-dependency and reliability of the forecast*, Annals of Geophysics, 53, 3, 129-140, 2010; doi: 10.4401 / ag-4761

Description:

The Hybrid Seismicity Method combines a classic time-independent smoothing algorithm based on a power-law kernel with a time-dependent rate-and-state friction model, which applies Coulomb stress changes. It was used for the CSEP project in Italy. The dataset was both tested for the clustered and declustered case, which resulted in better approximations with declustered datasets. In addition, the application of the rate-and-state friction model lead only to a marginal improvement. It was assumed that the improvement should behave better, the authors suggest to use more detailed information for the source fault model, because for this method just estimated scaling laws have been applied to retrieve fault parameters better data and scaling laws might lead to better results.

Due to the results of the CSEP project the HSM overestimated the total number of events during the testing period, but passed most of the applied test, except for the magnitude likelihood, where the HSM adequately forecasted the observe $M_L > 7$ events [2].

Regions & Catalogues:

Italy: Catalogo della Sismicità Italiana (used: 1985 – 2002), Bollettino Sismic Italiano (2003 - 2008)

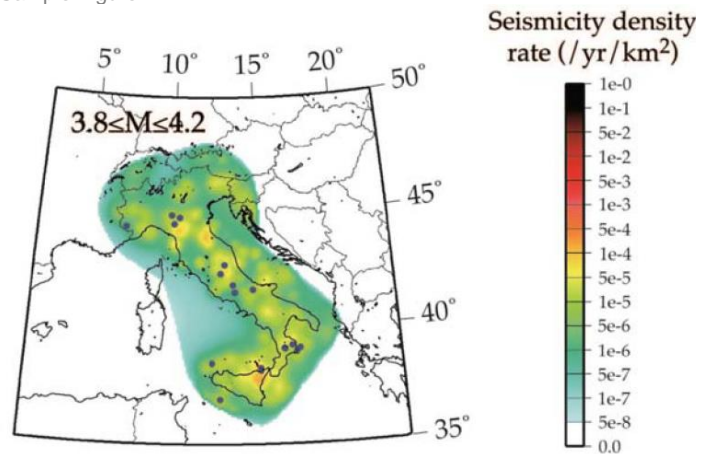
Input Parameters:

- Location
- Time
- Magnitude
- Focal mechanisms

Model Parameters:

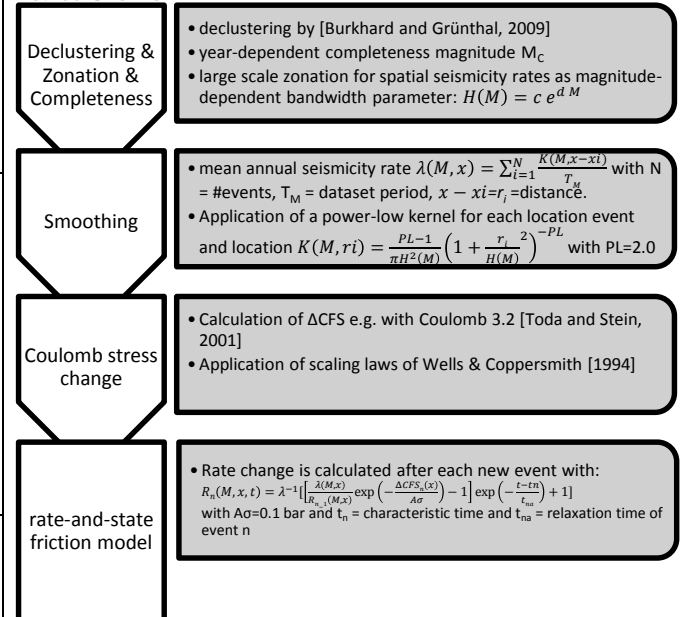
- b-value
- Smoothing
- Declustering
- Fault parameters

Sample Figure:



From [1]: Distribution of reference seismicity for local magnitudes between 3.8 and 4.2 based on a declustered dataset. The blue dots indicate earthquake which occurred during the testing period.

Method Overview:



Further publications:

²J. M. Werner, J. D. Zechar, W. Marzocchi, S. Wiemer - *Retrospective evaluation of the five-year and ten-year CSEP-Italy earthquake forecasts*, Annals of Geophysics, 53, 3, 2010; doi: 10.4401 / ag-4840

Long-term Stress Transfer (LTST)

Author & related publication:

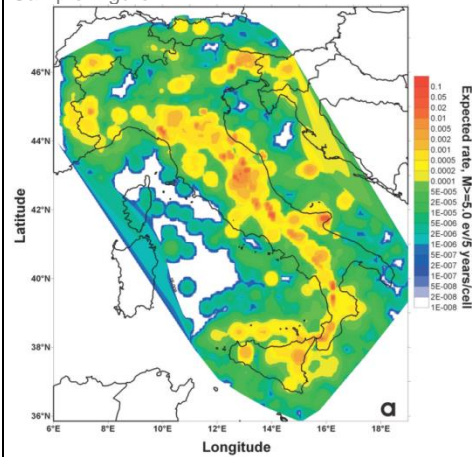
¹C.-H. Chan, M. Sorensen, D. Stromeyer, G. Grünthal, O. Heidbach, A. Hakimhashemi, F. Catalli – *Forecasting Italian seismicity through a spatio-temporal physical model: importance of considering time-dependency and reliability of the forecast*, *Annals of Geophysics*, 53, 3, 129-140, 2010; doi: 10.4401 / ag-4761

Description:

The LTST algorithm is based on the fusion of a statistical renewal model with a physical model. It considers fault interactions, which might increase or decrease future seismicity. The fault interactions are computed based on the co-seismic static permanent Coulomb stress change caused by all earthquakes since the last characteristic event on a certain fault segment.

This model can be used for long-term forecasting intervals by using two parameters, the average interevent time and the aperiodicity. To apply the method additional data, like the focal mechanisms, is necessary to cover the stress changes. Furthermore, the fault parameters of strike, dip, rake, dimensions and average slip are needed to perform computation. [1]

Sample Figure:

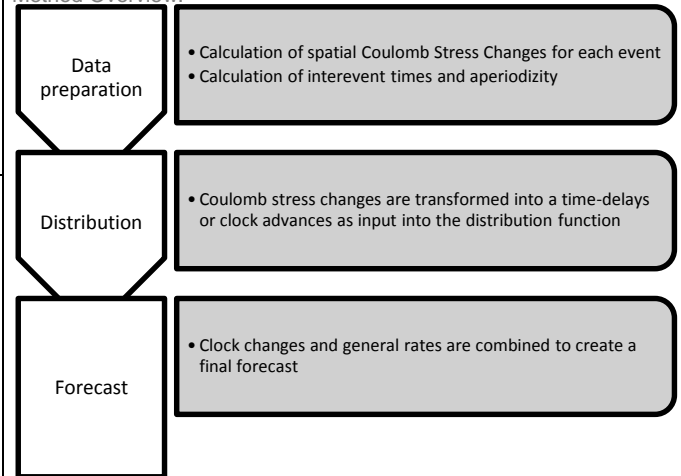


From [1]: 5-year forecast map of Italy, for events $M \geq 5$ earthquakes in Italy based on the LTST algorithm, starting from August 1, 2009.

Regions & Catalogues:

Italy: Catalogo Parametrico del Terremoti Italiani (1899 – 2004), DISS 3.1.0 seismogenic areas, INGV (2004 – 2009)

Method Overview:



Input Parameters:

- Location
- Time
- Magnitude
- Focal mechanisms

Model Parameters:

- Interevent times & aperiodicity
- Fault parameters

Further publications:

²R. Console, M. Murru, and G. Falcone – *Perturbation of earthquake probability for interacting faults by static Coulomb stress changes*, *Journal of Seismology*, 14, 67-77, doi: 10.1007/s10950-008-9149-4.

SHIFT (Seismic Hazard Inferred from Tectonics)

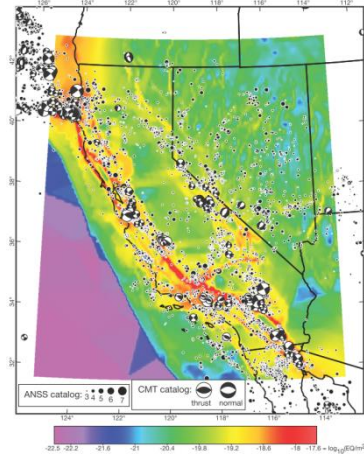
Author & related publication:

¹P. Bird, Z. Liu – *Seismic Hazard Inferred from Tectonics: California*, Seismological Research Letters Volume 78, 37-48, 2007

Description:

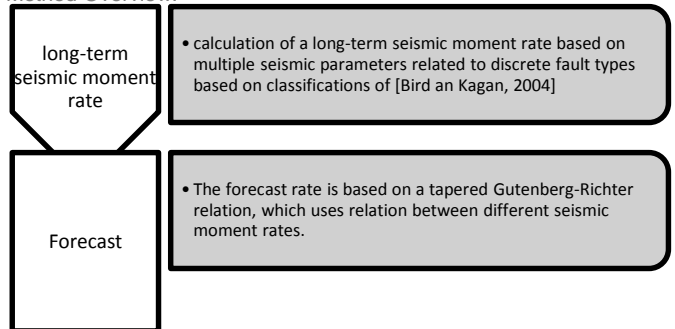
The SHIFT model for estimating long-term average seismicity of a certain region uses a local kinematic model of surface velocities and an existing global calibration of plate-boundary seismicity [1]. This global calibration is based on former publications of Bird e.g. [Bird and Kagan 2004]. It uses an approximation of the long-term average seismic moment rate and applies it to a tapered Gutenberg-Richter model. Due to the testing in the RELM project, the SHIFT model overestimated the number of events, which was related to the overall rates, which were much too high.

Sample Figure:



From [1]: Long-term forecast for the seismicity in the California region for a threshold magnitude of 5.663 according to the SHIFT model. The spatial integral states about 63 earthquakes per 25.75 years in the depth range 0-70 km.

Method Overview:



Regions & Catalogues:

California: Harvard CMT catalogue

Input Parameters:

- Geodetic data
- Geologic data
- Tectonic data
- Stress-directions

Model Parameters:

- Seismicity Parameters

Further publications:

²J.D. Zechar, D. Schorlemmer, M. J. Werner, M. C. Gerstenberger, D. A. Rhoades, T.H. Jordan – *Regional Earthquake Likelihood Models I: First-Order Results*, Bulletin of the Seismological Society of America, Vol. 103, No. 2A, pp. 787-798, April 2013, doi: 10.1785/0120120186

Fault-oriented Earthquake Forecast (FoEF)*

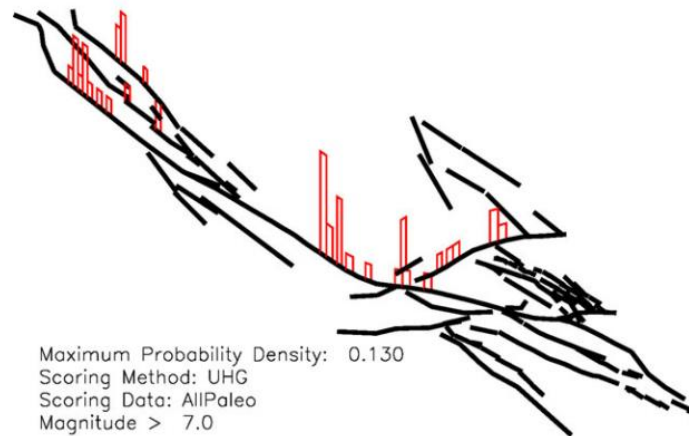
Author & related publication:

¹J. v. Aalsburg, J. B. Rundle, L. B. Grant, P. B. Rundle, G. Yakovlev, , D. L. Turcotte, etc.– *Space- and Time-Dependent Probabilities for Earthquake Fault System from Numerical Simulations: Feasibility Study and First Results*, Pure Applied Geophysics, 167, 2010, 697 - 977, doi: 10.1007/s00024-010-0091-3

Description:

FoEF uses topologically realistic numerical simulations for the strike-slip fault system in California to identify future rupture elements of the fault system. The Virtual California fault model was used to apply friction laws and other physical parameters. By tuning the model a stochastic set of earthquake series is calculated and compared to paleoseismic observations. To identify modeled time series which seem to reproduce historic data most accurately a time series score is applied. The models with the highest score are used to generate probability density function spatially distributed for each fault element, stating probabilities for participation in future large earthquake events.

Sample Figure:

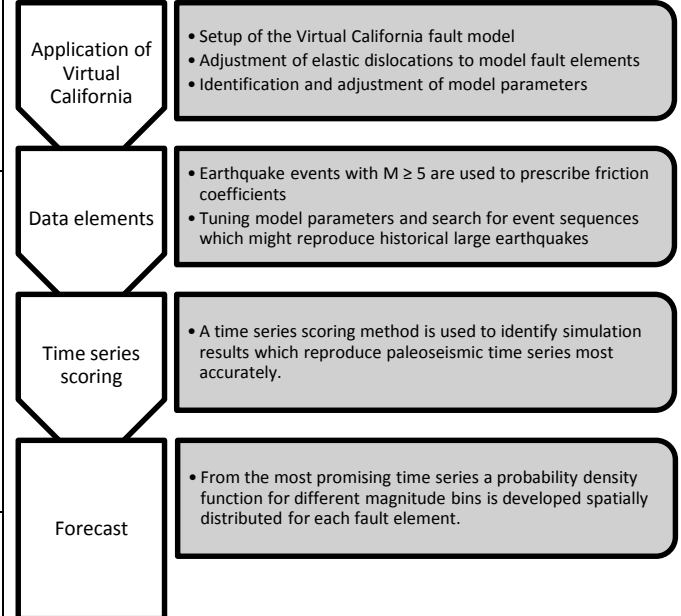


From [1]: Fault boundary map showing probabilities of participation of the next $M > 7$ earthquake.

Regions & Catalogues:

California: Paleoseismic Data for southern California

Method Overview:



Input Parameters:

- Virtual fault model
- Paleoseismic Data

Model Parameters:

- Physical parameters

Further publications:

Appendix B: Time-independent sample Method

This appendix shows the whole process of how to assemble a time-independent forecasting method. Key feature of this method will be the dynamic b-value, partially based on the approach of [Gulia et al., 2010].

The method will be based on an un-declustered dataset and will apply a simple self-normalizing Gaussian smoothing algorithm. It follows the following guideline:

1. Input and sort dataset
2. Calculate regional b-value
3. Calculate local b-values
4. Choose final local b-value based on maximum likelihood
5. Calculate smooth seismicity map
6. Calculate local earthquake rates

For the beginning, the dataset must be sorted and organized. For this approach only 4 parameters are necessary, time, magnitude, longitude and latitude. Important for the approach of local b-values is a large dataset. Depending on the data the completeness magnitude should be as low as possible to sufficiently estimate the Gutenberg-Richter relation.

The following program is built for a forecast in Turkey. The dataset covers approximately 1000 years and will be used down to a magnitude of 4.0. Due to data incompleteness, completeness periods for different magnitude ranges have to be applied. The completeness periods can be found in chapter 5.2.

Please note that this code is not part of the toolbox, it is a complete algorithm in one file, while the toolbox is a set of different functions. The toolbox function for local b-value calculation incorporates partial aspects of this code.

```
clear all; close all
%loading data
fid4=fopen('D:\...\dataset.txt','r');
list = textscan(fid4, '%f %f %f %f %f %f %f %f', 'delimiter','\t');
clear fid4

%sorting and organizing input data
year_list(:,1)=cell2mat(list(:,1));
month_list(:,1)=cell2mat(list(:,2));
day_list(:,1)=cell2mat(list(:,3));
mag_list(:,1) = cell2mat(list(:,8));
lat_list(:,1) = cell2mat(list(:,4));
long_list(:,1) = cell2mat(list(:,5));
k = [];
%selection element
for i = 1:length(mag_list)
    if mag_list(i) >= 5.0 & year_list(i)>= 1000 &
year_list(i)~=linspace(1995,2004,10) & long_list(i) <= 50 & long_list(i)
>= 20 & lat_list(i) <= 44 & lat_list(i) >= 32
        k = [k i];
    end
end
```



```
end
    k = [k i];
end
if isnan(month_list(i)) == 1
    month_list(i) = 1;
end
if isnan(day_list(i)) == 1
    day_list(i) = 1;
end
end
used_events = k;
%shrink dataset for the used_events
year_list = year_list(used_events,1);
month_list = month_list(used_events,1);
day_list = day_list(used_events,1);
lat_list= lat_list(used_events);
long_list = long_list(used_events);
mag_list = mag_list(used_events);

no_events = length(mag_list);
max_year = max(year_list);
```

Secondly, the global b-value has to be calculated. Therefore the dataset is sorted into magnitude bins for which the corresponding completeness period is applied. Afterwards the cumulative logarithmic observed annual rate is calculated and via a linear regression the b-value is calculated.

```
%-calculation-of-regional-b-value-----
%-----
spacing = 7;
m_space = linspace(5.0,7.5,spacing);
mc = 3.5;
%magnitude binning
bin_global = zeros(1,spacing);
for m=1:length(m_space)
    for i=1:no_events
        if m < length(m_space)
            if mag_list(i) >= m_space(m) && mag_list(i) < m_space(m+1)
                bin_global(m) = bin_global(m) +1;
            end
        else
            if mag_list(i) >= m_space(m)
                bin_global(m) = bin_global(m) +1;
            end
        end
    end
end
end

%cumulative magnitude annual rate
for m=1:(length(bin_global)-1)
    if m_space(m) < 5.5
        bin_global(m) = bin_global(m) / (max_year-1900);
    elseif m_space(m) < 6.0
        bin_global(m) = bin_global(m) / (max_year-1750);
    elseif m_space(m) < 6.5
        bin_global(m) = bin_global(m) / (max_year-1500);
    else
        bin_global(m) = bin_global(m) / (max_year-1000);
    end
end
```

```
    end
end
bin_global(m+1) = bin_global(m+1)/(max_year-1000);
for m=(length(bin_global)-1):-1:1
    bin_global(m) = bin_global(m) + bin_global(m+1);
end

bin_global = log10(bin_global);
%regression
p = polyfit(m_space,bin_global,1);
%regional b-value
b_global = -p(1)

LL_global = 0;
beta_global=b_global*log(10);
```

For the spatial discretization, a grid of $0.1^\circ \times 0.1^\circ$ is generated:

```
%-spatial-discretization-----
%-----
%Turkey: latitude    32 - 44
%           longitude: 20 - 50

k = 0;
space_long = 300;
space_lat = 120;
cell_size = 11.1;
for i = 1:space_lat
    for j = 1:space_long
        k = k+1;
        loc_lat(k) = 32 + 12./space_lat*(i-1);
        loc_long(k) = 20 + 30./space_long*(j-1);
    end
end
no_points = length(loc_lat);
```

For the calculation of the local b-value, all earthquakes within a circle of a certain radius are used. To find out which radius is the appropriate one, the likelihood for a set of radii is computed and finally compared based, together with the regional b-value, on the corrected Akkaike Information Criterion. From which the one with the smallest AIC_c is chosen.

```
%%
%-calculation-of-local-b-value-----
%-----
radii = linspace(10,100,10);
b_values = zeros(no_points,10);
AIC = zeros(no_points,10);
AIC_global = zeros(no_points,1);
for i=1:no_points
    for r = 1:length(radii)
        radius = radii(r);
        distance_list = zeros(1,no_events);
        %calculating distance between location and all events
        for j=1:no_events
```

Appendix B: Time-independent sample Method

```
d_lat = (loc_lat(i) - lat_list(j))*pi()/180;
d_long = (loc_long(i) - long_list(j))*pi()/180;
distance_list(j) = 2 * 6371 *
asin((sin(d_lat/2).^2+cos(loc_lat(i)*pi()/180)*cos(lat_list(j)*pi()/180)*si
n(d_long/2).^2).^0.5);
end
clear index
index = find(distance_list <= radius);
if isempty(index) == 0
    if max(mag_list(index)) ~= min(mag_list(index))
        if length(index) >= 5
            %magnitude binning
            bin_global = zeros(1,length(m_space));
            for m=1:length(m_space)
                if m<length(m_space)
                    bin_global(m) = length(find(mag_list(index)>=m_space(m) &
mag_list(index) < m_space(m+1)));
                else
                    bin_global(m) =
length(find(mag_list(index)>=m_space(m)));
                end
            end
            end
            %cumulative magnitude annual rate
            for m=1:(length(bin_global)-1)
                if m_space(m) < 5.5
                    bin_global(m) = bin_global(m)/(max_year-1900);
                elseif m_space(m) < 6.0
                    bin_global(m) = bin_global(m)/(max_year-1750);
                elseif m_space(m) < 6.5
                    bin_global(m) = bin_global(m)/(max_year-1500);
                else
                    bin_global(m) = bin_global(m)/(max_year-1000);
                end
            end
            end
            for m=(length(bin_global)-1):-1:1
                bin_global(m) = bin_global(m) + bin_global(m+1);
            end
            end
            if length(nonzeros(bin_global)) >= 2
                p =
polyfit(m_space(1:length(nonzeros(bin_global))),log10(nonzeros(bin_global))
',1);
                b_values(i,r) = -p(1);
                LL = 0;
                LL_global = 0;
                beta=b_values(i,r)*log(10);
                %calculating the likelihood for both the local as the
                %regional b-value
                for m=1:length(mag_list(index))
                    LL = LL + log10(beta*exp(-beta*(mag_list(index(m))-
mc))/(1-exp(-beta*(max(mag_list)-mc))));
                    LL_global = LL_global + log10(beta_global*exp(-
beta_global*(mag_list(index(m))-mc))/(1-exp(-beta_global*(max(mag_list)-
mc))));
                end
                AIC_global(i) = -2*max(LL_global)+2*0+(2*0*(0+1))/(no_events-0-
1);
                AIC(i,r) = -2*max(LL)+2*1+(2*1*(1+1))/(length(index)-1-1);
            end
            end
        end
    end
end
```

```
        end
    end
end
b_value_final = zeros(no_points,1);
used_radius = zeros(no_points,1);
%comparison of the AICs to choose the appropriate b-value and its
%corresponding used_radius
for i = 1:no_points
    if length(nonzeros(AIC(i,:))) >= 1
        index2 = find(AIC(i,:)==min(nonzeros(AIC(i,:))));
        used_radius(i) = radii(min((index2)));
        if AIC(i,index2) < AIC_global(i)
            b_value_final(i)=b_values(i,min(index2));
        else
            b_value_final(i)=b_global;
        end
    end
end
end
```

Finally to account for location uncertainty, the local b-values are smoothed. Using simply the mean over a certain circle around each point.

```
%-smoothing-b-values-----
%-----
stencil_size = 75; %smoothing distance
b_value_final_s=zeros(no_points,1);
for i=1:no_points
    distance_list = zeros(no_points,1);
    for j=1:no_points
        d_lat = abs((loc_lat(i) - loc_lat(j)))*pi()/180;
        d_long = abs((loc_long(i) - loc_long(j)))*pi()/180;
        distance_list(j) = 2 * 6371 *
asin((sin(d_lat/2).^2+cos(loc_lat(i)*pi()/180)*cos(loc_lat(j)*pi()/180)*sin
(d_long/2).^2).^0.5);
    end
    dist_index = find(distance_list<= stencil_size);
    b_value_final_s(i)=mean(nonzeros(b_value_final(dist_index)));
end
```

After all parameters are calculated, the dataset can be spatially smoothed by using a self-normalizing Gaussian kernel. At first the events are distributed over all grid cells and afterwards the smoothing is applied.

```
%%
%-spatial-smoothing-of-seismicity-----
%-----
corr_dist=40; %smoothing parameter
N = zeros(no_points,spacing);
N_i = zeros(no_points,spacing);
for i = 1:no_points
    for j = 1:no_events
        d_lat = abs((loc_lat(i) - lat_list(j))*110);
        d_long = abs((loc_long(i) - long_list(j))*110);
        if d_lat <= cell_size/2 && d_long <= cell_size/2
            for m = 1:spacing
                if mag_list(j)>= (5.0 + 0.5*(m-1)) & mag_list(j) < (5.0 +
0.5*m)
```

Appendix B: Time-independent sample Method

```
                N(i,m) = N(i,m) + 1/(max_year-10-period_list(m));
            end
        end
    end
end

normalizer = zeros(no_points,spacing);

for i = 1:no_points
    for j = 1:no_points
        d_lat = (loc_lat(i) - loc_lat(j))*pi()/180;
        d_long = (loc_long(i) - loc_long(j))*pi()/180;
        dist = 2 * 6371 *
asin((sin(d_lat/2).^2+cos(loc_lat(i)*pi()/180)*cos(loc_lat(j)*pi()/180)*sin
(d_long/2).^2).^0.5);
        if dist <= 3*corr_dist
            for m=1:spacing
                N_i(i,m) = N_i(i,m) + N(j,m)*exp(-dist^2/(corr_dist^2));
                normalizer(i,m) = normalizer(i,m) + exp(-
dist^2/(corr_dist^2));
            end
        end
    end
    for m=1:spacing
        N_i(i,m) = N_i(i,m)/(normalizer(i,m));
    end
    i/no_points
end
for i=1:no_points
    for m=(spacing-1):-1:1
        N_i(i,m) = N_i(i,m)+N_i(i,m+1);
    end
end
```

Finally the a-value is calculated for each location following the approach of chapter 4.1.3. Afterwards the rate and the probability for each magnitude bin and location can be computed.

```
%%
%- -rate-calculation-----
%------

forecast=zeros(no_points,7);
P = zeros(no_points,7);
m=linspace(5,8,7);
forecast_period = 10;
m_min=5;
for mag=1:length(m)
    forecast_magnitude = m(mag);
    forecast(:,mag)=10.^(log10(N_i(:,1))-
b_value_final_s*(forecast_magnitude-m_min));
    P(:,mag)=1-exp(-forecast(:,mag).*forecast_period);
end
```

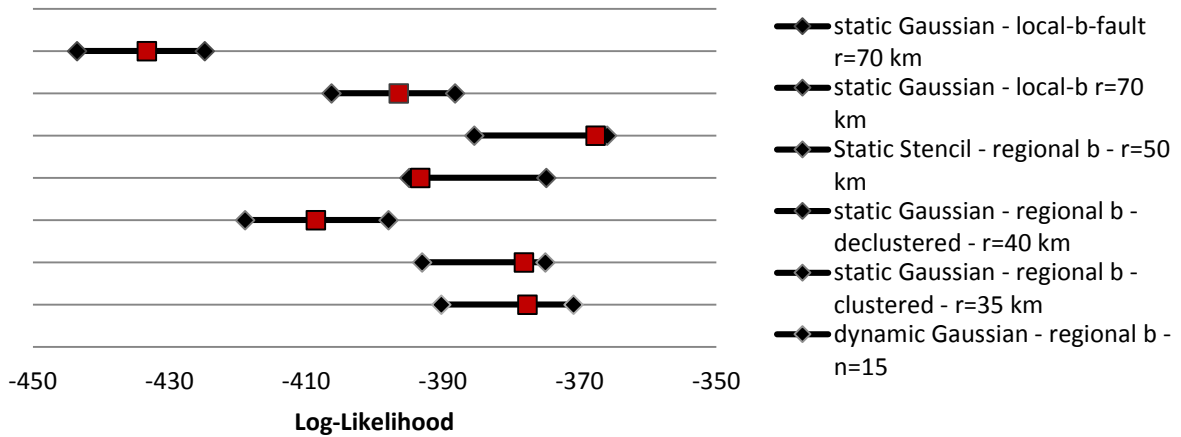
Appendix C: Time-independent Test Results

Spatial and temporal likelihood comparisons for the tested time-independent methods, where the lines represent the 95% confidence interval of the stochastic earthquake density, and the red point represents the likelihood of the observed events. Applied on Turkey and Italy of the period from 1995 to 2005, 1985 to 1995 and 1975 to 1985.

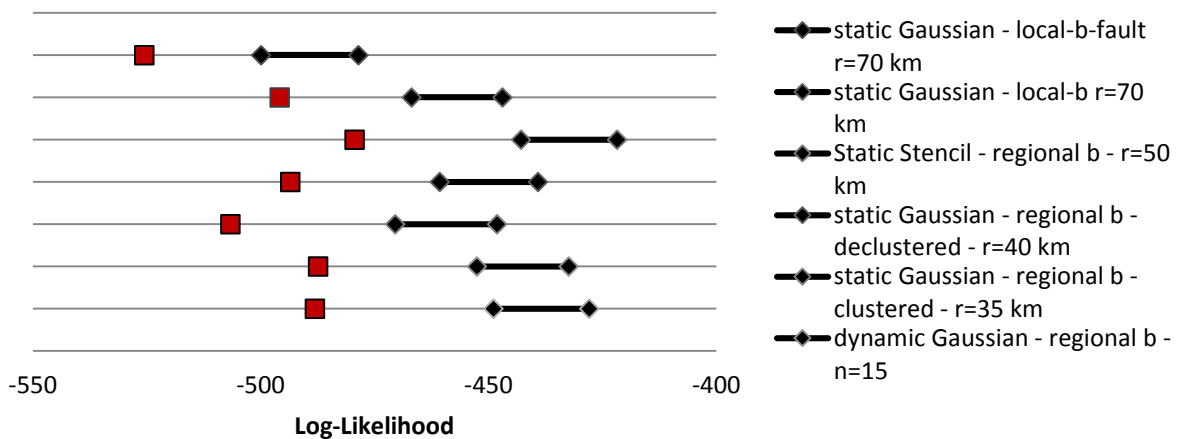
A detailed description of the testing procedure and the related methods which have been tested is given in chapter 5. The S-Test denotes the quality of spatial accuracy of the tested method, while the M-Test does the same for the magnitudes. The forecast of a method is assumed to be consistent with the observation if the log-likelihood of the forecast is in the 95% reliability range of stochastically computed forecasts. Alternatively the forecast is assumed to be consistent if the observation is more likely (value closer to 0) than 50% of the forecasts. In direct comparison, the forecasts whose mean exactly fits the likelihood (red dot is in the center the black bar) of the observation is assumed to be the best result for a certain period.

Turkey: S-Tests

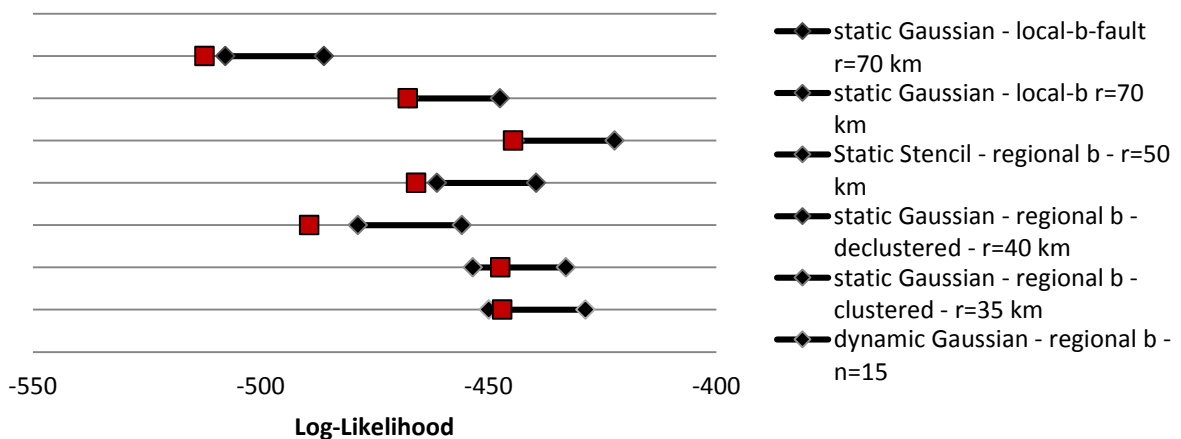
S-Test Likelihood Comparison for 1995 - 2005, Turkey



S-Test Likelihood Comparison for 1985 - 1995, Turkey

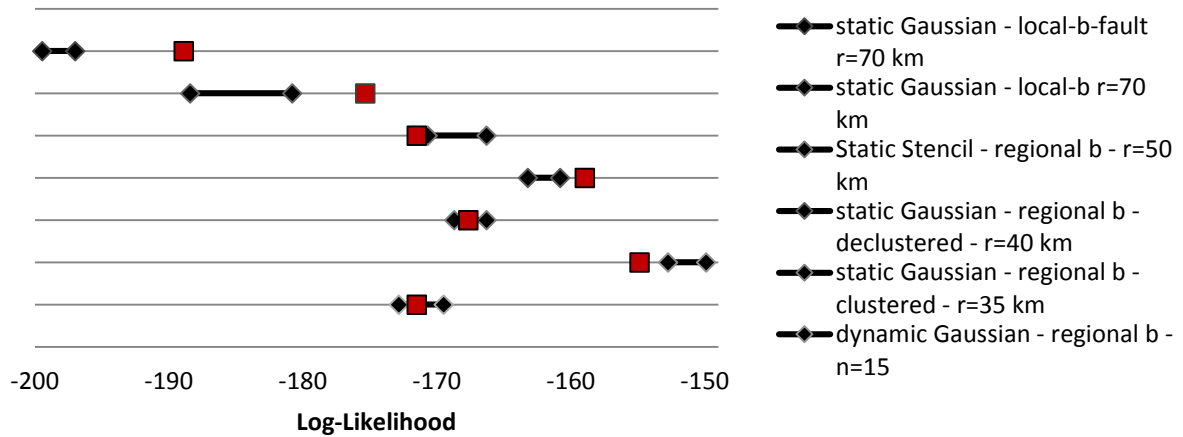


S-Test Likelihood Comparison for 1975 - 1985, Turkey

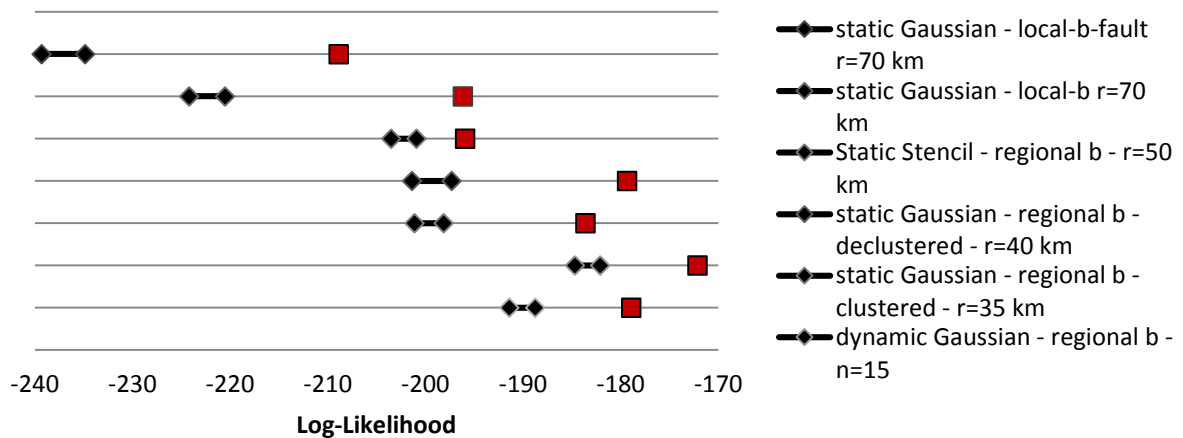


Turkey: M-Tests

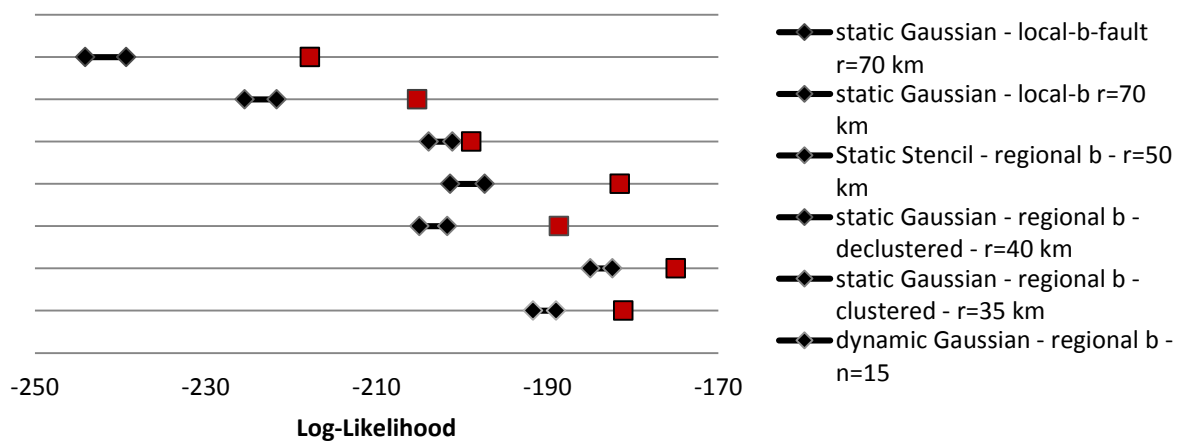
M-Test Likelihood Comparison for 1995- 2005, Turkey



M-Test Likelihood Comparison for 1985 - 1995, Turkey

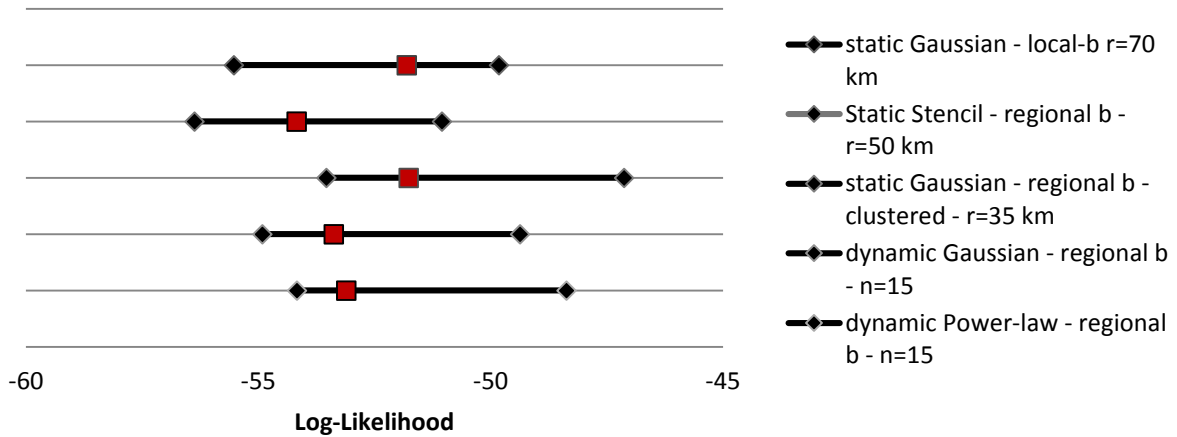


M-Test Likelihood Comparison for 1975 - 1985, Turkey

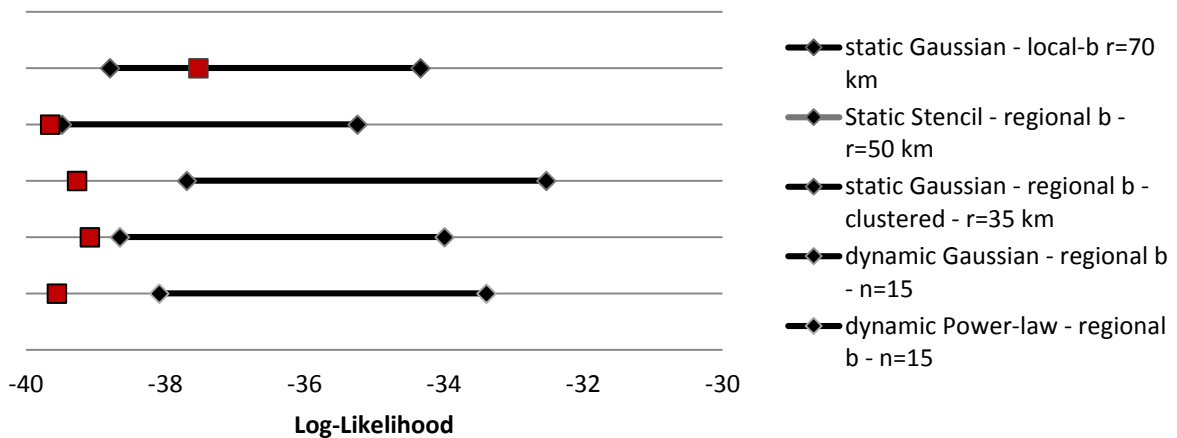


Italy: S-Tests

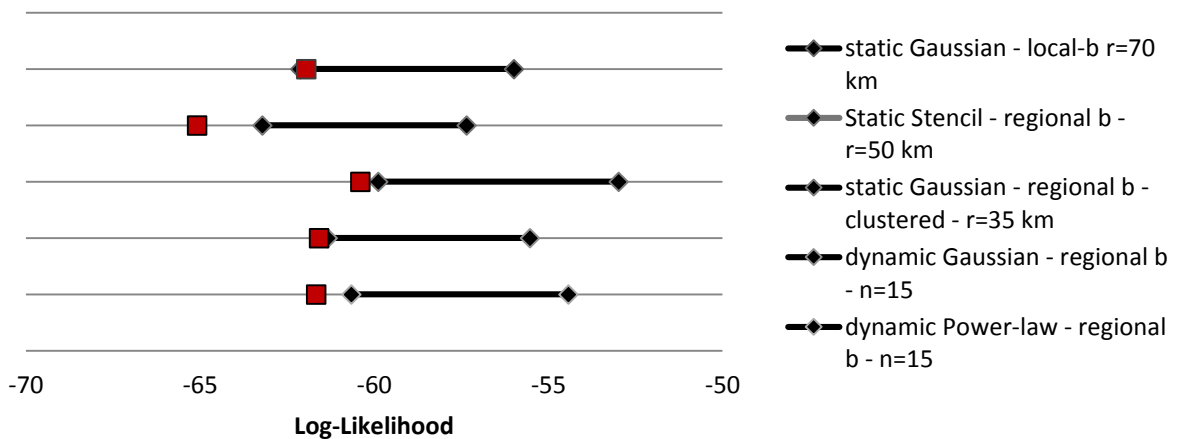
S-Test Likelihood Comparison for 1995- 2005, Italy



S-Test Likelihood Comparison for 1985- 1995, Italy

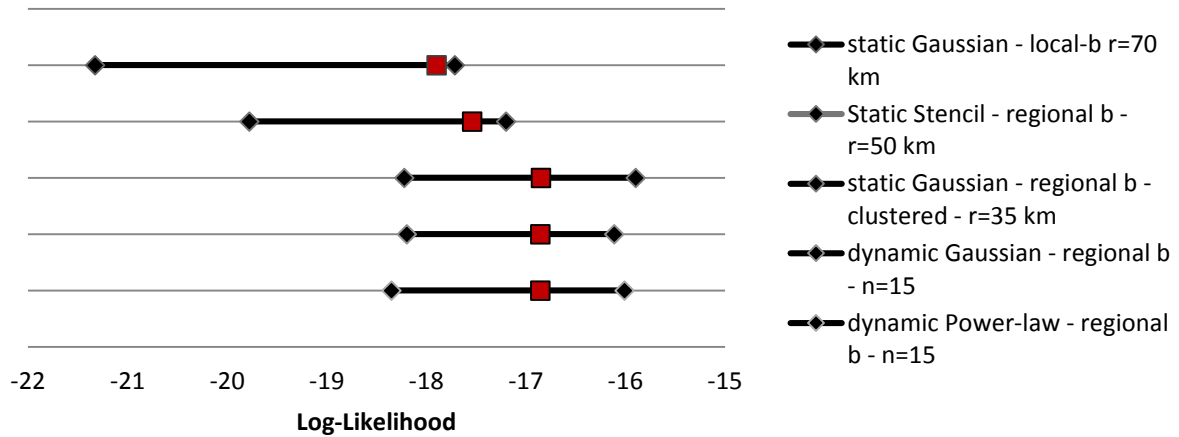


S-Test Likelihood Comparison for 1975- 1985, Italy

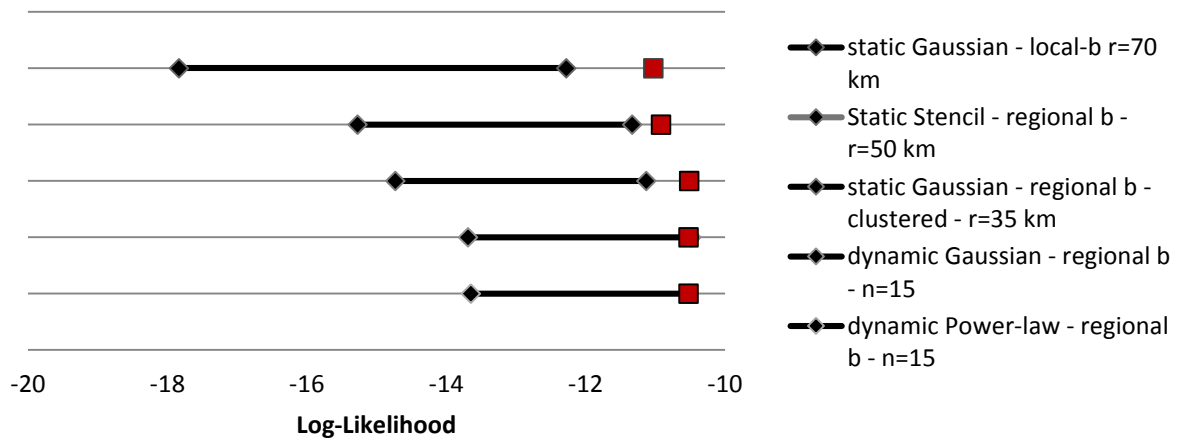


Italy: M-Tests

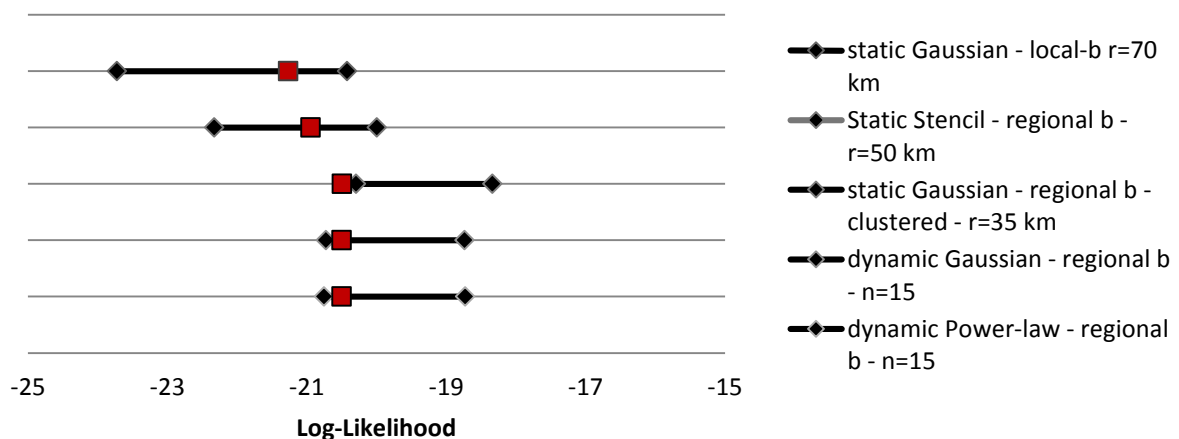
M-Test Likelihood Comparison for 1995- 2005, Italy



M-Test Likelihood Comparison for 1985- 1995, Italy



M-Test Likelihood Comparison for 1975- 1985, Italy



Appendix D: Time-independent Method Toolbox

During this thesis a lot of different algorithms and codes have been assembled and coded. A set of them, which cover most of the described methods and approaches is given on a CD with this thesis. This CD contains:

1. the time-independent method toolbox
2. a set of time-dependent methods
3. the Slip Accumulation method (together with necessary fault data)
4. a set of declustering algorithms
5. the earthquake catalogues

The references for the different methods and datasets are given in the related chapters of this text book. In the following, the readme of the CD is shown, which explains the content in more detail. All codes are written in Matlab©.

The toolbox does not contain exactly the same methods which have been tested in this thesis. It rather gives a range of assembling possibilities and stable algorithms. The time-independent toolbox is an easy-to-use tool to generate simple time-independent forecasting methods. The codes can be of course further calibrated and advanced for more complex algorithms.

```
-----  
-State-of-the-Art-Review-and-Analysis-Earthquake-Forecasting--  
-Dipl.-Ing.-Andreas-Schaefer-----  
-----
```

This CD was assembled and developed during the Masterthesis of Dipl.-Ing. Andreas Schaefer about as aState-of-the-Art Review and Analysis of Earthquake Forecasting. It provides essential code elements and developments for earthquake forecasting. Details about the algorithms are given in the thesis.

```
-----  
-Time-independent-Toolbox-----  
-----
```

The first set of codes is for time-independent forecasting methods and is meant as a toolbox to easy assemble future time-independent forecasting algorithms. The user can choose between different options for spatial smoothing, catalogue declustering and Gutenberg-Richter handling. The codes can be

used to smooth with or without magnitude binning. The following overview shows how a time-independent algorithm can be assembled:

1. import data
2. calculate / set b-value
3. spatial discretization
4. spatial smoothing with magnitude bins
5. Option: local b-value calculation
6. Probability Calculation

-Time-dependent-Code-Samples-----

In addition, this CD contains three time-dependent forecasting methods. Two of them have been reconstructed based on published approaches, Pattern Informatics (PI) and Epidemic-type of Aftershock Sequences (ETAS), the third one was developed by the author and introduces time-dependent b-values. The time-dependent b-value method and the ETAS method are calibrated for Turkey, while the PI method is also applicable for Italy.

- Pattern Informatics (PI)
- Epidemic-Type of Aftershock Sequences (ETAS)
- time-dependent b-values (tdb)

-Slip-Accumulation-Method-----

This method was developed by the author to give a quite simple example of the development of a hybrid method which incorporates fault-based slip rates. The method is calibrated both for Turkey and Italy.

-Data-----

Data given on this CD is referenced in the related textbook. In total, to regions, Italy and Turkey, are given with historical catalogues. Furthermore a simplified version of the SHARE fault database is given. The data is used for scientific purpose only.

-CSEP-Testing-Algorithms-----

Together with the time-independent methods a set of stochastic likelihood tests was reconstructed based on the testing procedure of the CSEP project. These algorithms calculate likelihood scores for magnitude (M-test) and spatial (S-test) scales and the Poisson probability of the total observation density (N-test).

-Test-Results-----

Almost all test results which have been developed in this thesis project are also given as Excel sheets.

The following is covered:

- time-independent likelihood test results (M & S & N-tests) for Turkey and Italy
- ETAS test results both for background seismicity and aftershock activity.

©Andreas_Schaefer

For further questions, please inform:
aschaefer.engineering@gmail.com

The Toolbox itself just uses the file `main.m` as the starting point from which different subfunction can be called. The following list shows all functions which are included in the toolbox.

- `main.m` main file from which the time-independent method can be assembled
- `spat.dist.m` function for spatial discretization
- `smoothing_static.m` function for static spatial smoothing, supports different distribution functions (Gaussian, Power law, Donut, Stencil/Moore neighborhood)
- `smoothing_dynamic.m` function for dynamic spatial smoothing, see above
- `calc_b_global.m` function to calculate a b -value for the whole earthquake catalogue
- `calc_b_local.m` function to calculate local b -value based on a maximum likelihood principle
- `CSEP_testing.m` includes the likelihood testing procedure for time-independent methods

The content of the file `main.m` is given below:

```
%-import-dataset-----  
%-----  
  
load('Turkey_declustered.mat') %import data  
%year_list  
%month_list  
%day_list  
%lat_list  
%long_list  
%mag_list  
%no_events  
max_year=max(year_list); %determine most recent entry on an annual basis  
  
%possible files:  
%'Turkey_clustered.mat'  
%'Turkey_declustred.mat'  
%'Italy_clustered.mat'  
  
%adding restrictions to the catalogue, here: Turkey  
min_year=1000;  
min_mag=5.0;  
min_long=25;  
max_long=45;  
min_lat=36;  
max_lat=42;  
  
k = [];  
for i = 1:length(mag_list)  
    if mag_list(i) >= min_mag & year_list(i)>= min_year ...  
        & long_list(i) <= max_long & long_list(i) >= min_long ...  
        & lat_list(i) <= max_lat & lat_list(i) >= min_lat  
        k = [k i];  
    end  
end
```

```
end
if isnan(month_list(i)) == 1
    month_list(i) = 1;
end
if isnan(day_list(i)) == 1
    day_list(i) = 1;
end
end
used_events = k;

year_list = year_list(used_events,1);
month_list = month_list(used_events,1);
day_list = day_list(used_events,1);
lat_list= lat_list(used_events);
long_list = long_list(used_events);
mag_list = mag_list(used_events);

%%
%-spatial-discretization-----
%-----
%creates a grid starting from the minimum longitude(min_long) and the
%minimum latitude (min_lat) and ending at the maximum longitude (max_long)
%and the maximum latitude (max_lat). The spacing is set by default to about
%10 km
min_long=24;
min_lat=35;
max_long=46;
max_lat=44;

[loc_long,loc_lat,cell_size,no_points]=...
    spat_dist(min_long,max_long,min_lat,max_lat);

%options: e.g.
%Turkey: latitude:   35 - 44
%         longitude:  24 - 46
%Italy:   latitude:   35 - 50
%         longitude:   5 - 20

%%
%-Spatial-Smoothing-----
%-----
%choice of the following spatial smoothing algorithms
%the difference between static and dynamic indicates whether the smoothing
%kernel distance adjusts itself based on the earthquake density or not.

%static / dynamic Gaussian
%static / dynamic Power-law
%static / dynamic Donut
%static Stencil

%additionally it is possible to activate or deactivate magnitude binning
%for smoothing purposes. In the following code, binning is active

%magnitude bins
m_space=linspace(5,7.5,6);
%completeness data for the magnitude bins (here: Turkey)
completeness=[1900 1750 1500 1000 1000 1000];

%completeness and m_space must have the same length!
```

```
method='Gaussian'; %Gaussian / Powerlaw / Donut / Stencil

density=smoothing_static(method,50,long_list,lat_list,cell_size,...
    loc_long,loc_lat,mag_list,m_space,completeness,year_list,max_year);

%optional dynamic smoothing
%density=smoothing_dynamic(method,10,long_list,lat_list,cell_size,...
%    loc_long,loc_lat,mag_list,m_space,completeness,year_list,max_year);

%%
%-b-value-calculation-----
%-----

b_local=zeros(no_points,1);
%global_bvalue
%b_global is one single b_value for the whole region
b_global=calc_b_global(mag_list,m_space,completeness,max_year);

%option
%b_local is vector of location-dependent b_values
%b_local=calc_b_local(b_global,long_list,lat_list,loc_long,...
%    loc_lat,mag_list,completeness,m_space,max_year);

%assign local vector of b_values (if no local b_values are computed, the
%global b_value is assigned)
b_local(b_local==0)=b_global;

%%
%-probability/rate-calculation-----
%-----

%Forecast Period
%the following simple probability calculator uses the number of earthquakes
%of the minimum magnitude.
%alternatively it is possible to estimate an a-value via all different
%magnitude bins

m_min=min(m_space); %minimum magnitude bin
forecast=zeros(no_points,length(m_space));
forecast_period=10; %period of the forecast time interval
P=forecast;
for m=1:length(m_space)
    forecast_magnitude= m_space(m); %magnitude for which a forecast is made

    %calculate the rate of a certain magnitude
    for i=1:no_points
        forecast(i,m)=10.^(log10(density(i,1))-
b_local(i)*(forecast_magnitude-m_min));
    end

    %Poisson-probability of occurrence
    P(:,m)=1-exp(-forecast(:,m).*forecast_period);
end
```